

**INFLUENCE OF PROCESSING ON MICROSTRUCTURE
AND PROPERTIES OF Al-Al₂O₃ NANOCOMPOSITES**

BY

MUHAMMAD SHAH ZEB KHAN

A Thesis Presented to the
DEANSHIP OF GRADUATE STUDIES

KING FAHD UNIVERSITY OF PETROLEUM & MINERALS

DHAHRAN, SAUDI ARABIA

1963 ١٣٨٣

In Partial Fulfillment of the
Requirements for the Degree of

MASTER OF SCIENCE

In

MATERIALS SCIENCE AND ENGINEERING

MAY 2016

KING FAHD UNIVERSITY OF PETROLEUM & MINERALS
DHAHRAN- 31261, SAUDI ARABIA
DEANSHIP OF GRADUATE STUDIES

This thesis, written by **Muhammad Shah Zeb Khan** under the direction his thesis advisor and approved by his thesis committee, has been presented and accepted by the Dean of Graduate Studies, in partial fulfillment of the requirements for the degree of **MASTER OF SCIENCE IN MECHANICAL ENGINEERING**.



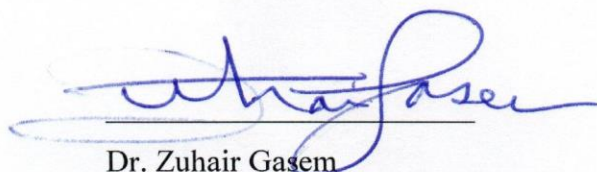
Dr. Saheb Nouari (Advisor)



Dr. AbulFazal M. Arif (Member)

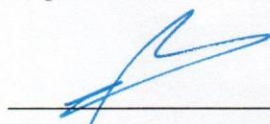


Dr. Sohail Akhtar (Member)



Dr. Zuhair Gasem

Department Chairman



Dr. Salam A. Zummo
Dean of Graduate Studies



19/6/16

Date

© Muhammad Shah Zeb Khan

2016

This work is dedicated to my mother for her matchless support and efforts.

ACKNOWLEDGMENTS

All thanks belong to Almighty Allah, who guided and blessed me with the courage and strength to conduct and accomplish this research work. I am indebted to my parents and family members for their love, support and encouragement. Their patience and sacrifices will remain my inspiration throughout the life.

I would like to express my sincere gratitude to my thesis advisor Dr. Saheb Nouari, Assoc. Prof. Department of Mechanical Engineering, KFUPM, who supervised this work and played vital role in guiding and handling technical aspects throughout the research. His kind support and cooperation will never be forgotten as He paved the way towards timely and successful completion of thesis. I am very much grateful to Dr. Abulfazal Arif & Dr. Sohail Akhtar from Department of Mechanical Engineering, KFUPM for their valuable suggestions and guidance.

Technical support and assistance from Dr. Abbas Saeed Hakeem, Research Scientist, Center of Excellence in Nanotechnology, KFUPM, in using Scanning Electron Microscope & Spark Plasma Sintering equipment is greatly acknowledged. Also I acknowledge Dr. Naseer Iqbal, Center of Excellence in Nanotechnology, KFUPM, for his timely help to review this work. A necessary thanks to all my colleagues especially Usama Siddiqui & Khawaja Mohammad who provided valuable support, advices and comments to refine this work. I am also in debt to all my friends and colleagues for giving me such a wonderful time.

Further thanks to technical staff members Mr. Latif and Mr. Sadaqat material science laboratory for their help and assistance in using different laboratory equipment.

CONTENTS

ACKNOWLEDGMENTS	III
LIST OF FIGURES	VII
LIST OF TABLES	X
ABSTRACT.....	XII
ARABIC ABSTRACT	XIV
CHAPTER 1 INTRODUCTION.....	1
CHAPTER 2 LITERATURE REVIEW	5
2.1 Composites.....	5
2.2 Metal Matrix Nanocomposites (MMNCs)	6
2.3 Strengthening Mechanisms	8
2.3.1 Load Transfer Effect	8
2.3.2 Hall-Petch Strengthening	9
2.3.3 Orowan Strengthening.....	10
2.3.4 CTE & EM Mismatch	12
2.3.5 Sum of Contributions	13
2.4 Mechanically Milled Nanocomposites.....	16
2.4.1 Mechanical Milling	16
2.4.2 Principle and Mechanism of Mechanical Milling	16
2.4.3 Milling Parameters	21
2.5 Mechanically Milled Al-Al ₂ O ₃ MMNCs.....	23
2.6 Consolidation of MMNCs	25

2.6.1	Spark Plasma Sintering	25
2.6.2	Principle and Mechanism of Sintering	27
2.6.3	Sintering Parameters	30
2.6.4	Spark Plasma Sintered Al-Based Composites	32
2.7	Mechanical Properties	34
2.7.1	Hardness	34
2.7.2	Compressive Strength	36
2.8	Thermal Properties.....	36
2.9	Coefficient of Thermal Expansion (CTE)	38
2.10	Motivation & Objectives	40
 CHAPTER 3 MATERIALS AND EXPERIMENTAL PROCEDURES		41
3.1	Raw Materials	41
3.2	Experimental Procedures.....	42
3.2.1	Mechanical Milling	42
3.2.2	Scanning Electron Microscopy (SEM).....	44
3.2.3	X-Ray Diffraction (XRD)	44
3.2.4	Spark Plasma Sintering (SPS)	46
3.2.5	Optical Microscopy (OM)	51
3.2.6	Density	51
3.2.7	Hardness	53
3.2.8	Compression Strength	53
3.2.9	Thermal Characterization	55
3.2.10	Coefficient of Thermal Expansion.....	55

CHAPTER 4 RESULTS & DISCUSSION	56
4.1 Powder Synthesis	56
4.2 X-Ray Diffraction	65
4.2.1 Pure Aluminum	65
4.2.2 XRD of 24h Milled Nanocomposites	67
4.2.3 Crystallite Size	69
4.3 Densification & Microstructure.....	71
4.4 Mechanical Properties	77
4.4.1 Hardness	77
4.4.2 Compression Test.....	80
4.5 Thermal Properties.....	89
4.5.1 Thermal Conductivity	89
4.5.2 Thermal Diffusivity.....	91
4.5.3 Heat Capacity	93
4.5.4 Coefficient of Thermal Expansion	94
CHAPTER 5 CONCLUSIONS	98
REFERENCES.....	99
VITAE.....	111

LIST OF FIGURES

Figure 2.1. Classification of composites/nanocomposites based on the type of matrix	6
Figure 2.2 Possible distribution of the matrix and reinforcement phases in a nano-composites [31]	7
Figure 2.3 Interaction between particles and a dislocation [69].	11
Figure 2.4 Schematic representation of microstructure-based transition mechanism from micro- to nano-Al-SiC composite [93]	15
Figure 2.5 Crushing of powder particles during mechanical milling	17
Figure 2.6 Types of impacts during the process of mechanical milling	17
Figure 2.7 To synthesize the metastable phase "energize and quench" method [49]	18
Figure 2.8 After collision size and shape change of different milling system [60]	19
Figure 2.9 The development of composite after high energy mechanical milling [48].....	21
Figure 2.10 SPS sintering stages/steps [44]	27
Figure 2.11 (a) DC pulse current flow through the particles (b, c) material transfer path during sintering [44, 74]	28
Figure 2.12 Spark plasma sintering set up	29
Figure 2.13 Diamond pyramid indenter used for the Vickers test [73]	35
Figure 2.14 Schematics of Dilatometer [91]	38
Figure 3.1 Sintering stages and parameters	47
Figure 4.1. (a) FE-SEM micrograph of Al powder and (b) TEM micrograph of Al ₂ O ₃ nano powder.....	56
Figure 4.2. FE-SEM micrographs of Al-10 vol.% Al ₂ O ₃ composite powder mechanically alloyed for (a) 3 h; (b) 6 h; (c) 20 h; (d) 24 h.....	58

Figure 4.3 FESEM micrographs of powders containing (a) 2 vol.% of Al_2O_3 (b) 15 vol.% of Al_2O_3 milled for 24h.	59
Figure 4.4 X-Ray mapping of Al- 10 vol. % Al_2O_3 milled for 24h.	61
Figure 4.5 X-Ray Mapping of Al-2% vol. Al_2O_3 milled for 24h.	62
Figure 4.6 X-Ray Distribution of Al-5% vol. Al_2O_3 milled for 24h.	63
Figure 4.7 X-ray mapping of Al-15% vol. Al_2O_3 milled for 24h.	64
Figure 4.8 XRD-Spectrum of pure aluminum (a) Unmilled (b) Milled for 24h.	65
Figure 4.9 XRD spectra of Al- Al_2O_3 composites mechanically milled for 24 h (a) 2 vol. %, (b), 10 vol. %, and (c) 15 vol. % Al_2O_3	67
Figure 4.10 Crystallite size of (1) Al MA for 24 h, and Al- Al_2O_3 composites (2) 2 vol. %, (3), 10 vol. %, and (4) 15 vol. % mechanically alloyed for 24 h.	69
Figure 4.11 Optical micrographs (x 500) of un-milled aluminum sintered for (a) 5 min (b) 20 min, and aluminum milled for 24h and sintered for (c) 5 min, (d) 20 min.	72
Figure 4.12 Optical micrographs (x 200) of Al-15 vol.% Al_2O_3 composite milled for 24h and sintered for (a) 5 min and (b) 20 min.	74
Figure 4.13 Relative density of sintered samples. (1) Al, (2) Al MA for 24 h, and Al- Al_2O_3 composites (3) 2 vol.%, (4), 10 vol.%, and (5) 15 vol.%.	75
Figure 4.14 Hardness of sintered samples. (1) Al, (2) Al MA for 24 h, and Al- Al_2O_3 composites (3) 2 vol.%, (4), 10 vol.%, and (5) 15 vol.%.	77
Figure 4.15 Compressive properties of samples sintered at 550°C, 50MPa, 200°C/min for 20m.	81

Figure 4.16 FESEM images showing fracture surfaces of (a) P-Al-unmilled (b) P-Al–24h and (c) Al-Al ₂ O ₃ 10% vol. nanocomposite, sintered at 550°C, 50MPa, 200°C/min for 20minutes.....	88
Figure 4.17 Thermal conductivities of spark plasma sintered pure Al-unmilled, pure Al and Al- Al ₂ O ₃ 10 % vol. nanocomposite milled for 24h.	90
Figure 4.18 Thermal diffusivity of spark plasma sintered pure Al-unmilled, pure Al and Al- Al ₂ O ₃ 10 % vol. nanocomposite milled for 24h.	91
Figure 4.19 Heat capacity of spark plasma sintered pure Al-unmilled, pure Al and Al- Al ₂ O ₃ 10 % vol. nanocomposite milled for 24h.....	93
Figure 4.20 CTE variations with temperature for (a) pure Al unmilled, (b) milled 24h, and (c) Al- Al ₂ O ₃ 10% vol. nanocomposite.....	94
Figure 4.21 Average CTE at 450 °C for pure Al unmilled, milled 24h, and Al- Al ₂ O ₃ 10% vol. nanocomposite	96

LIST OF TABLES

Table 3.1 Chemical composition of pure aluminum powder.....	41
Table 3.2 Size distribution in Al powder	41
Table 3.3 Summary of ball milling process parameters	43
Table 3.4 Spark plasma sintering process parameters	46
Table 3.5 Experimental parameters, to investigate the microstructure and densification of sintered monolithic Al and nanocomposites.	49
Table 3.6 Experimental parameters, to investigate the mechanical properties of sintered monolithic Al and nanocomposites.....	50
Table 3.7 Experimental parameters, to investigate the thermal properties of sintered monolithic Al and nanocomposites.....	50
Table 3.8 Theoretical density of nanocomposites.....	52
Table 3.9 Experimental conditions, to measure the coefficient of thermal expansion (CTE) using dilatometer.....	55
Table 4.1 Crystallite size of α -Al and mechanically milled aluminum nanocomposites ..	70
Table 4.2 Hardness (MPa) of spark plasma sintered materials.....	79
Table 4.3 Experimentally calculated properties of samples sintered at 550°C, 50MPa, 200°C/min, and 20m.	80
Table 4.4 Mechanical properties of materials sintered using spark plasma sintering	83
Table 4.5 Parameters used to estimate the yield strength of Al-Al ₂ O ₃ nanocomposites [94].....	84
Table 4.6 Theoretical and experimental values of compressive yield strength of developed nanocomposites and monolithic Al.....	85

Table 4.7 Thermal properties of nanocomposite including monolithic Al, sintered at 550°C, 50MPa, 200°C, 20 m.....	89
--	----

ABSTRACT

Full Name : Muhammad Shah Zeb Khan
Thesis Title : Influence of processing on microstructure & properties of Al-Al₂O₃ nanocomposites
Major Field : Materials Science & Engineering
Date of Degree : May, 2016

Metal matrix nanocomposites are advanced materials developed using ceramic nano-reinforcements and nanocrystalline metal matrices. These composites have outstanding properties and high potential for large number of functional and structural applications. Despite the importance of Al-Al₂O₃ metal matrix nanocomposites, work pertaining to their processing using mechanical alloying and spark plasma sintering is very scarce in the literature. The objective of this research work is to explore the possibility to synthesize nanocrystalline aluminum and homogenous Al-Al₂O₃ nanocomposite powders using mechanical alloying and consolidate them through spark plasma sintering technique. The second objective is to investigate the influence of milling and sintering conditions on the microstructure, densification, mechanical and thermal properties of the developed materials. Scanning electron microscopy, x-ray diffraction and mapping were used to characterize the powders and sintered samples. Density and hardness of sintered samples were measured using densimeter and hardness tester, respectively. Compressive properties of the developed materials were evaluated using universal testing machine. A thermal analyzer was used for thermal characterization i.e. thermal conductivity, thermal diffusivity, and specific heat capacity. A dilatometer was used to measure the coefficient of thermal

expansion of the sintered samples. It was observed that the milling of pure aluminum for 24 h reduced its crystallite size to less than 100 nm. For Al-Al₂O₃ nano-composites, milling for 24 h decreased the crystallite size of the aluminum phase and resulted in uniform dispersion of the reinforcement. Sintering of the synthesized powders led to the grain growth. Al₂O₃ contributed to growth inhibition when samples were sintered for 20 minutes; and improved the hardness but reduced densification. The Al-10 vol. % Al₂O₃ nanocomposite showed the highest Vickers hardness value of 1463 MPa. Mechanical milling for 24 h and the addition of 10% volume fraction of Al₂O₃ ceramic nanoparticles increased the compressive strength. A 111.5 % increase in compressive strength was observed for 10% by volume Al-Al₂O₃ nanocomposite. Furthermore, addition of Al₂O₃ nanoparticles decreased thermal properties but increased thermal stability of the developed materials.

ARABIC ABSTRACT

ملخص الرسالة

الاسم الكامل: محمد شاه زيب خان

عنوان الرسالة: تأثير التصنيع على البنية المجهرية و خصائص مركبات النانوية للألمنيوم و أكسيد الألمنيوم.

التخصص: علم و هندسة المواد

تاريخ الدرجة العلمية: مايو- 2016

تعتبر المركبات النانوية ذات الأساس المعدني من المواد المتقدمة و التي تطورت بإستخدام مواد نانوية مقوية سيراميكية داخل أساسات نانو بلورية معدنية. تتمتع هذه المركبات بخصائص بارزة و إمكانية كبيرة لتطبيقها في عدد كبير من التطبيقات الوظيفية و الهيكلية.

بصرف النظر عن أهمية المركب النانوي ذو الأساس المعدني (الألمنيوم و أكسيد الألمنيوم). فإن الدراسات المتعلقة بتصنيعها بإستخدام السبك الميكانيكي والتلبيد بدرجة الحرارة البلازما هي نادرة جدا في الوسط البحثي. إن الهدف الرئيسي من هذا البحث هو إستطلاع إمكانية تصنيع مسحوق بلورات الألمنيوم النانوية و مسحوق المركب النانوي للألمنيوم و أكسيد الألمنيوم بإستخدام طريقتي السبك الميكانيكي و التلبيد بدرجة الحرارة البلازما. والهدف الثاني هو دراسة تأثير ظروف الطحن والتلبيد على البنية الذرية و الكثافة و الخواص الميكانيكية والحرارية.

تم استخدام المجهر الإلكتروني و جهاز حيود الأشعة السينية وتخطيطها لتحديد خصائص المساحيق والعينات المتكلسة. تم قياس كثافة وصلابة العينات المتكلسة باستخدام مقياس الكثافة واختبار الصلادة. تم فحص الخصائص الإنضغاطية للمواد التي تم تطويرها باستخدام اختبار آلة الضغط. تم استخدام المحلل الحراري لتوصيف الخصائص الحرارية ، مثل كل من : الموصلية الحرارية و الانتشار الحراري والسعة الحرارية. تم استخدام مقياس التوسع لقياس معامل التمدد الحراري للعينات المتكلسة.

لوحظ أن طحن الألمنيوم لمدة 24 ساعة يعمل على خفض حجم بلوراته إلى أقل من 100 نانومتر. أما بالنسبة للمادة المركبة النانوية من الألمنيوم و أكسيد الألمنيوم فإن الطحن لمدة 24 ساعة خفض حجم البلورة للألومنيوم وساعد في توزيع أكسيد الألمنيوم (المقوي) بانتظام. عملية التليد للمساحيق المصنعة عملت على نمو حجم البلورات. عندما تم تليد العينات لمدة 20 دقيقة، ساهم أكسيد الألمنيوم على تثبيت النمو وتحسين الصلابة لكنها عملت على خفض الكثافة. أظهر مركب الألمنيوم المقوى بـ 10% من أعلى قيمة صلابة فيكرز (1463 ميجا باسكال). أدت عملية الطحن الميكانيكي لمدة 24 ساعة و من ثم إضافة 10% من أكسيد الألمنيوم إلى زيادة قوة تحمل الضغط بمعدل 111.5%. علاوة على ذلك فإن إضافة أكسيد الألمنيوم النانوي السيراميكي أدى إلى إنخفاض الخواص الحرارية ولكن زاد من الاستقرار الحراري لهذه المركبات المطورة.

CHAPTER 1

INTRODUCTION

Metal Matrix Composites (MMC) constitute of metallic matrix that are reinforced with rigid ceramic particles in order to obtain improved mechanical properties of monolithic metals. In the past, the practice of making alloy from two or more metals was frequently employed for optimization of numerous properties. The addition of rigid particles in metal matrix composites improved their toughness, young's modulus, strength, corrosion and wear resistance [1-4]. These enhanced properties, enable composites materials for light weight and high strength applications like military, aerospace & automotive industries [5-7, 10].

MMCs family comprises of three different classes; Continuous fiber reinforced MMCs, short fibers or whiskers reinforced MMCs and particle reinforced MMCs. From these three categories particle reinforced MMCs is low in cost due to its cheap fabrication and equally optimized properties [1]. Therefore, it is among the most attractive procedure that has been employed commercially. Moreover, second phase particles are used in particulate MMCs that could be of range from 10nm to 500 μ m. If the dimension of one or more constituent particle is observed less than 100 nm then it is said to be metal matrix nanocomposites (MMNCs). By proceeding to nanoscale for MMNCs, it is known that these materials show excellent properties than MMCs and hence exhibited significantly improved ductility, fracture toughness, machinability, tribological, thermal and electrical properties [19]. Small volume fraction of rigid particles can also enhance aforementioned properties appreciably [20-22]. For example, the addition of 1 vol.% Si₃N₄ (10nm)-Al matrix enhances the tensile strength of composite comparable to that of 15% SiC (3.5 μ m)-Al

matrix composite manufactured by the same powder metallurgical technique [23]. It is observed that the yield strength of smaller size (10nm) with minor volume is almost equal to that of the bigger size (3.5 μ m) reinforcement with larger volume.

Literature indicates that the particle reinforced MMCs are the best and cheaper to fabricate the MMNCs. Particulate reinforced MMNCs can be classified into two different methods; in-situ and ex-situ composites [12-19]. In the in-situ method the reinforcement is the product of chemical reaction between the raw materials used while ex-situ method employs external reinforcement [24]. The ex-situ is further categorized into solid state (powder metallurgy) and liquid state (casting) processing. In processing of liquid state composites, the distribution of reinforcement is obtained by die casting, squeeze casting, infiltration, ultrasonic cavitation, mechanical stirring and spraying [24, 25]. There are many limitations in casting of metal matrix nanocomposites fabrication. During casting, chances of external contamination and irregular dispersion of reinforcement are frequent so the ultrasonic waves are used to disperse the Al₂O₃, SiC in Al and Mg [26, 27]. Secondary phase formation is also expected during processing at higher temperatures [28, 29]. Poor wettability, porosity and irregular dispersion of reinforcement are the common problems in the liquid state processing. The other method of ex-situ is solid state processing which consist on powder grinding, mixing and then sintering. The solid state technique is observed helpful in resolving the shortcomings of the liquid state processing [24, 29-32].

Powder metallurgy employs cold isotatic pressing (CIP), hot isotatic pressing (HIP), hot pressing, hot extrusion, hot rolling, microwave sintering and spark plasma sintering [5, 25, 33]. Spark plasma sintering (SPS) is a non-conventional solid state processing technique. This is a modern and a very effective technique in order to consolidate the milled powders.

DC current pulse and uniaxial pressure are provided at the same time. The DC current can provide heat to the pressed powder up-to 2400 °C [34]. And with the proper cooling rate, the time required for cooling the sintered job is also reduced. Microstructure can be preserved using heating rate 200 °C/min with least grain growth [35]. This process is binder-less and does not require any pre-compaction. Few samples of Al 6061 alloy were sintered using HIP, MW, SPS and tube furnace and it was observed that the sintering obtained by SPS has highest densification.

In powder metallurgy (PM) technique, materials are processed through mechanical milling. It involves severe plastic deformation which results in to grain size reduction, uniform dispersion and prevention of the unwanted brittle phases. The best milling was achieved by Frisch Pulverisette-4-mill and SPEX 9000 to achieve uniform dispersion of Lead in Aluminum matrix [36]. Aluminum is considered as the dream metal in MMCs for its outstanding properties like higher strength with light weight, low melting point, good formability and corrosion resistance. There are number of reinforcements that can be used such as Al_2O_3 , AlB_2 , AlN , TiC , Al_4C_3 , SiC , WC , TiB_2 and TaC in order to enhance various properties of aluminum [24-37]. With the help of these rigid reinforcements aluminum based MMNCs have very broad range applications in automotive, aerospace industries, high pressure and temperature requirements, turbines, structural material and other mechanical parts. Al_2O_3 is found to have excellent properties lesser COF, high hardness, strength, specific modulus, wear resistance, oxidation and corrosion resistance. Aluminum based metal matrix with alumina reinforcement was found to have potential applications in military, automotive and aerospace applications [5, 19]. It was observed that the alumina has better wettability and thermal stability in aluminum matrix. Al- Al_2O_3 nanocomposites

are not been explored completely therefore there is a scope of exploration and enhancement in the mechanical properties of Aluminum. Synthesis of Al-Al₂O₃ nanocomposites have done by the help of mechanical milling proceeded with spark plasma sintering in the past [41, 42]. But the above mentioned limitations of the composites have not been resolved and the effect of SPS parameters were not investigated completely. These are the core issues that caused hindrance in the mass production of MMNCs. Therefore, this work focuses on achieving uniform dispersion of reinforcement in the matrix, which is ultimately responsible for improving the various properties of the nanocomposites. The uniform dispersion of different compositions is characterized and the effect of milling on dispersion is observed. Different parameters of SPS are also investigated and a correlation between microstructure and densification is developed as discussed in the relevant sections.

CHAPTER 2

LITERATURE REVIEW

2.1 Composites

Composites are defined as the materials made up of chemically different and insoluble constituents. These constituents may be macro or microscopic scale. It is a very broad definition; which covers a lot of materials like different layers of sand, chalk and stones, human body and wood etc. Material scientists and industrialists use another definition; a material consist of different constituents, which are mixed physically by pre-mixing them together in order to achieve some optimized properties of monolithic materials [38]. Metal matrix composites (MMCs) are comprised of a softer phase called as matrix that possess good formability, thermal conductivity and ductility. While, the other phase contains some hard or rigid particles that are dispersed in the matrix phase called reinforcement. Reinforcement possess higher stiffness and strength than matrix and its addition improves few specific properties in the matrix. The reinforcement can have different type of morphology and geometry like particulate or whiskers (oriented or disoriented). The classification of composites as shown in fig.2.1 is based on the following details:

- 1) Type of matrix e.g., polymer, ceramic, metal etc.
- 2) Type of reinforcement; chemical nature (oxides, carbides, nitrides) and shape includes (particulate, whiskers, continuous fibers or discontinuous fibers)
- 3) The processing route (In-situ or ex-situ) [31]

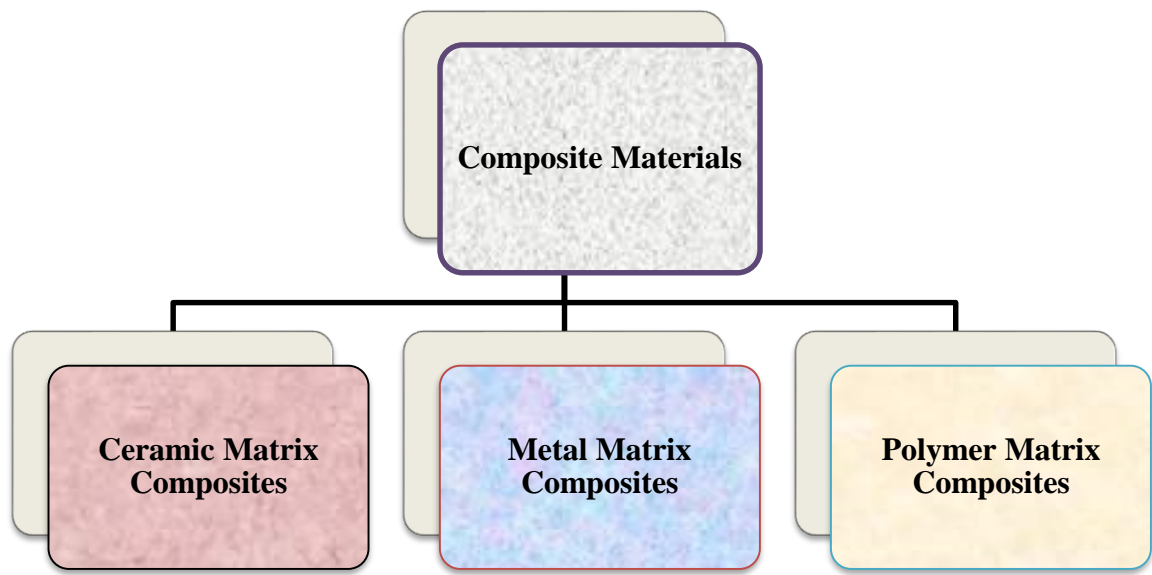


Figure 2.1. Classification of composites/nanocomposites based on the type of matrix

2.2 Metal Matrix Nanocomposites (MMNCs)

Aluminum based metal matrix composites are the most widely used MMCs now a days. The ceramic phase (Al_2O_3 , SiC , AlN) which is hard and brittle should ideally be uniformly dispersed in the aluminum matrix to improve its mechanical, thermal, wear, surface and other structural properties. Metal matrix composites have also shown improvement in other properties like creep resistance, high specific stiffness and strength [29]. Due to these excellent properties, aluminum based MMCs are extensively used in automotive and aerospace industries. The optimized development of MMNCs has led to the precise achievement of properties. Metal matrix nano-composites are defined as the composites in which one or more constituents should have the grain size less than 100nm [40]. The diagrammatic representation of reinforcement in the matrix is shown in fig 2.2 There are two types of hexagons, open and filled, former represents matrix phase and later shows the reinforcement either single or multiple.

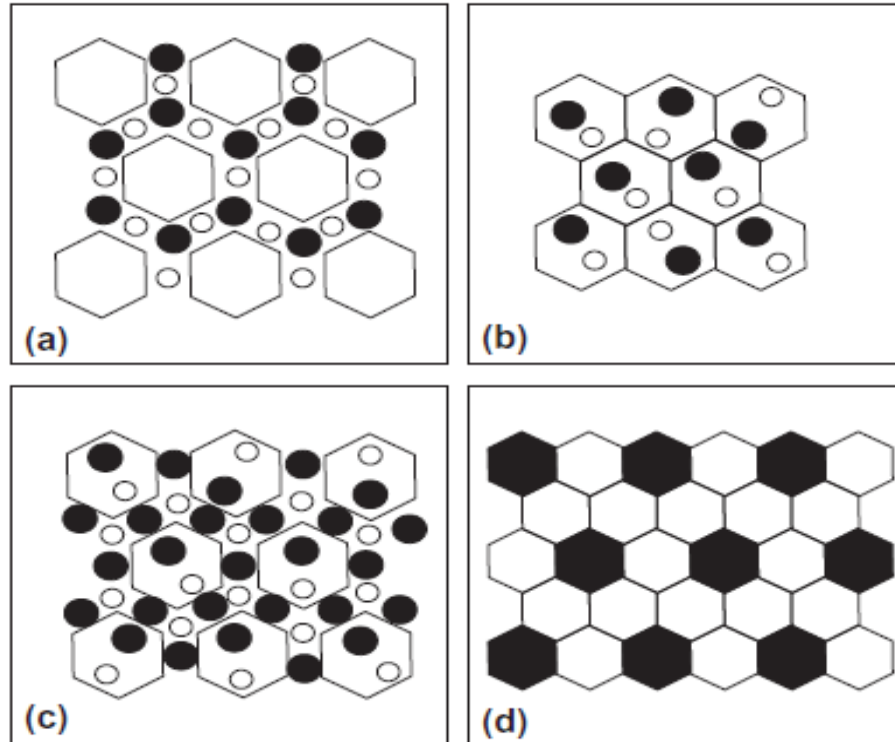


Figure 2.2 Possible distribution of the matrix and reinforcement phases in a nano-composites [31]

In fig.2.2 (a) the 2nd phase rigid particles are distributed around the grain boundaries of matrix or basic phase, (b) shows the 2nd phase particles inside the matrix, (c) represents the 2nd phase particles both at grain boundaries and inside the matrix and (d) depicts the uniform distribution of reinforcement in the matrix [31].

Razavi Hesabi Z et al. [41, 42] investigated the sintering behavior of Aluminum (pure) with 5%-Al₂O₃ by volume. The consolidation/ sintering involved rearrangement of particles in 1st-stage, whereas in the 2nd- stage plastic deformation of the powder grains took place. The metal matrix nano-composite with reinforcement Al-CNT, Al-B₄C, Mg-SiC, Ti-SiC, Cu-CNTs, Al-Al₂O₃, Mg-SiC, Al-SiC, Al-CNT, Mg-Y₂O₃, Al-Diamond, and Zn-SiC using powder metallurgy have also been successfully prepared [40].

There are few challenges associated with the development of MMNCs as mentioned below;

- Non-homogeneous dispersion and agglomeration of reinforcement in the matrix.
- Strengthening mechanism; the bonding between interfaces should be high to get best mechanical properties.
- Grain growth during the process of sintering.
- Economy/ cost effectiveness of the developed nanocomposites [44, 45].

2.3 Strengthening Mechanisms

Plastic deformation is entirely based upon dislocation movement. The hindrance to the movement of dislocations upon application of applied force is known as strengthening. The mechanical strength of MMNCs increases due to a variety of strengthening mechanisms benefactions i.e. load transfer effect (LTE), Hall-Petch Strengthening (HPS), Orowan strengthening (OS), mismatch of thermal expansion coefficient (CTE) and elastic modulus (EM). These strengthening mechanisms are discussed below individually;

2.3.1 Load Transfer Effect

In a composite, the prime important function for addition of reinforcement in the matrix is to bear the major part of applied load, while the matrix binds the reinforcement particles together, and also distributes and transmits the applied load to the reinforcement [80, 81]. Generally, applied load transfers from softer matrix to comparatively stiffer and harder reinforcement particles. This transfer of load contributes to the strength enhancement of the matrix material. Mechanical processing and addition of nanometer sized reinforcement particles induces strong cohesion between the matrix and reinforcement at atomic level. In

fact, the nanoscale particles are directly bonded to the matrix. This bonding depends upon the proper wetting between the reinforcement and matrix. Formation of bonding may take place due to reaction or dissolution of particles and metal matrix [3, 79, 80]. Nardone and Prewo modified the shear lag model for the prediction of the strength contributed to composite due to load transfer, the relation is given in below equation 2.1;

$$\Delta\sigma_{LT} = v_p \sigma_m \left[\frac{(l+t)A}{4l} \right] \quad (2.1)$$

where volume fraction (V_p), yield strength (σ_m), l and t are the size reinforcement particles in both (parallel and perpendicular) directions to the applied load.

2.3.2 Hall-Petch Strengthening

Hall Petch strengthening is a type of strengthening based upon the fact that not all the grains in the material are aligned in a single direction. Therefore, it is difficult for a dislocation moving in a specific plane in one crystal to travel over to another grain in the same plane. A material having finer grains have more disorder regions (GBs) and provides more resistance to the movement of dislocations. Therefore, material with smaller grains become harder and stronger than the coarse-grained materials having lesser number of grain boundaries. The relationship between yield strength and the grain size which is termed as the Hall Petch given below in equation 2.2;

$$\Delta\sigma_{H-P} = \sigma_o + \frac{k_y}{\sqrt{d}} \quad (2.2)$$

where σ_{H-P} is Hall-Petch yield stress, d is the average diameter of grain, and k_y is the constant for the specific material (locking parameter) [67].

The addition of ceramic particles plays an important role in the growth of grains in metal matrix composites. These particles interact with the GBs and act as pin points to restrict the further grain growth. The increase in volume fraction (v_p) and the decrease in particle diameter (d_p) of reinforcement results in a finer grain structure in the matrix. Zener derived to determine the maximum matrix grain size theoretically [3]. The Zener equation is given below.

$$dm = \frac{4ad_p}{3v_p} \quad (2.3)$$

2.3.3 Orowan Strengthening

Dislocations can travel in a dispersion strengthened matrix in two ways. Either they can cut by the precipitate particles or bend around and bypass the particle. Cutting of particles through the dislocations usually take place if the slip planes are continuous from the matrix through the precipitate particle and when almost equal force is required to travel the dislocation in the matrix and the inclusion particles (precipitate). Small particles are comparatively easier to cut by the dislocations than the coarse grained particles and are called segregated solute atoms. Ease of shearing or cutting depends upon few particle properties i.e. stacking fault energy, modulus effect, morphology, lattice friction and coherency of strains. When the slip planes are not continuous within matrix and the second phase particles (abrupt change in orientation is observed) then cutting of particles is not possible. In these conditions, dislocations try to bend around the particles and bypass it. This behavior is known as Orowan strengthening, the phenomenon is shown in the fig. 2.3 Non-shearable nanoparticles act as barriers in movement of dislocations and promote

dislocations bending or bowing around the particles that is called as Orowan loops formation under applied external load.

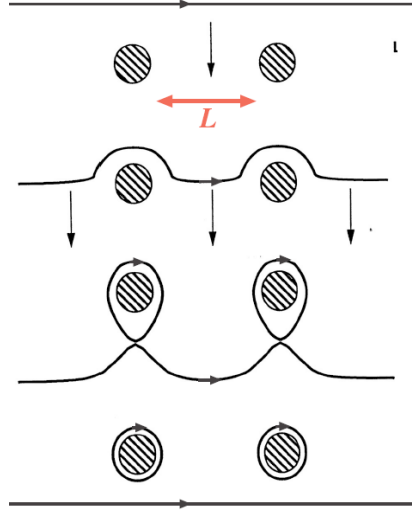


Figure 2.3 Interaction between particles and a dislocation [69].

The basic equation for the Orowan shear stress determination is given in equation 2.4:

$$\tau_o = \frac{G}{\lambda} \quad (2.4)$$

where G is the shear modulus of the matrix material, and λ is the average interspacing between particles. When the particles are harder and of submicron size, the strengthening is achieved through Orowan strengthening as it becomes more effective as inclusion particle size reduces [3, 21].

The extent of distribution of the second phase particles determines the degree of strengthening. The relationship between particle distribution and volume fraction, average particle diameter and mean interspacing of particles is expressed in the equation 2.5 as mentioned [21]:

$$\lambda = \frac{4(1-f)r}{3f} \quad (2.5)$$

where f is the volume fraction of spherical particles of radius r . The inter-particle spacing should be typically few hundred angstroms. The purpose of the addition of hard but small particles in soft metals or alloys to provide the hurdles and obstacles to the movement of dislocations and also to enhance the stiffness of the composite than monolithic metals or alloys [21, 67]. One modified form of Orowon-Ashby relation is shown in equation 2.6:

$$\Delta\sigma_{or} = \frac{0.13bG}{r\left(\sqrt[3]{\frac{1}{2}v_p-1}\right)} \ln\left(\frac{r}{2b}\right) \quad (2.6)$$

where G is the shear modulus of the matrix material, b is the burgers vector [3, 21].

2.3.4 CTE & EM Mismatch

As a result of cooling and straining, formation of geometrically necessary dislocations (GNDs) take place due to the mismatch between the coefficient of thermal expansion (CTE) and elastic modulus (EM) of matrix and inclusion. The density of GNDs produced by the mismatch between CTE and EM can be determined from the following expressions 2.7 & 2.8:

$$\rho^{CTE} = \frac{A\Delta\alpha\Delta T v_p}{b d_p(1-v_p)} \quad (2.7)$$

$$\rho^{EM} = \frac{6v_p}{\pi d_p^3} \varepsilon \quad (2.8)$$

where geometric constant (A), the difference in CTE ($\Delta\alpha$) and the difference between test and processing temperatures (ΔT).

The overall strengthening due to CTE and EM can be estimated by using Taylor's equation as given 2.9 [3];

$$\Delta\sigma_{CTE+EM} = \sqrt{3}\beta Gb(\sqrt{\rho^{CTE}} + \sqrt{\rho^{EM}}) \quad (2.9)$$

2.3.5 Sum of Contributions

By summing each of the previously explained strengthening effects and mechanisms, the final strength can be determined for a specific composite (σ_c), by employing yield strength of the matrix (unreinforced) as given below;

$$\sigma_c = \sigma_m + \sum_i \Delta\sigma_i \quad (2.10)$$

where σ_m is the yield strength of the matrix (unreinforced), $\sum \Delta\sigma_i$ is the single strengthening effects. There are several other methods to estimate σ_c . One of the simple approach to calculate the final strength of the composite by taking the square root of summation of single strengthening contribution ($\sum \Delta\sigma_i$) as shown below:

$$\sigma_c = \sigma_m + \sqrt{\sum_i \Delta\sigma_i^2} \quad (2.11)$$

By considering the combine effect of Orowan strengthening, CTE mismatch and load bearing, the final strength of composite can also be estimated as following;

$$\sigma_c = (1 + 0.5v_p)(\sigma_m + A + B + \frac{AB}{\sigma_m}) \quad (2.12)$$

where A & B are the coefficients of CTE mismatch and Orowan effect respectively [3, 78, 79]. A and B can be calculated using the following relations;

$$A = 1.25G_mb \sqrt{\frac{12\Delta\alpha\Delta T v_p}{bd_p(1-v_p)}} \quad (2.13)$$

$$B = \frac{0.13G_mb}{d_p[(\frac{1}{2v_p})^{\frac{1}{3}} - 1]} \ln \frac{d_p}{2b} \quad (2.14)$$

It has been reported that when the particulate size of reinforcement is lesser than 50nm, the Orowon effect and CTE mismatch are the major contributors in strengthening of a particulate composite [3, 78-81]. The overall strengthening is considered to be a cumulative effect of all the previously mentioned effects. D. Liu et al. [90] reported that the strengthening of MMNCs is mainly affected by both the grain boundaries and presence of impurities and second phase particles. While it is approximated due to difficulty in determining the precise effect of individual mechanisms. Effect of grain size and second phase particles can be schematically illustrated in fig. 2.4.

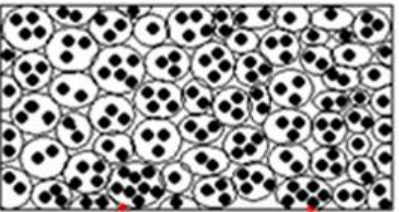
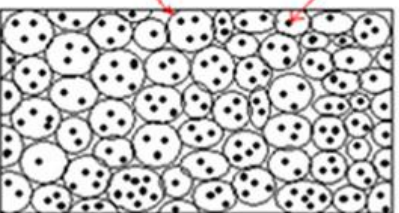
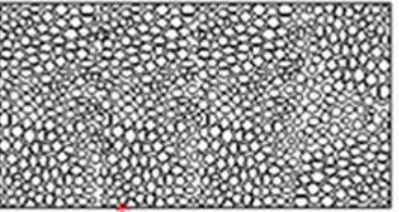
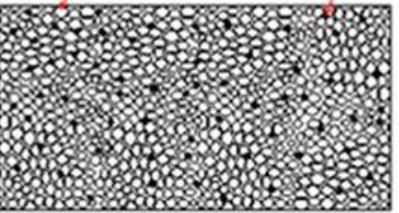
Morphology	Operating Mechanism
<div data-bbox="435 310 490 436" style="display: inline-block; transform: rotate(-90deg);">micro Al micro SiC</div>  <div data-bbox="435 592 490 718" style="display: inline-block; transform: rotate(-90deg);">micro Al nano SiC</div> 	<p style="text-align: center;">Hall-Petch + Orowan looping</p>
<div data-bbox="435 825 490 951" style="display: inline-block; transform: rotate(-90deg);">nano Al</div>  <div data-bbox="435 1077 490 1203" style="display: inline-block; transform: rotate(-90deg);">nano Al nano SiC</div> 	<p style="text-align: center;">Hall-Petch + Grain boundary sliding</p>
	<p style="text-align: center;">Hall-Petch + Grain boundary pinning</p>

Figure 2.4 Schematic representation of microstructure-based transition mechanism from micro- to nano-Al-SiC composite [93]

2.4 Mechanically Milled Nanocomposites

2.4.1 Mechanical Milling

Mechanical milling is a technique in which a charge (powder) is placed in a container (vials) and high energy impact is provided by rotation [46]. Advanced nanomaterials can be produced by this non-conventional solid state method. This technique is utilized to obtain the optimal structures, mechanical and physical properties. It is also called mechanical alloying by some researchers for cases in which solid solution formation is expected. Reactive milling is referred to the powders in which some reactions take place in the milling process and ultra-fine particles dispersion takes place. Using the milling technique amorphous, metastable, nano-crystalline, novel materials and metal-ceramic composites can be manufactured [47, 48]. Mechanical milling and mechanical alloying are technically two different terms; mechanical alloying involve with the material transfer for homogenization while the mechanical milling doesn't require any material transfer [49].

2.4.2 Principle and Mechanism of Mechanical Milling

Mechanical milling is a method of synthesizing various materials at non-equilibrium conditions. This technique involves the loading of elemental or pre alloyed powder with grinding balls in a container (vial) which are then subjected to heavy deformation by centrifugal forces. The crushing of powder grains take place as shown in the figure 2.5. During the process of milling different type of impact load are applied to the powder as a result of ball-ball and ball to wall collisions, as shown in fig. 2.6. Milling also enables homogeneous dispersion of reinforcement in the matrix which imparts the desired properties in developed composites.

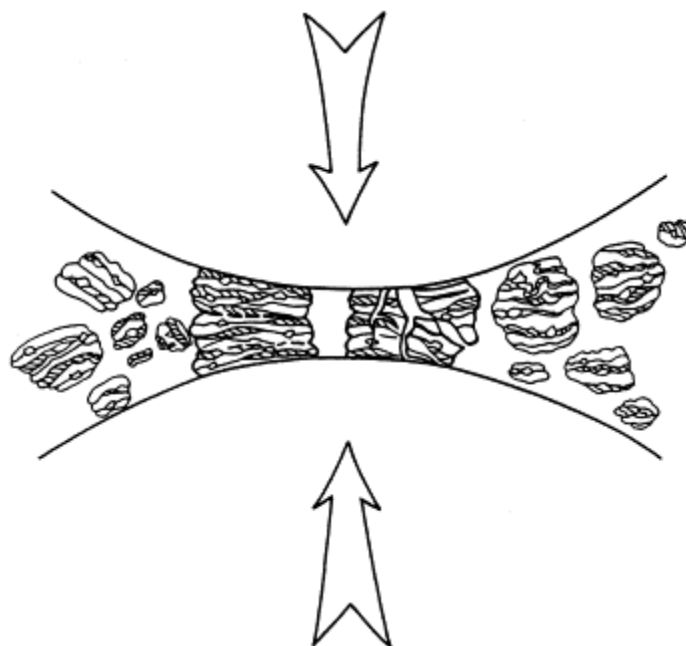


Figure 2.5 Crushing of powder particles during mechanical milling

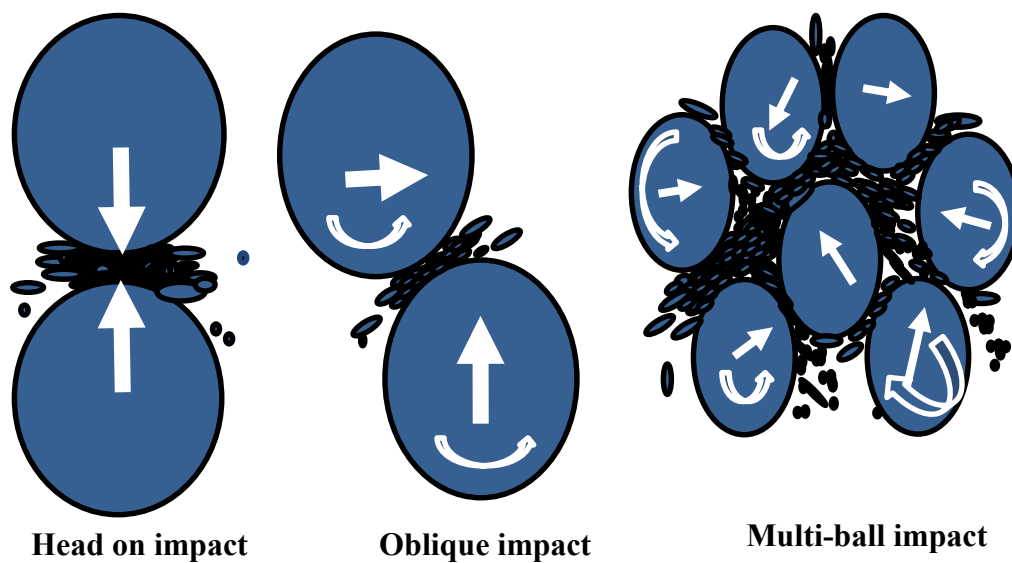


Figure 2.6 Types of impacts during the process of mechanical milling

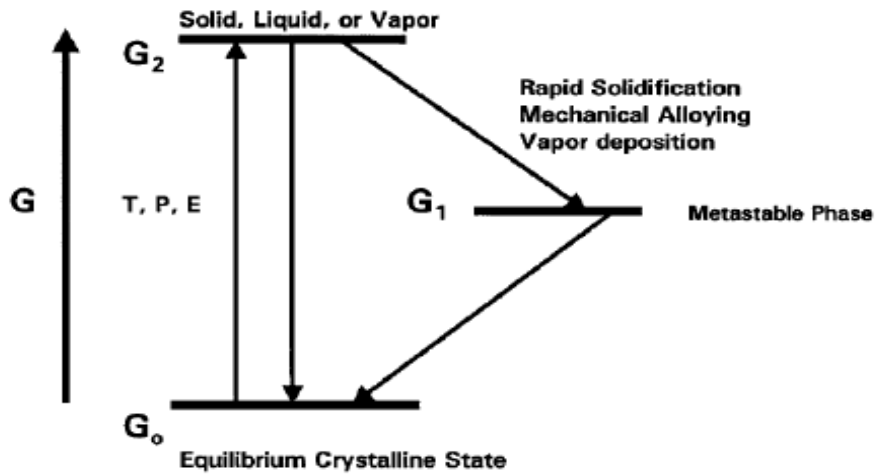


Figure 2.7 To synthesize the metastable phase "energize and quench" method [49]

Fig.2.7 illustrates formation of metastable phase by the provision of external energy, and this metastable phase further went through the equilibrium state. There are few processes taking place during the mechanical milling; plastic deformation, cold welding and fracturing.

Optimum ball milling process depends on two following factors:

1. The rate of fracturing should be balanced with cold welding rate.
2. Average particles should be relatively coarser.

The purpose of mechanical milling is to prepare the powder for further processing i.e. sintering/consolidation. Materials consisting of more than one phase/constituents can be homogenize and mixed by using mechanical milling [49]. The process of ball milling can be divided into the following 4-stages on the basis of microstructure;

- At the start of the milling process the particles flattening takes place as illustrated in the fig.2.8 is called initial stage. Different ranges of particles sizes

are utilized in the processing. This stage is insufficient to obtain the homogenization of the reinforcement in the matrix.

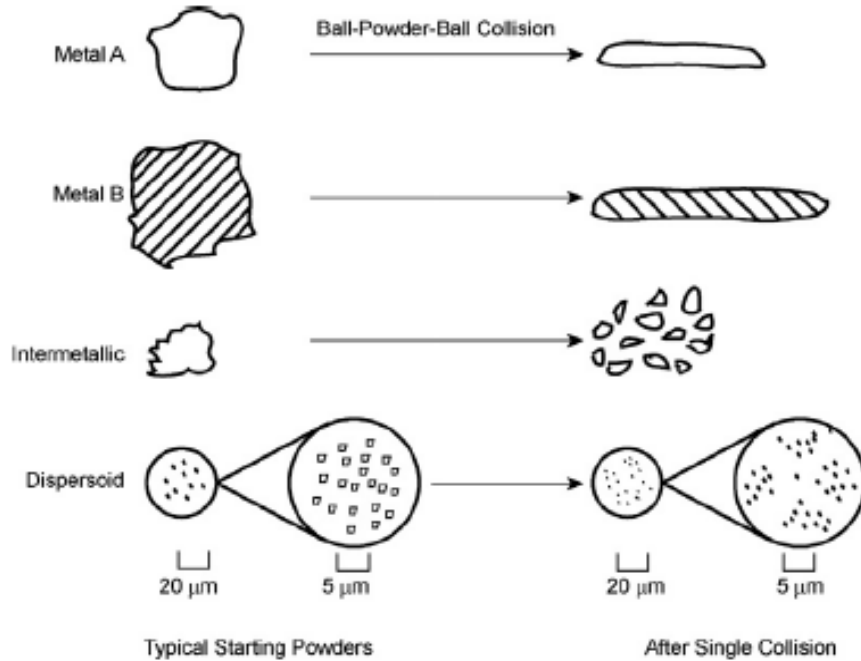


Figure 2.8 After collision size and shape change of different milling system [60]

- In the intermediate stage, the fracturing and cold welding take place. Welding is more dominant; therefore, it results in lamellar structure with reduced size of particles [49].
- Further grain size reduction along with the homogenization of the reinforcement in the matrix takes place at macroscopic level in the final stage. During this process the equilibrium obtained between cold welding and fracturing. [46].
- The last stage in the milling process is called completion stage. In this stage, the extreme deformation of particles occurs and no further optimization is expected.

In the milling process, vials (container) are placed on the stage of milling machine, and the stage is responsible to rotate the vials having powder particles in it. The balls in the vials collide with each other and with the walls of the vials. During this collision, some powder is trapped between the balls and the wall of the vials. This collision provides impact energy to the powder and deforms it permanently which further lead to fracture [40]. It actually happens in the case of ductile materials, while for brittle materials relatively longer time is require to flatten, cold weld and fracture the grains.

An equilibrium between cold welding and fracturing might be achieved during the milling process. Cold welding usually induces the agglomeration of particles, which is balanced with the fracturing or reduction of the particles. The formation of composite can be seen in the fig. 2.9. The milling process induces severe plastic deformation in the powder in the form of defects, stacking faults, dislocations, grain boundaries and vacancies and also allows the two species to get homogenize during the process.

There are three different possible systems during the milling:

- 1) Ductile-ductile
- 2) Brittle-brittle
- 3) Ductile-brittle

In the brittle-brittle system there is no possibility for alloying due to lack of ductility that induces cold welding. Alloying is also reported for some cases in the brittle-brittle systems.

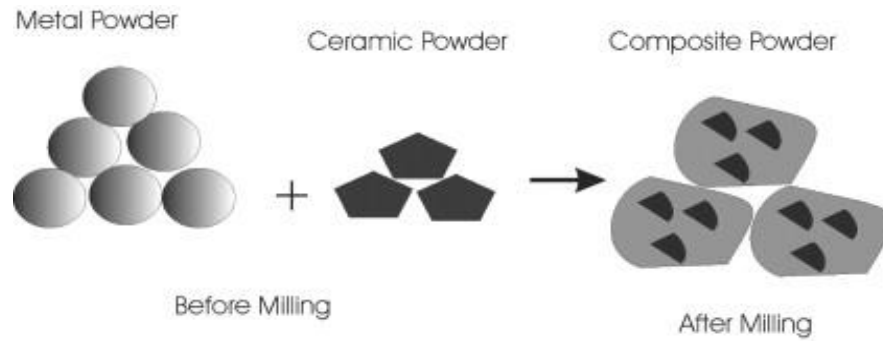


Figure 2.9 The development of composite after high energy mechanical milling [48]

2.4.3 Milling Parameters

Type of Mill: It depends on few factors like the quantity of powder, final constitution required, capacity, controlled environment and speed of rotation. Suryanarana et al. [49] specified the SPEX mill shaker for the purpose of alloy screening, while Fritsch Pulverisette planetary ball mills used for large quantity powder production.

Milling Container: The material of vials/ container should be harder than the powder being milled. Common materials include tool steel, tempered steel, hardened steel, tungsten carbide and tungsten carbide cobalt steel [47].

Milling Speed: The speed depends on the type of ball mill and the purpose of milling. Higher milling speeds induce larger deformation and strains in the powders. Above a certain limiting speed, the balls will be pinned to the walls of the vials and the purpose of inducing strains and stresses in the material powder will not be accomplished. Temperature also increases during the milling, and it can decompose the non-equilibrium phase, which can also cause the formation of crystalline or amorphous structure in the powders [49].

Milling Time: On the basis of all previous milling conditions the time of milling has to be decided. More milling time can increase the chances of contamination. The intensity of

milling, the type of mill used, temperature and environment and ball to powder ratio are the deciding factor for the time of milling.

Grinding Medium: The size and density of milling balls influence the end product after the process of milling. High density balls impart more strain and energy to the powders. The difference in size and density can affect the crystalline or amorphous phase formation and its grains size.

Ball to Powder Ratio (BPR): This is also called charge ratio (CR). It is actually the ratio between the mass of the milling balls and the powders. 10:1, 50:1, 100:1 are the BPR ratios found in the literature. Higher ball to powder ratios result in the quicker milling process [50].

Extent of Filling the Vials: Half of the vials should be filled with the powder [49].

Milling Atmosphere: Vials of the mill used should be in the inert environment in order to avoid any kind of chemical reactions during the process. It also prohibits the air having solid particles to contaminate the charge. Milling atmosphere also affect the formation of different phases in the powder.

Process Controlling Agent: It is used mostly for lubrication purposes it minimize the effect of cold welding. It also helps to minimize agglomeration. Common PCAs are ethanol, methanol, hexane and stearic acid. PCAs in the form of liquid are preferable for solid; homogeneous distribution of particle size can be achieved. The addition of PCA induces some impurity in the powder called yield. Yield induces low level impurity in the process. Therefore, PCAs of low impurity level are required as a lubricant.

Temperature of Milling: Temperature has a great influence on milled powders because of diffusion. Milling temperature affects the solid solubility concentration or type and

quantity of phase formed. For higher milling temperature the solid solubility decreases as reported [49]. Higher the milling temperature greater is the amount of amorphous phase formation in the powder.

2.5 Mechanically Milled Al-Al₂O₃ MMNCs

B. Prabhu et al [43] ball milled and characterized the metal matrix nanocomposite of aluminum with reinforcement of alumina with different fractions 20, 30 and 50 percent by volume using high energy milling technique. Different particles sizes for alumina reinforcement were employed including 5 μ m, 150nm and 50nm in the aluminum matrix. After 20 h of milling uniform distribution of alumina reinforcement was observed in aluminum matrix. The BPR ratio kept 10:1 in the high energy milling SPEX. X-Ray mapping, SEM, XRD and EDS used to confirm the uniform distribution at different parameters. A uniform distribution of finest particles (50nm) with 50% by volume of reinforcement was observed in aluminum matrix. No phase transformation for alumina was observed after 20 h of milling.

Mehdi Rahimian et al [42] mechanically milled alumina reinforcement in the matrix of aluminum in order to meet the most recent demands of industry. They investigated the effect of alumina particle size, sintering time and temperature on different properties of aluminum based metal matrix composites. The alumina particles of different sizes 48 μ m, 12 μ m and 2 μ m were used. The time and temperature for sintering in the range 30-90 min with 500-600 °C temperature range. Optical microstructure was revealed by the help of metallography technique and correlated with different properties including yield strength, hardness, density and compressive strength. It was observed that as the particle size of

alumina decreases the increase in density, hardness, compressive strength and yield strength obtained. These properties also depend on the sintering time and temperature.

Z. Razavi Hesabi et al [41] processed Al–Al₂O₃ metal matrix composite by using mechanical milling technique proceeded with the uni-axial loading compaction and conventional sintering. Densification and the effect of reinforcement was studied by comparing monolithic aluminum and composite sintered samples. The milling was prolonged for 72k seconds or 20 h using the planetary ball mill. 1.5% by weight stearic acid was used as process controlling agent (stearic acid). The processing of powder was taken place in the presence of high purity argon environment. The rotational speed kept 250rpms with 10:1 ball to powder ratio.

H. Mahboob et al [39] manufactured Al–Al₂O₃ composite material with the help of mechanical milling technique and investigated the microstructure. The powder of aluminum and alumina were used with specific particle size weight percentage and milled in a horizontal ball mill. The charge powder was allowed to mill for specified time and then pressed and sintered in argon environment. The powder was characterized microstructurally by SEM. It was observed that higher the milling time, the better is the distribution of reinforcement in the matrix. The process involved a ball to charge ratio 20:1. Steel balls of different diameter ranges were used (15.8 to 24.4mm) with slow rotational speed 85rpm milling time kept up to 15h. The milled powder was analyzed at eight different intermediate milling times to determine the milling time effect on the composite.

S.S. Razavi Tousi et al [42] fabricated the aluminum-based nanocomposite using submicron sized alumina reinforcement. From various experimental analysis, it was concluded that the size, morphology and the press-ability of the reinforcement powder have

strong effect on the properties of composite. Uniform distribution of alumina particles in the aluminum matrix was confirmed by SEM. Aluminum with 20 wt.% of alumina reinforcement (.5-.8 μm) milled in planetary ball mill for 25h. The BPR ratio was kept 15:1 with 250 revolution per minute speed. Stearic acid with 3% by weight was utilized as process controlling agent. The argon atmosphere was provided.

2.6 Consolidation of MMNCs

There are two major categories of sintering called as conventional and non-conventional. Conventional sintering includes; hot isostatic pressing (HIP), cold isostatic pressing (CIP) and tube furnace sintering, while non-conventional sintering includes; spark plasma sintering (SPS), plasma activated sintering (PAS), electro-consolidation and micro wave sintering (MWS).

2.6.1 Spark Plasma Sintering

It is a consolidation technique in which the powder particles are joined together at high temperature and pressure is provided simultaneously; to get a densified material by gradually reducing the volume of the pores and spaces between them. It is a diffusion assisted technique usually utilized for the synthesis of refractory materials having higher melting points and cannot be manufactured by the casting. Now a days, this technique is being utilized for metals, alloys, composites and intermetallics as well. Pores are present at initial compaction due to availability of high energy sites, providing a high temperature, the atoms diffuse to the point of contact between the particles which result into bonding and the shrinkage of the pores present between the particles. The successful sintering of the materials results into the best densification by minimizing the amount of pores.

Densification depends upon sintering temperature, time, mechanism, average particle size of powder, initial powder density and the size distribution of the powder particles [47].

Another type of sintering called liquid state sintering, involves a constituent which has lower melting point than others and acts as binder upon melting during the process of sintering.

Spark plasma sintering (SPS) falls under the category of plasma activated sintering (PAS). It is one of the two categories of electric current assisted/activated sintering (ECAS). SPS has also referred as field assisted sintering (FAST), pulsed electric current sintering (PECS) or plasma activated sintering (PAS). SPS involves simultaneous application of pulsed electrical high energy, low voltage, spark pulse current and pressure directly on the materials to be sintered. The process should not be confused with some other types of RS. The criteria with which RS processes can be differentiated include apparatus used and type of the wave form in the applied current. ECAS is an advanced technique in recent times due to its numerous advantages such as;

1. Quicker heating rate.
2. Flexible and controllable process parameters.
3. Pre compaction is not required.
4. High temperature ceramics and long fibers can be sintered.
5. Lesser holding time needed which eliminate the formation of new phases and grain growth.
6. Highly densified sintered parts obtained almost near to theoretical density [38].

2.6.2 Principle and Mechanism of Sintering

Spark plasma sintering is usually performed in four major stages as illustrated in fig. 2.11. In the first stage, the air and gas removal is takes place to generate vacuum in the chamber up to certain limit. In the second stage, the pressure is applied uni-axially along the die and proceeded to third step, involve resistance heating and holding the system for desired time. Final stage involves the cooling at specific cooling rate. During the process, at the points of contacts of the particles, a localized high temperature generation take place up to 10,000 °C which causes evaporation and melting of the contacting powder particles.

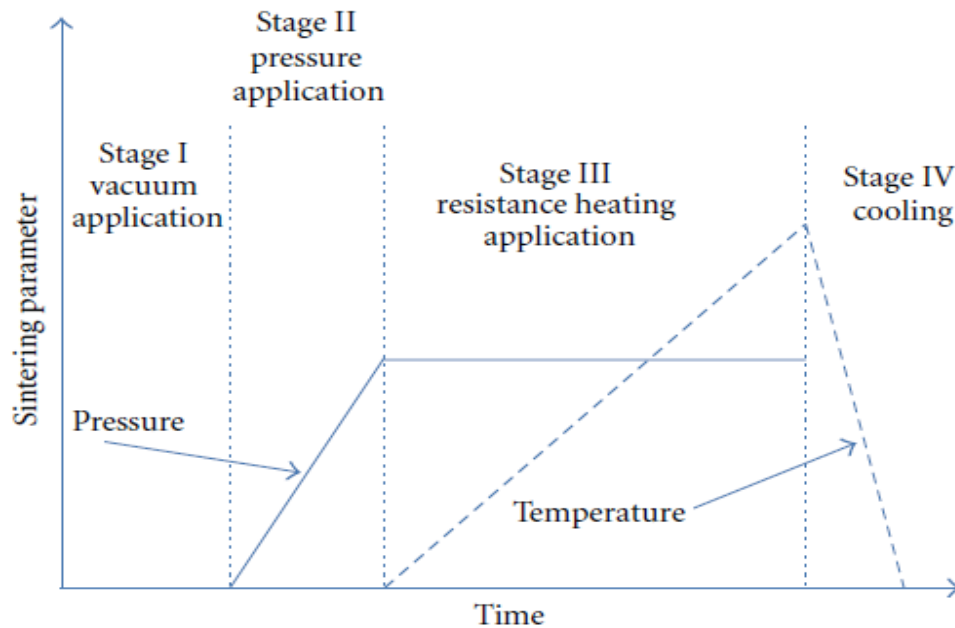


Figure 2.10 SPS sintering stages/steps [44]

Fig. 2.11 (a, b & c) illustrates the pulse current heating at point of contacts and the materials diffusion and formation of necking due to high localized temperature. The provision of current and pressure simultaneously along with the ample localized temperature due to pulse heating, led to the densification of the particles with lesser grain growth.

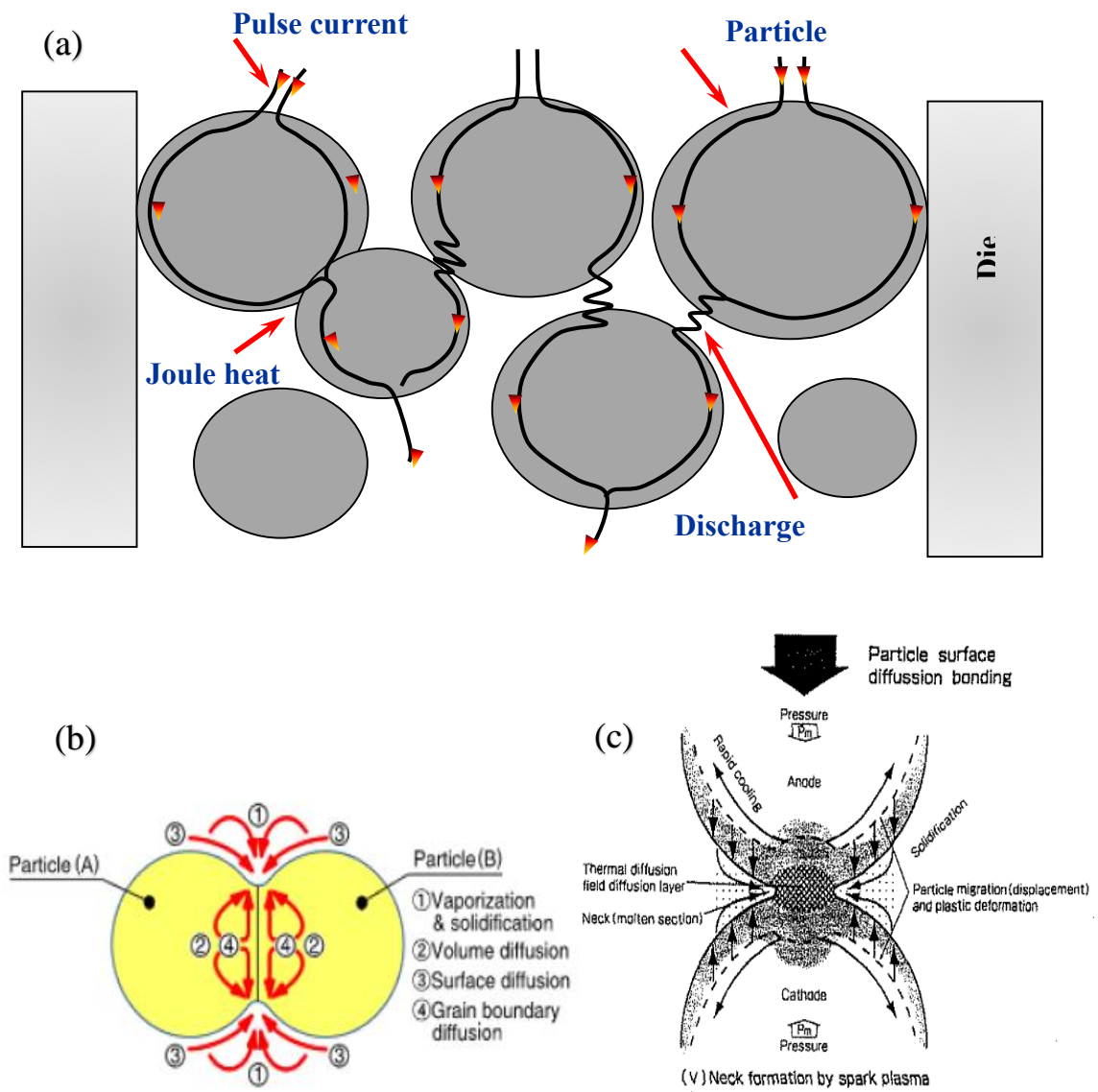


Figure 2.11 (a) DC pulse current flow through the particles (b, c) material transfer path during sintering [44, 74]

The overall schematic of spark plasma sintering technique is shown in the figure 2.12. The machine is equipped with uniaxial press, punches (electrodes), die holding stage, thermocouple, pyrometer, vacuum chamber, DC pulse generator and pressure measuring units [44].

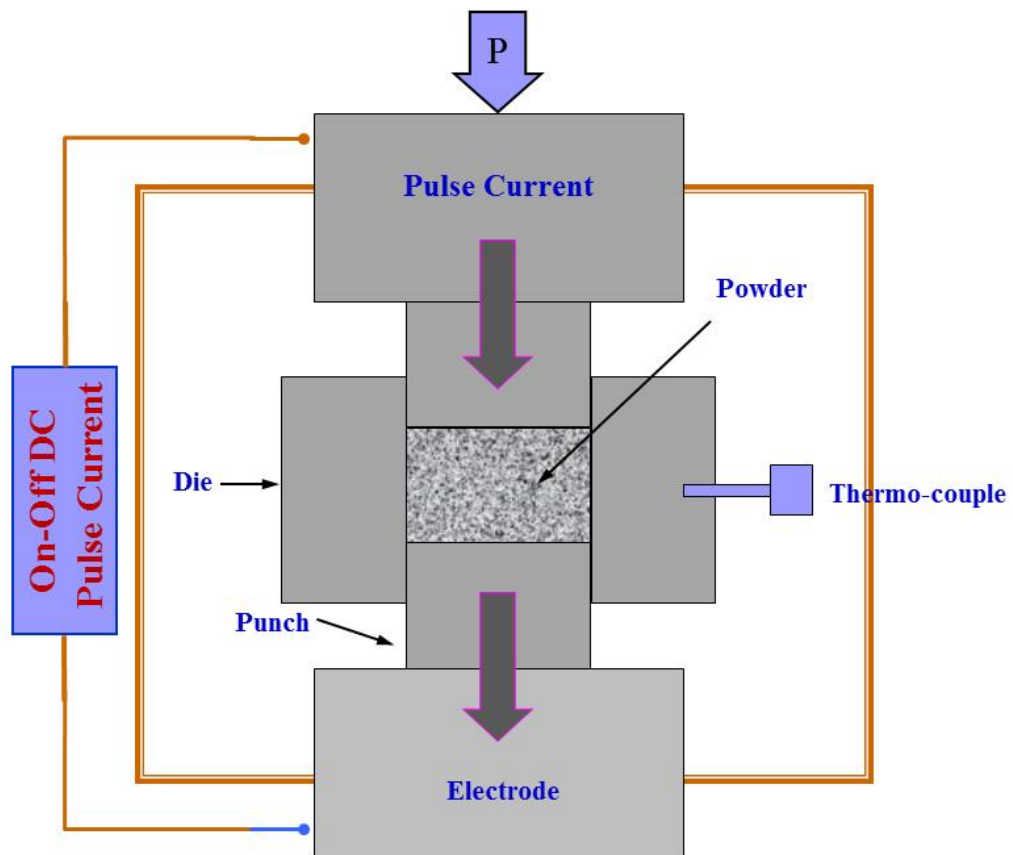


Figure 2.12 Spark plasma sintering set up

2.6.3 Sintering Parameters

2.6.3.1 Sintering Pressure

Spark plasma sintering is one of the pressure assisted sintering technique. To assist the densification of specimen the pressure is applied through the upper and lower punches. In some cases the densification of specimens is less sensitive to the applied pressure during sintering of Al2124 and Al6061 alloys by SPS [35]. With respect to the effect of pressure, it was concluded that, the relationship between applied pressure and specimen's properties is not well defined. In contrast, it has been reported by many researchers that pressure plays a great role in achieving dense sintered sample [37, 45, 50]. The densification is extremely fast when pressure is involved. It allows low sintering temperature which in turn minimizes grain growth.

2.6.3.2 Sintering Temperature

Sintering proceeds mainly by diffusion. As a result sintering temperature plays a vital role. However, excessive temperature causes grain growth. Therefore, there is a need to identify the maximum temperature that gives optimum densification and gives minimum grain growth as well. Usually sintering temperature is estimated between .7-.9 of melting point m_p of material [67].

In [45], the relationship between density and temperature was formulated as in equation 2.15;

$$\rho = s \left(\frac{T}{T_m} \right) + b \quad (2.15)$$

where, ρ is relative density, s temperature sensitivity, T and T_m are sintering and melting temperature respectively and b is the intercept on density axis. It shows that densification

increases with sintering temperature. However, the temperature sensitivity determines whether density will be affected by sintering temperature or not. If temperature sensitivity is high then material's density will be dependent on temperature.

2.6.3.3 Sintering Time

Sintering time is also a key factor to avoid the grain growth while achieving good densification. The required time to sinter a given material depends on the heating rate; high heating rate implies short sintering time. At constant sintering parameters (i.e. pressure, temperature and heating rate), increase in time increases densification to a limiting value after which there will be grain growth.

2.6.3.4 Heating Rate

The heating rate in spark plasma sintering is higher than the conventional sintering contributing to fast sintering time associated with SPS. There is a significant difference from the conventional sintering as heating rates can go as high as high as 1000 °C/min. Higher heating rates can be used to restrain powders grain growth. Smaller particle size enhanced the heating rate effect on consolidation of different powder materials.

2.6.4 Spark Plasma Sintered Al-Based Composites

As it is explained earlier; in the literature section, there are number of rigid particle reinforcements i.e. oxides, carbides & nitrides etc. to be used in aluminum based metal matrix composites. Al_2O_3 is found to have excellent properties, lesser coefficient of friction (COF), high hardness, strength, specific modulus, wear resistance, oxidation and corrosion resistance [41]. As a result of attractive physical and mechanical properties of Al- Al_2O_3 , it has found wide applications including aerospace, automobiles industry, electronic heat sinks, automotive drive shafts, ground vehicle brake rotors, jet fighter aircraft fins, explosion engine components etc. aluminum based metal matrix with alumina reinforcement was found to have potential applications in military, automotive and aerospace applications. It was observed that the alumina has better wettability and thermal stability in aluminum matrix. Al- Al_2O_3 nanocomposites has not been explored completely, therefore, there is a room of exploration and enhancement in the mechanical properties of aluminum [42].

Zhang et al. [48] synthesized the Al- 20 vol.% SiC composite powders through mechanical milling and then consolidated with SPS. Pure Aluminum milled with two different sizes of reinforcements ($12\mu\text{m}$ and $45\mu\text{m}$). The sintering took place at applied pressure 30MPa and maximum temperature 590°C for 10 min holding time with heating rate 50°C .

Saheb et al. [56] critically studied and fabricated the mechanically milled pristine Al with different volume percentages of Alumina 2%, 10% & 15% as reinforcement. The influence of reinforcement content, milling and sintering conditions, on the microstructure, densification, and hardness of the developed materials was investigated. It was found that

milling of pure aluminum for 24 h decreased its crystallite size less than 100 nm. For Al- Al_2O_3 nanocomposites, milling for 24 h decreased the crystallite size of the aluminum phase and resulted in uniform dispersion of the reinforcement. Sintering of the synthesized powders led to grain growth. Al_2O_3 contributed to grain growth inhibition when samples were sintered for 20 minutes. Milling improved hardness of aluminum but reduced its densification. Addition of Al_2O_3 nanoparticles resulted in further improvement of hardness. The Al-10 vol. % Al_2O_3 nanocomposite had the highest Vickers hardness value of 1460 MPa. The sintering was done at 550 °C with pressure applied 50 MPa with different sintering time 5, 10, 15 & 20 mins. The heating rate was kept 200 °C/min.

Yadav et al. [45] investigated the spark plasma sintering of aluminum Matrix composites. The composite was manufactured by mechanically milling pure aluminum with 2, 10, 15 & 20 wt% of SiC powders. The sintering parameters were; sintering temperature 600 °C, pressure 40 MPa with heating rate and cooling rate of 100°C /min. The influence of reinforcement on the density and hardness were observed. It was found that the density decrease as we increase the percentage of reinforcement. It is attributed with the phenomenon of grain boundary inhibition due to the rigid particles. It was also observed in the SEM micrographs, there were scratches and porosity voids during polishing. The hardness increases with increasing the reinforcement amount, it implies with the pinning of dislocations at the reinforcement cites.

2.7 Mechanical Properties

2.7.1 Hardness

It is the measurement of material resistance to localized plastic deformation i.e. indent or scratch. This test consist on pressing the surface of material with the help of indenter (of known geometry and mechanical properties). It is an essential property for metallurgists, tribologists and fracture mechanics engineers while designing of any component, selection of the material, and machining/manufacturing processes to obtain the desire properties in the end or final product. The shape of indenter may vary from type of test as following;

- Brinell test (spherical indenter)
- Rockwell test (conical indenter)
- Vicker's or Knoop test (pyramidal indenter)

The hardness tests are classified on the basis of numerous criterions; type of measurement (Brinell, Vickers, knoop), nature of the test (static or dynamic/scratch) and magnitude of load.

On the basis of magnitude of the load, hardness tests are classified as;

- Macrohardness (load > 1kgf)
- Microhardness (1gf < load < 1kgf)
- Nanoindentation (load may be as small as 0.1mN)

In 1925 R.Smith and G. Sandland introduced Vickers hardness test for the first time. This test was also termed by the shape of the indenter i.e. 136° diamond pyramid hardness test. Vickers-Armstrong limited, Kent, England; manufactured first hardness tester and become

familiar across the world. Therefore, this apparatus and test was recognized as the name Vickers [21, 67, 73]. The shape of indenter used for Vickers hardness testing is shown in the fig. 2.13.

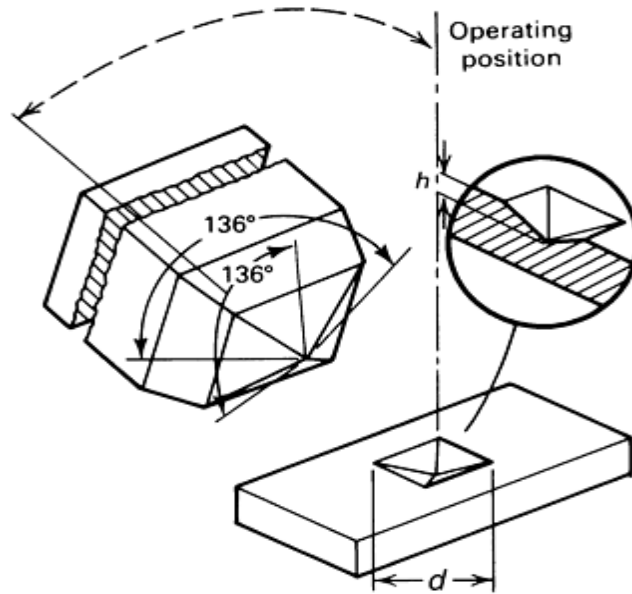


Figure 2.13 Diamond pyramid indenter used for the Vickers test [73]

2.7.2 Compressive Strength

Compression test is frequently used to determine the compressive properties of materials subjected to compressive loading. It also helps to determine the design and analysis of structures which are under compression. Compressive properties include modulus of elasticity, compressive strength, yield stress and the deformation beyond the yield point [73]. These properties are parallel with tensile test but in compression loading state. Selection of the specimen dimensions is very important to perform the testing. Length to diameter (L/D) ratio is the key factor in the selection of the specimens dimension in order to perform the test effectively. The testing specimens should be a right cylindrical shape [55].

2.8 Thermal Properties

Metal matrix composites of high thermal conductivity have numerous advantages for use in industrial electronic packaging and thermal management applications. The outstanding properties of MMCs i.e. thermal conductivity, tailorable coefficient of thermal expansion (CTE) and relatively low density make it suitable for industrial use. Tailorable CTE has an advantage of matching the CTE of semiconductor materials such as silicon, gallium arsenide, or alumina [51]. The requirement of thermal conducting materials is not only the high thermal conductivity but also the low coefficient of thermal expansion in order to maintain the integrity of the small circuits in the area of electronics (semi-conductors usually have lower CTE) [52]. High thermal conducting materials are also used as heat sinks and heat spreaders because of their ability to conduct the heat, and are, therefore, used in electronics [54].

Many reinforcements can be added to aluminum based composites like SiC, alumina and graphite. But literature suggests that the SiC and graphite react with aluminum and form aluminum carbide which is brittle in nature and produces interfacial mismatch which consequently weakens the material. Silicon also dissolves in aluminum and reduces its melting point which is also harmful to use the materials at higher temperatures. Alumina is stable oxide which does not react with aluminum but it has lower thermal conductivity and more prone to form agglomeration. The thermal conductivity of aluminum based metal matrix composite is greatly influenced by the reinforcement and its volume fraction present [52, 53].

According to Wiedemann-Franz law, thermal conduction is dominated by electrons in metallic materials [89];

$$K_e = \frac{\pi^2}{3} \left(\frac{k_b}{e} \right)^2 \sigma T \quad (2.15)$$

where K_e is the electrical conductivity, k_b is Boltzman constant, e is electron charge, T is absolute temperature and σ is electrical conductivity.

2.9 Coefficient of Thermal Expansion (CTE)

The importance of MMNCs due to lower coefficient of thermal expansion in the structural design, mechanical systems electronic and electronic packaging industry had been explained earlier. The dimensional changes in the aluminum based metal matrix upon exposure to heating can be observed by the help of dilatometer. Schematics of a dilatometer are given in fig. 2.14. In general the thermal expansion behavior of these composites is the result of numerous parameters; the phases present & their stability, the volume fraction of second phase particles, distribution of reinforcement in the matrix, type and amount of stresses induced during the processing and synthesizing[59].

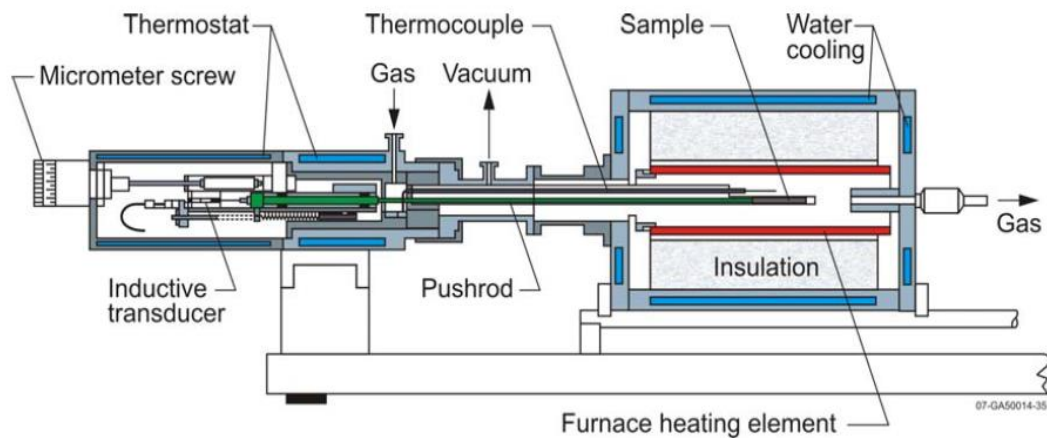


Figure 2.14 Schematics of Dilatometer [91]

In literature, it was found that there are few models which are used to calculate the CTE theoretically. Three of them are mentioned below. These models play a major role in comparison with the calculated values of COF for developed composite.

The models are given as following:

1) Rule of mixture

$$\alpha_M = V_1\alpha_1 + V_2\alpha_2 \quad (2.16)$$

2) Turner model

$$\alpha_M = \frac{V_1\beta_1 + V_2\beta_2}{V_1B_1 + V_2B_2} \quad (2.17)$$

3) Kerner model

$$\alpha_M = \alpha_1 + V_2(\alpha_1 - \alpha_2) * \frac{\beta_1(3B_2 + 4G_1)^2 + (B_2 - B_1)(16G_1^2 + 12G_1B_2)}{(4G_1 + 3B_2)[4V_2G_1(B_1 - B_2) + 3B_1B_2 + 4G_1B_1]} \quad (2.18)$$

In above three models, α stands for CTE, V is the volume fraction, B & G are bulk and shear moduli, and the subscripts M, 1, and 2 belongs to the composite, matrix and reinforcement phases, respectively [88].

2.10 Motivation & Objectives

The development of nanoparticle reinforced metal matrix nanocomposites for commercial applications is still facing numerous challenges, which include inhomogeneous microstructures, due to nanoparticles agglomeration, the grain growth if sintering is required, and the limitations on the amount of the produced material. Adequate work has been done on Al-Al₂O₃ nanocomposites, however, work dedicated to processing of these nanocomposites using mechanical milling and spark plasma sintering is very scarce in the literature. The objective of this research work is to explore the possibility to synthesize nanocrystalline aluminum and homogenous Al-Al₂O₃ nanocomposite powders using mechanical milling and consolidation through spark plasma sintering technique. The second objective is to investigate the influence of processing on the microstructure, densification, mechanical and thermal properties of the developed materials.

CHAPTER 3

MATERIALS AND EXPERIMENTAL PROCEDURES

This chapter presents properties of materials used in experimental program as well as the experimental procedures followed during synthesis and characterization of nanocomposites.

3.1 Raw Materials

Pristine aluminum and α -Al₂O₃ powder used in as received conditions. Pure aluminum powder (99.88% purity with an average particle size of 33 μ m) purchased from Aluminum Powder Company (Alpoco Ltd). The composition of as received powder is given in table 3.1. Size distribution of pure aluminum is also enlisted in table 3.2.

Table 3.1 Chemical composition of pure aluminum powder

Elements	Al	Fe	Si	Ti	Ga	Ni	Cu, Mn, Pb, Zr, Zn, Cr
wt. %	99.88	0.074	0.024	0.006	0.006	0.005	0.001 each

Table 3.2 Size distribution in Al powder

Size (μ m)	%
63	0
53	1
45	11
38	11.4
< 38	76.6

α -Al₂O₃ (99.85% pure with an average particle size of 150 nm) with spherical morphology, supplied by ChemPUR Germany. Pristine aluminum milled for 24h and different volume fraction of alumina in aluminum were selected as following for further experimentation;

- Pure aluminum milled for 24h
- 2%-Al₂O₃ by volume in aluminum matrix milled for 24h (2.92 % by weight)
- 5%-Al₂O₃ by volume in aluminum matrix milled for 24h (7.20 % by weight)
- 10%-Al₂O₃ by volume in aluminum matrix milled for 24h (14.07 % by weight)
- 15%-Al₂O₃ by volume in aluminum matrix milled for 24h (20.64 % by weight)

3.2 Experimental Procedures

3.2.1 Mechanical Milling

Aluminum and alumina were weighed by using electronic weighing balance to prepare the nominal composition of 2, 5, 10 & 15 vol. % of metal ceramic composites. Additionally, pure aluminum was also milled as a reference material. Mechanical milling technique was used to homogenize the powder mixtures. A planetary ball mill (Fritsch Pulverisette, P5, Idar-Oberstein, Germany) was used to conduct the mechanical milling experiments. The mentioned powders were milled for 24 h in the argon environment to avoid the oxidation of deformed powders while milling. Weight ratio of ball to powder kept 10:1 at 200 rpm. Hardened stainless steel balls (10mm diameter) were used in 250 ml by volume stainless steel containers (vials). Materials transfer is difficult in stainless steels balls and powders. Stearic acid (1.5 wt. % of the total charge) was used as process controlling agent to minimize the sticking of material inside the vials and balls surface. PCA also controls the excess of cold welding during milling. Each powder was milled for 24 hrs. The milling

conditions were kept constant for all the milled materials. The milling process was interrupted after 0.5, 1, 2, 3, 4, 5, 6, 8, 10, 15, 20 & 24h of milling in order to monitor the morphological and structural changes during the milling. 1 g of powder was obtained after each designated cycle along with the SS balls to keep ball to powder ratio 10:1. Stainless steel spatula was used to remove the sticky materials from the walls of vials as Al is highly ductile. The process of milling was not continuous for 24 h. After each hour of milling, a stay period of 1 or 1.5 h was provided to dissipate the generated heat while collision between balls, powders & walls of vials. Because heat might help the powders to get oxidize. The summary of ball milling process parameters are listed in the table 3.3.

Table 3.3 Summary of ball milling process parameters

Sr. #	Materials & milling parameters	Amount/ Quantity	Units
1	Purity of aluminum	99.88	%
2	Purity of Alumina	99.95	%
3	Particle size of Al	33	μm
4	Particle size of alumina	150	nm
5	Ball Size	10	mm
6	Weight of one ball	3.98	g
7	Ball to powder ratio	10:1	ratio
8	Total charge	20	g
9	Stearic Acid	1.5	%
10	Density of Al	2.7	g/cm^3
11	Density of Al_2O_3	3.98	g/cm^3
12	Inert Environment	Argon	-

3.2.2 Scanning Electron Microscopy (SEM)

Morphology and microstructure of as received and milled powder were determined by the help of field emission scanning electron microscope (FE-SEM) equipped with energy dispersive spectroscopy (EDS). JEOL (model JSM 6460) and Tescan Lyra-3 was used for the characterization. Small amount of powder was placed on aluminum holders having copper double side tape and gold coated for 15 seconds in order to avoid accumulation of electrons on the powder which causes charging. The morphology of milled powders was determined using secondary electron detector. Back scattering electron detector was used to visualize the compositional contrast between Al, Al₂O₃ excessive regions. Elemental composition was confirmed using energy dispersive spectroscopy (EDS) analysis. X-ray elemental mapping was performed to examine the distribution of the reinforcement in the matrix. 20 frames for each composition were recorded altogether. The microscopy of sintered and sintered-fractured samples was also done.

3.2.3 X-Ray Diffraction (XRD)

The structural characterization of the powders milled and unmilled was obtained using Bruker D8 X-ray diffractometer, USA, using Cu K-Alpha radiation with a wavelength $\lambda = 0.15405$ nm with 30 kV and step increment in diffraction angel was 0.02/sec. The XRD patterns were recorded in diffraction angel range of 30-80 degrees with step increment of 0.02/sec. The XRD peaks obtained from the pattern were analyzed using standard XRD procedure [51]. The effect of milling on crystallite size and lattice strains was also investigated using following equation 2.19:

$$B_r \cos\theta = \frac{k\lambda}{L} + \eta \sin\theta \quad (2.19)$$

Where B_r is the full width at half-maximum (FWHM) of the diffraction peak after instrument correction, k is constant (with a value of 0.9); λ is wavelength of the x-ray radiation ($\lambda = 0.15405$ nm); L and η are crystallite size and lattice strain, respectively; and θ is the Bragg angle.

$$B_r^2 = B_{obs}^2 - B_i^2 \quad (2.20)$$

The B_r is related to the measured width of the peak (B_{obs}) and peak broadening caused by factors except the particle size effect (B_i), frequently called instrumental broadening factor and calculated using a fully annealed sample, through the formula given in equation 2.20”.

3.2.4 Spark Plasma Sintering (SPS)

Spark plasma sintering machine (FCT system, Germany) model-HP D 5 was used to consolidate the mechanically alloyed powders. Disc shaped specimens were prepared using a graphite die of 20 mm diameter. A compaction pressure of 50 MPa and heating rate of 200°C /min were used in all sintering experiments. Aluminum un-milled and milled for 24 h, and Al-Al₂O₃ nano-composite powders containing 2, 5, 10, and 15 vol. % Al₂O₃ milled for 24 h were sintered. The samples were sintered at a temperature of 550°C for holding times of 5, 10, 15 and 20 minutes. The process parameters are enlisted in the table 3.4.

Table 3.4 Spark plasma sintering process parameters

Sr. #	Parameters	Quantity/Values
1	Graphite die	20mm
2	Amount of powder	5g
3	Sintering Temperature	550 °C
4	Applied Pressure	50 MPa
5	Heating Rate	200 °C/min
6	Sintering Time	5 &20min

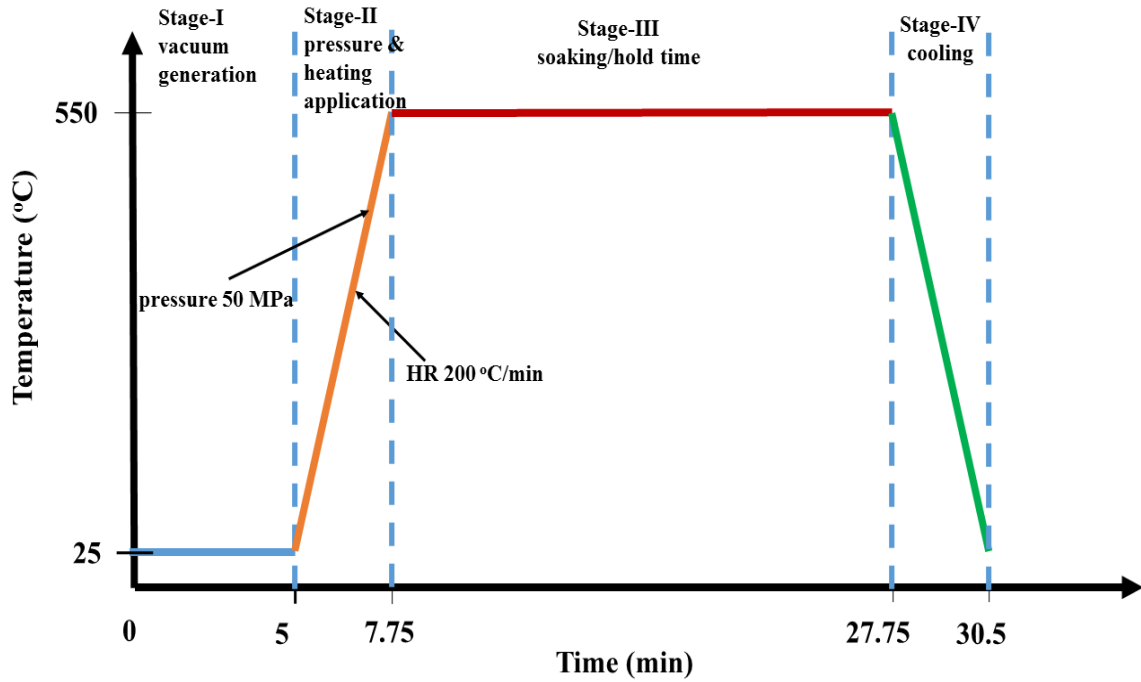


Figure 3.1 Sintering stages and parameters

The pure aluminum un milled and milled for 24 h also sintered using the SPS technique for the comparison with the developed composites. While using the die of 20mm, 5 g of each composition was put in graphite die after placing graphite foil lining inside. The purpose of this lining is to reduce the friction between the graphite die walls and the powder, also to avoid sticking of sample powder inside the die after the sintering. To avoid the powder sticking on punches, round graphite foils of the same size of punches are placed at the top and bottom ends of the dies, this also blocks the movement of powder outside the die while applying high pressure and temperature. At the start of the experiment 3kN force was applied initially at the rate of 5mm/min. Pulse pattern utilized during the experimentation was 4:1. Ultra-high vacuum of 0.4 hPa was generated for the experiment run. Kanthal K-type thermocouple was inserted in the die hole for the purpose of monitoring the exact temperature of die. Using all the above conditions totally 24 samples

were prepared for further characterization i.e. microstructural, mechanical & physical properties. In fig. 3.1 the scheme of the overall process is shown using the given conditions in tables 3.5 & 3.6.

Pure Al unmilled, pure Al milled for 24 h and Al-Al₂O₃ 10 vol. % composite milled for 24h were selected to undergo thermal analysis and compression test. In order to determine thermal conductivity, six samples were prepared using 25 mm diameter graphite die by keeping the conditions constant. The die punches were shortened by 3mm in order to prepare the bigger thickness samples. 16 g powder was put into the graphite die and samples obtained had the height of 12-13 mm. which is suitable to determine the thermal conductivity of the metallic materials; since metals have very high thermal conductivity, therefore, bigger thickness samples were developed.

Table 3.5 Experimental parameters, to investigate the microstructure and densification of sintered monolithic Al and nanocomposites.

Sample	P (MPa)	Temp. (°C)	Time (min)	H.R (°C/min)
Al				
Al-1	50	550	5	200
Al-2	50	550	10	200
Al-3	50	550	15	200
Al-4	50	550	20	200
Al-24h milled				
Al-24h-1	50	550	5	200
Al-24h-2	50	550	10	200
Al-24h-3	50	550	15	200
Al-24h-4	50	550	20	200
Al- 2 vol. % Al₂O₃				
Al- 2 vol. % Al ₂ O ₃ -1	50	550	5	200
Al- 2 vol. % Al ₂ O ₃ -2	50	550	10	200
Al- 2 vol. % Al ₂ O ₃ -3	50	550	15	200
Al- 2 vol. % Al ₂ O ₃ -4	50	550	20	200
Al- 5 vol. % Al₂O₃				
Al- 5 vol. % Al ₂ O ₃ -1	50	550	5	200
Al- 5 vol. % Al ₂ O ₃ -2	50	550	10	200
Al- 5 vol. % Al ₂ O ₃ -3	50	550	15	200
Al- 5 vol. % Al ₂ O ₃ -4	50	550	20	200
Al- 10 vol. % Al₂O₃				
Al- 10 vol. % Al ₂ O ₃ -1	50	550	5	200
Al- 10 vol. % Al ₂ O ₃ -2	50	550	10	200
Al- 10 vol. % Al ₂ O ₃ -3	50	550	15	200
Al- 10 vol. % Al ₂ O ₃ -4	50	550	20	200
Al- 15 vol. % Al₂O₃				
Al- 15 vol. % Al ₂ O ₃ -1	50	550	5	200
Al- 15 vol. % Al ₂ O ₃ -2	50	550	10	200
Al- 15 vol. % Al ₂ O ₃ -3	50	550	15	200
Al- 15 vol. % Al ₂ O ₃ -4	50	550	20	200

Table 3.6 Experimental parameters, to investigate the mechanical properties of sintered monolithic Al and nanocomposites.

Sample	P. (MPa)	Temp. (°C)	Time (min)	H.R (°C/min)
Al				
Al-1	50	550	20	200
Al-24h milled				
Al-24h-1	50	550	20	200
Al- 10 vol. % Al₂O₃				
Al- 10 vol. % Al ₂ O ₃ -1	50	550	20	200

Table 3.7 Experimental parameters, to investigate the thermal properties of sintered monolithic Al and nanocomposites.

Sample	P. (MPa)	Temp. (°C)	Time (min)	H.R (°C/min)
Al				
Al-1	50	550	40	200
Al-24h milled				
Al-24h-1	50	550	40	200
Al- 10 vol. % Al₂O₃				
Al- 10 vol. % Al ₂ O ₃ -1	50	550	40	200

3.2.5 Optical Microscopy (OM)

The microstructural investigation of sintered specimens was performed using optical microscope Meji MX7100. Disc shaped developed samples were cut along cross section using precision cutting machine. During the cutting fresh sweat water was used as coolant in order to avoid heating of the sample. Mounting of the cut samples was performed using hot mounting press by keeping the applied pressure 5 bar at 180 °C with transparent polymeric material (Lucite). The mounted samples further proceeded with grinding using different grades of emery papers. Fine polishing was done by using diamond paste and alumina suspension on nylon and canvas cloth respectively. The polished sample were etched by the help of Keller's reagent in order to reveal the microstructure [50] soaking each sample in solution for 10 to 20 seconds. Then microstructural images of the samples were recorded at different magnifications.

3.2.6 Density

Density measurement was performed on polished Al and other synthesized composite samples using Archimedes principle. METTLER TOLEDO (Model AG285) electronic balance with and accuracy of ± 0.0001 g was used to weigh the polished samples. Deionized water was used as an immersion fluids. The density determination using mentioned principle involves the weighing the samples in air and di-ionized water. The equation 2.21, relation used to calculate the density is also mentioned below

$$\rho_o = \frac{A}{A-B} * (\rho_l - \rho_a) + \rho_a \quad (2.21)$$

where ρ_o is density to be calculated, A and B are weights of sample in air and liquid respectively, ρ_l and ρ_a are densities of liquid and air respectively.

The density of pure Al and Alumina are 2.7 g/cm³ and 3.98 g/cm³ respectively. Hence, the density of composites can be estimated theoretically using equation

$$\rho_c = \rho_m V_m + \rho_r V_r \quad (2.22)$$

where ρ_m and ρ_r are the densities of matrix and reinforcement respectively, V_m and V_r are the volume fractions of matrix and reinforcement, respectively. With this, the theoretical densities of the composites are obtained and given in table 3.8. After obtaining the densities of the samples, relative density was calculated using above equation.

$$\text{Densification} = \frac{\text{Calculated density } \rho_c}{\text{Theoretical Density}} * 100 \quad (2.23)$$

Table 3.8 Theoretical density of nanocomposites.

Composite	Theoretical Density (g/cm ³)
Al-2-Vol% Alumina	2.73
Al-5-Vol% Alumina	2.76
Al-10-Vol% Alumina	2.83
Al-15-Vol% Alumina	2.89

3.2.7 Hardness

Vickers's MMT-3 Digital Micro Hardness Tester, Buehler, USA was used to obtain micro hardness of the sintered specimens. Hardness profiles was determined by recording twelve readings in a row, using 100 gf load applied for time of 10s. The micro hardness was the average of the recorded values from each sample. Vicker's hardness (HV) is calculated using the following formulae;

$$HV = \frac{0.18911 F}{d^2} \quad (2.23)$$

where, 'F' is the applied load, while 'd' represents the length of the diagonals of indent or pyramid shape impression. It is important to note that the distance between two indents should be 2.5 times of the diameter of the indent.

3.2.8 Compression Strength

Instron 3367, USA universal testing machine was used for the compression strength determination. According to ASTM E89-A the specimen dimensions and testing parameters were selected; the disc shaped sintered samples were machined through edm wire cutter in the size; diameter 6mm (± 0.02 mm) with length 12mm (± 0.02 mm). The machined specimens were cut in the mentioned dimensions in order to keep the aspect ratio (L/D) 2 which is the key parameter as per given in the standards. The samples undergone testing at a strain rate of .127mm/min [55]. Cylindrical samples were cut down using electrical discharge wire cutting/machining (EDM). Four cylindrical samples of dimensions length x diameter (12mm x 6mm) obtained from the sintered disc. Pure aluminum (both milled for 24h, unmilled) and Al-10 vol%. Al₂O₃ composite 24h milled

were investigated experimentally and compared with theoretical values to estimate the behavior of material under compression. Pure Al and Al-Al₂O₃ 10% by vol. mechanically milled for 24h proceeded with consolidation through spark plasma sintering. The conditions for spark plasma sintering was; pressure 50MPa, sintering temperature 550 °C, heating rate 200 °C/min with sintering time 20 minutes. 20 mm die was utilized for first batch of samples and total 3 samples each from one composition were prepared using the same conditions. In order to get adequate height of samples after sintering, the die punches were ground to increase the internal volume of the die. 18 g of powder for each of three composition was placed in the die and approximately 12-14 mm height disc shaped samples obtained after sintering. Compressive strength was determined by using ASTM E89-A standard test. The testing parameters and dimensions of the samples were selected according to the standard test. The test was performed on the testing conditions given in the ASTM standard. Axial compressive loading was provided to each sample until the fracture occurs.

3.2.9 Thermal Characterization

Thermal conductivity of sintered monolithic aluminum milled, un-milled and Al-10 vol. % alumina composite was determined using thermal constraint analyzer Model TPS 2500s by hot disc company. Kapton sensor was used to measure the thermal conductivity at 19 °C. Thermal conductivity (λ) was calculated by using the relation; $\lambda = k \times \rho \times C_p$. Where ρ and C_p are the density and specific heat of the material respectively [77].

3.2.10 Coefficient of Thermal Expansion

Dilatometer (model L75 Horizontal) was used to measure the coefficient of thermal expansion of all the sintered samples. The heating and cooling rate kept 5 °C /min with the dimensional changes were recorded between 25-450 °C of temperature range. The experimental conditions are given in table 3.9.

Table 3.9 Experimental conditions, to measure the coefficient of thermal expansion (CTE) using dilatometer

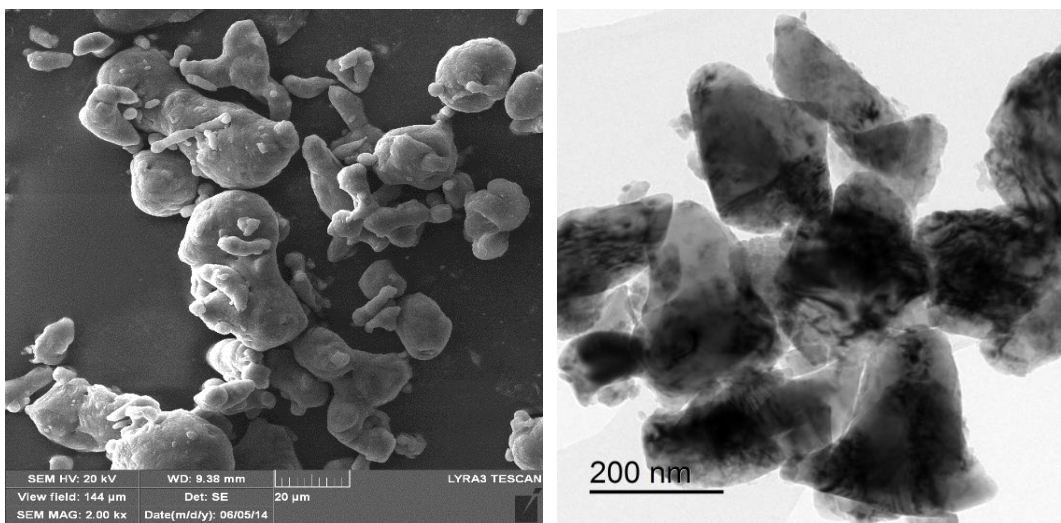
Parameters	Specifications
Sample initial length	12mm
Sample Holder (Crucible)	Alumina
Sample Nature	Metallic
Sample Geometry	Cylindrical
Temperature Range	25-450 °C
Heating Rate	5 °C /min

CHAPTER 4

RESULTS & DISCUSSION

4.1 Powder Synthesis

FE-SEM micrograph of aluminum powder is shown in figure 4.1 (a). Its particles are not uniform and have different sizes and shapes. They show a varying size distribution which is also in agreement with the data provided by the vendors. From the fig. 4.1 it can be clearly observed that most of the particles are approximately 20~50 μm in size. A TEM micrograph of as-received Al_2O_3 nano powder is presented in fig. 4.1 (b). The Al_2O_3 nano powder have particles with different morphologies and average particle size of 150 nm. It can be noticed that Al_2O_3 nanoparticles are agglomerated because of their small particle size and high surface energy.



(a)

(b)

Figure 4.1. (a) FE-SEM micrograph of Al powder and (b) TEM micrograph of Al_2O_3 nano powder.

Al-Al₂O₃ powders were milled for different milling times to achieve uniform dispersion of reinforcement in the matrix. Fig. 4.2 shows typical FE-SEM micrographs of Al-10 vol. % Al₂O₃ powder milled for (a) 3 h; (b) 6 h; (c) 20 h; and (d) 24 h. The morphology and size of aluminum particles changed with milling time. Initially, milling led to flattening of particles, which results in increase in the particle size. However, at longer milling time of 24 h, figure 4.2 (d), milling led to decrease in particle size which is attributed with the phenomenon of fracturing during milling, as cold welding and fracturing takes place simultaneously in the process of milling. The particle becomes flattened at early stages of milling till 15 h and it can be observed in the figures while this phenomenon is also noticed in the literature [9, 29]. This flattening takes place due to the cold welding of the grains during the process of milling.

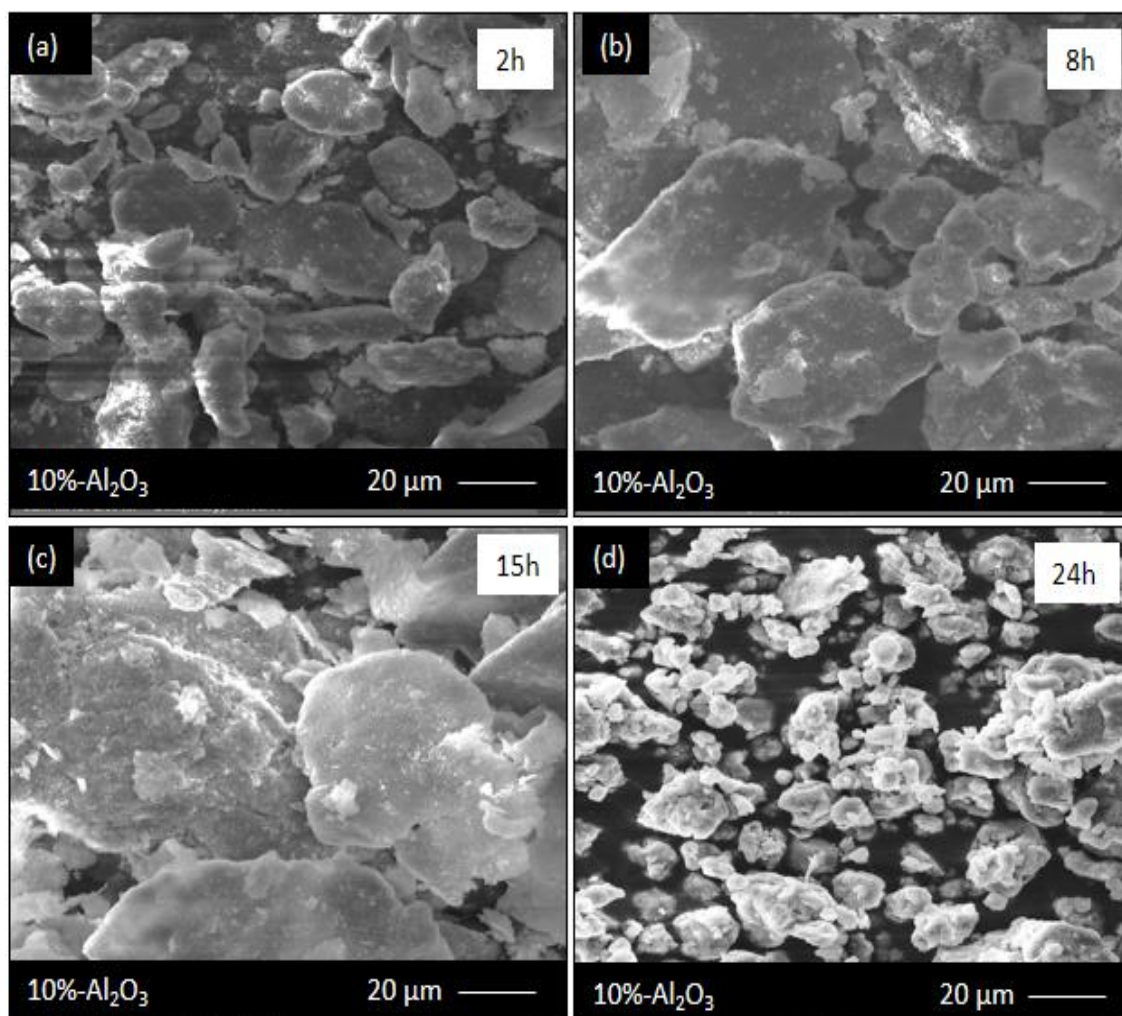


Figure 4.2. FE-SEM micrographs of Al-10 vol.% Al₂O₃ composite powder mechanically alloyed for (a) 3 h; (b) 6 h; (c) 20 h; (d) 24 h.

Figure 4.3 (a) and (b) show FE-SEM micrographs of powders containing 2 and 15 vol. % of Al_2O_3 , respectively, milled for 24 h. The nanocomposite powders reinforced with 2 and 15 vol.% of Al_2O_3 nanoparticles showed similar behavior compared to the Al-10 vol.% Al_2O_3 composite. Analysis of the size and morphology of aluminum particles in powders containing 2, 10, and 15 vol.% Al_2O_3 and milled for 24 hours shows that higher the Al_2O_3 content, smaller will be the particle size; and more equisized particles were formed. Therefore, it can be concluded that, under the same milling conditions, the increase in Al_2O_3 content enhanced the milling effect. The same effect was observed in Al-SiC nanocomposites where SiC was reported to enhance the milling effect in mechanically alloyed Al-SiC nano-composites prepared under milling speed of 200 rpm, milling time up to 20 h, and BPR of 10:1. This is due to the fact the increase in reinforcement volume fraction leads to the increase in milling rate and reduces the time to reach a balance between fracturing and re-welding of the milled particles [12].

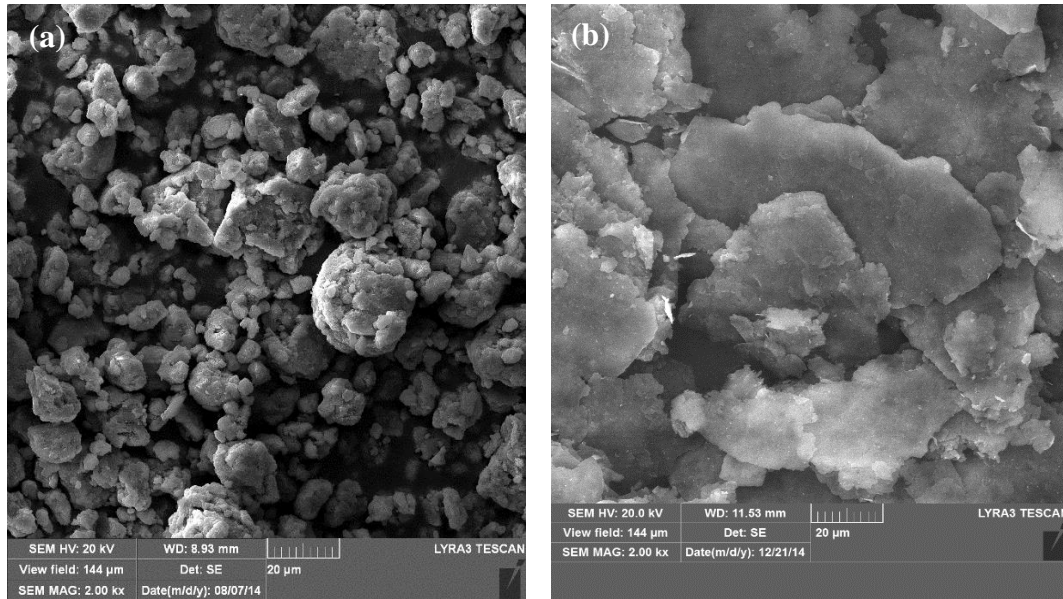


Figure 4.3 FESEM micrographs of powders containing (a) 2 vol.% of Al_2O_3 (b) 15 vol.% of Al_2O_3 milled for 24h.

Elemental mapping of aluminum and oxygen in Al-10 vol. % Al_2O_3 nanocomposite was performed for mechanically milled 2h, 8h, 15h, and 24h. X-Ray mapping is used to observe the uniform distribution of the reinforcement in the matrix. Oxygen map shows the uniform distribution of alumina in the matrix of aluminum. In SEM micrograph, the grains were found to be flattened and agglomerated due to initial stage of ball milling [49]. This results in poor distribution of alumina in the aluminum matrix. For each volume fraction, smaller milling time showed alumina agglomeration. But as we proceeded to higher milling times, the distribution became finer and uniform. The number of dots in each map represent the quantity of relevant element in the selected area, for higher milling time the number of dots are increased and can be clearly observed.

Fig. 4.4 presents the effect of mechanical milling time on the uniform distribution of reinforcement in the matrix for Al-10 vol. % Al_2O_3 nanocomposite. It is clear that as we proceed to higher milling time the distribution of O becomes uniform in the matrix. This trend is in complete agreement with [31, 43], in which uniform distribution of alumina was achieved after 20h of milling. Figures 4.5, 4.6 & 4.7 are the x-ray maps of 2, 5 & 15 % by vol. Al- Al_2O_3 composite milled for 24 h.

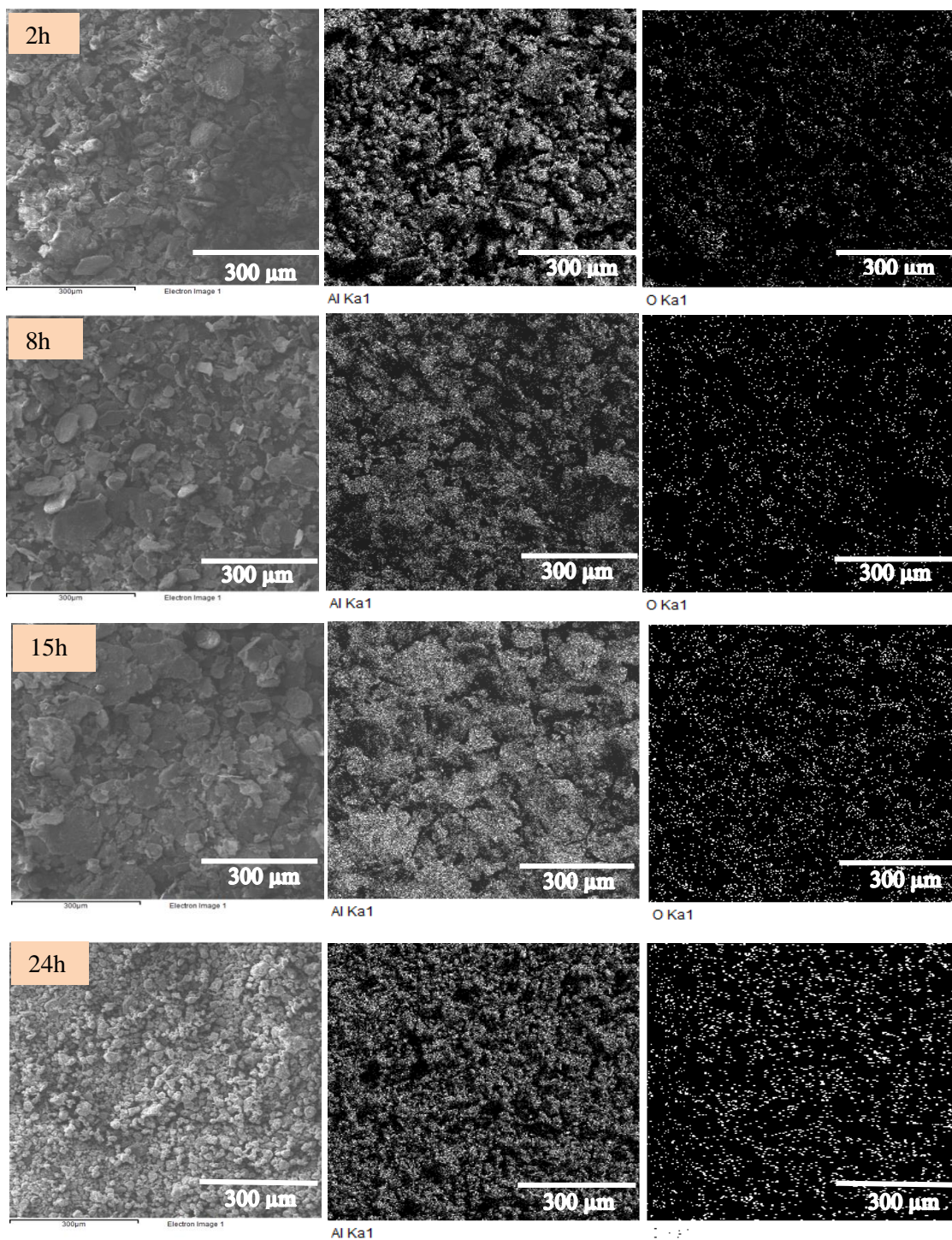


Figure 4.4 X-Ray mapping of Al- 10 vol. % Al_2O_3 milled for 24h.

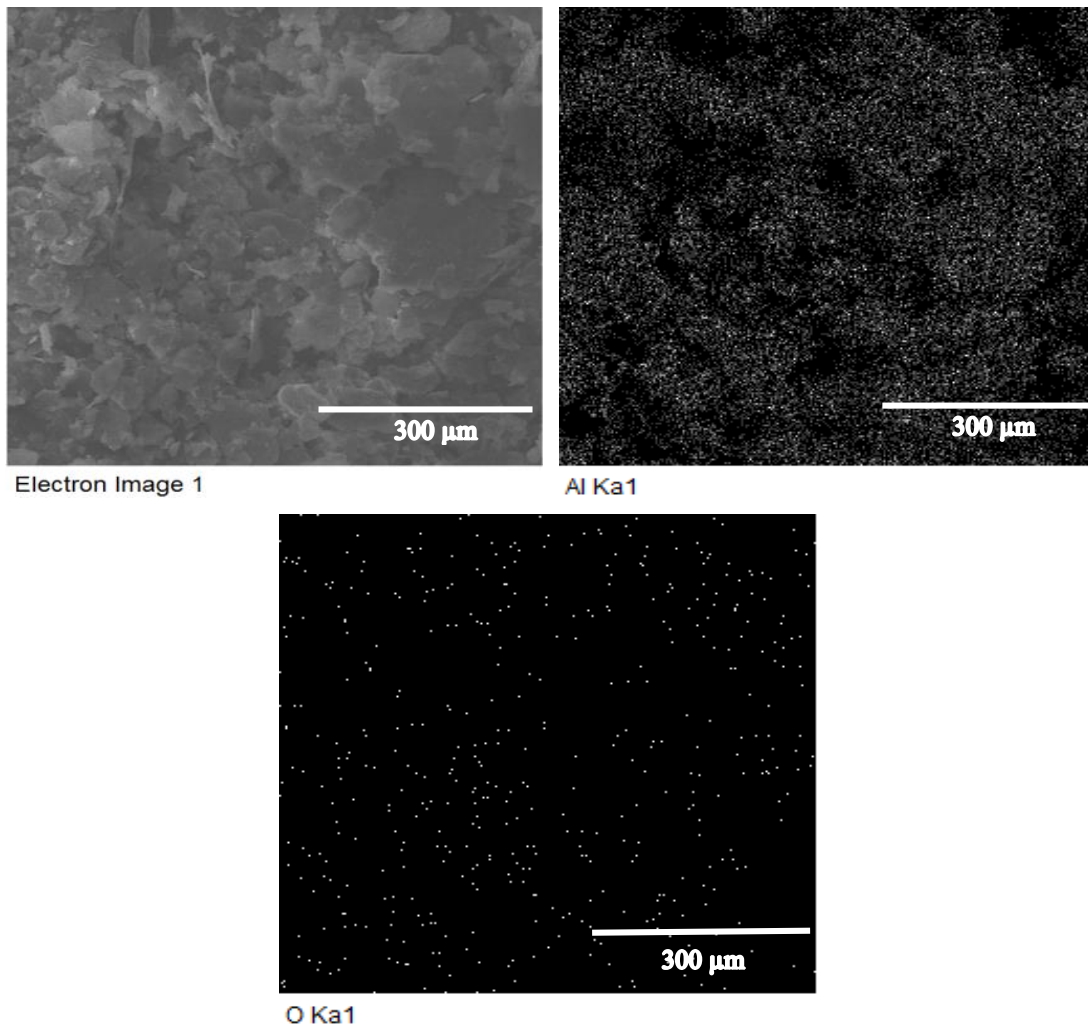


Figure 4.5 X-Ray Mapping of Al-2% vol. Al_2O_3 milled for 24h.

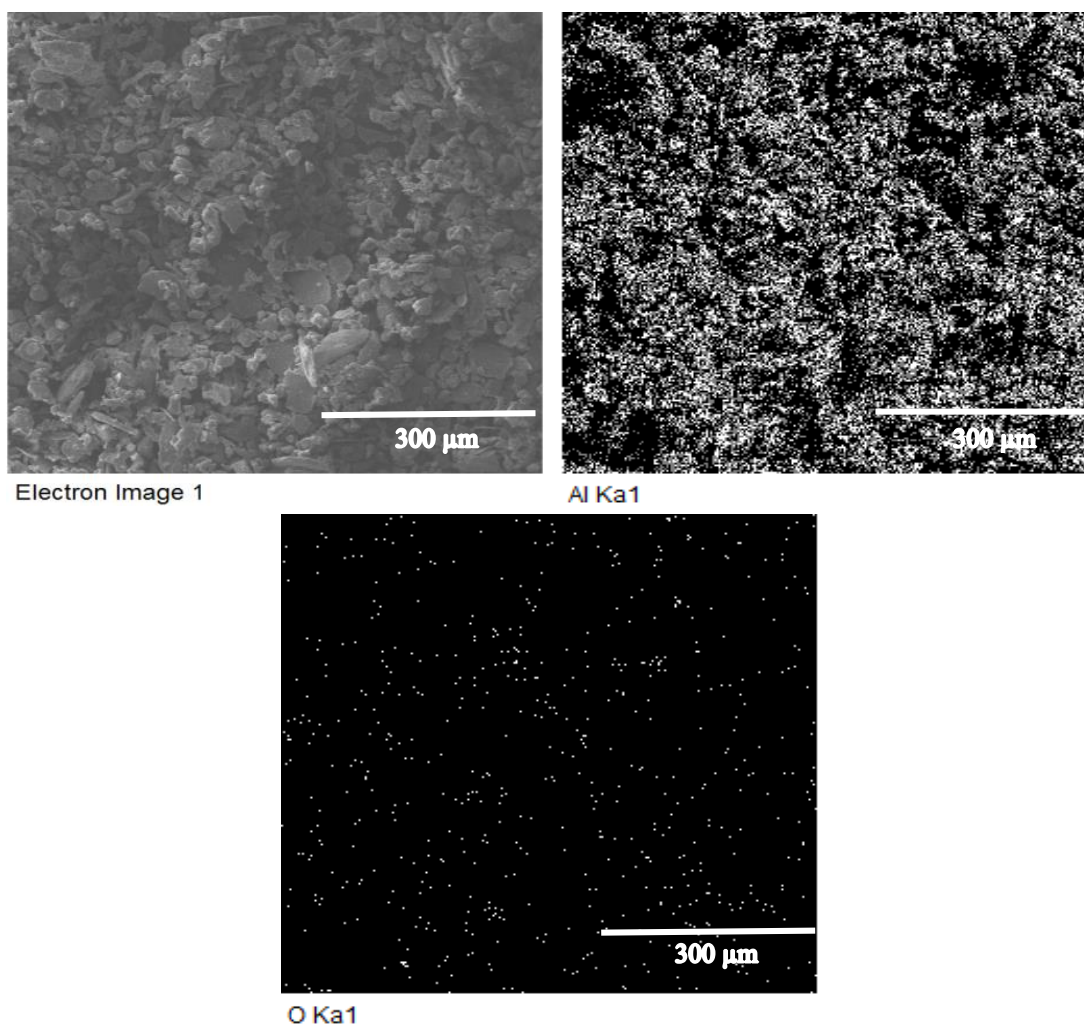


Figure 4.6 X-Ray Distribution of Al-5% vol. Al_2O_3 milled for 24h.

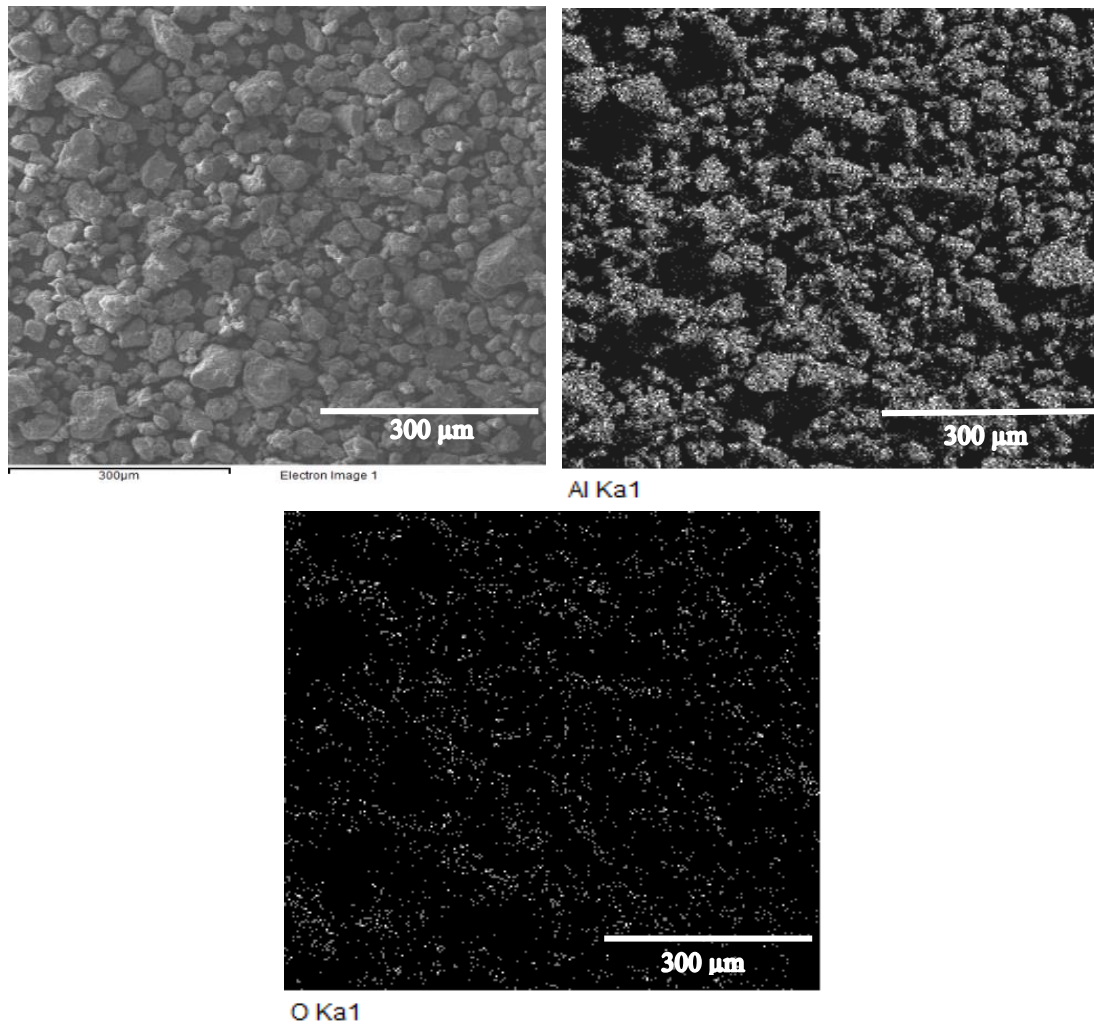


Figure 4.7 X-ray mapping of Al-15% vol. Al₂O₃ milled for 24h.

4.2 X-Ray Diffraction

4.2.1 Pure Aluminum

Phase analysis and crystal structure determination of milled powders was carried out using XRD technique. Fig. 4.8 shows the XRD pattern for pure aluminum in as received condition (a) without milling and (b) with 24 h of milling. The XRD pattern is indexed according to the FCC structure having the lattice parameter $a = .404 \text{ nm}$.

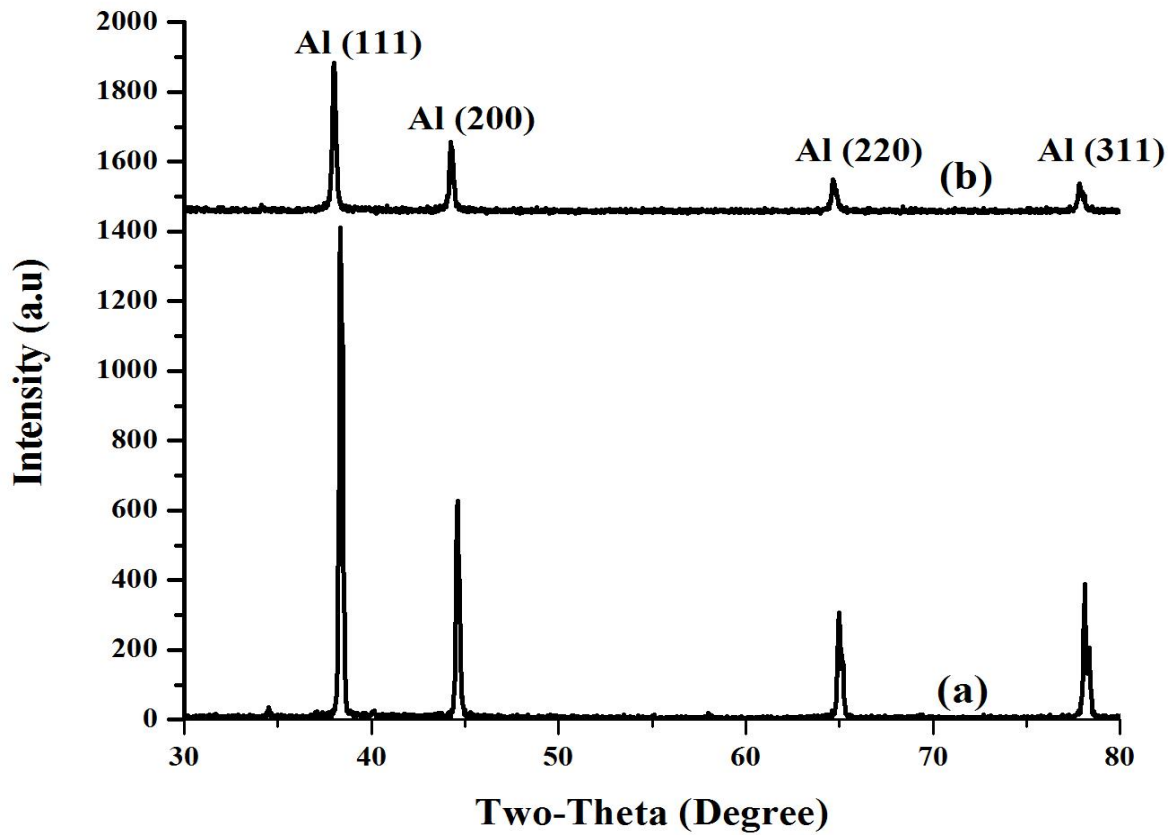


Figure 4.8 XRD-Spectrum of pure aluminum (a) Unmilled (b) Milled for 24h

In the XRD pattern, the intensity difference and peak broadening can be observed clearly. For aluminum in unmilled form, the intensity is almost 4 times larger than the aluminum milled for 24 h. The decrease in intensity is related with the peak broadening and also associated with the reduction in crystallite size and induction of strains after severe plastic deformation after the 24 h of milling [31].

The decrease in crystallite size usually takes place in three stages, “The first stage is characterized by the formation of shear bands with high density of dislocations. In the second stage, annihilation and recombination of these dislocations give rise to small angle grain boundaries separating the individual grains. In the last stage of milling, the orientation of the single crystalline grains become random with respect to their adjacent grains” [65].

4.2.2 XRD of 24h Milled Nanocomposites

Fig. 4.9 shows the XRD spectrum for mixture of milled powder in different vol. fractions. The XRD peaks for α -aluminum can be clearly observed in the spectrum but the peaks of alumina are not visible for 2% volume fraction Al-Al₂O₃ composite which is milled for 24hrs. This is attributed with the fact that there present a very low concentration of alumina in the matrix which is insufficient to be detected by the help of XRD. While in 10 and 15 vol. % of alumina nanocomposites, the amount of alumina is quite sufficient to be detected using XRD technique. The peaks of alumina are detected for 10 and 15 vol. % of alumina nanocomposites, although the intensity of detected peaks is very low.

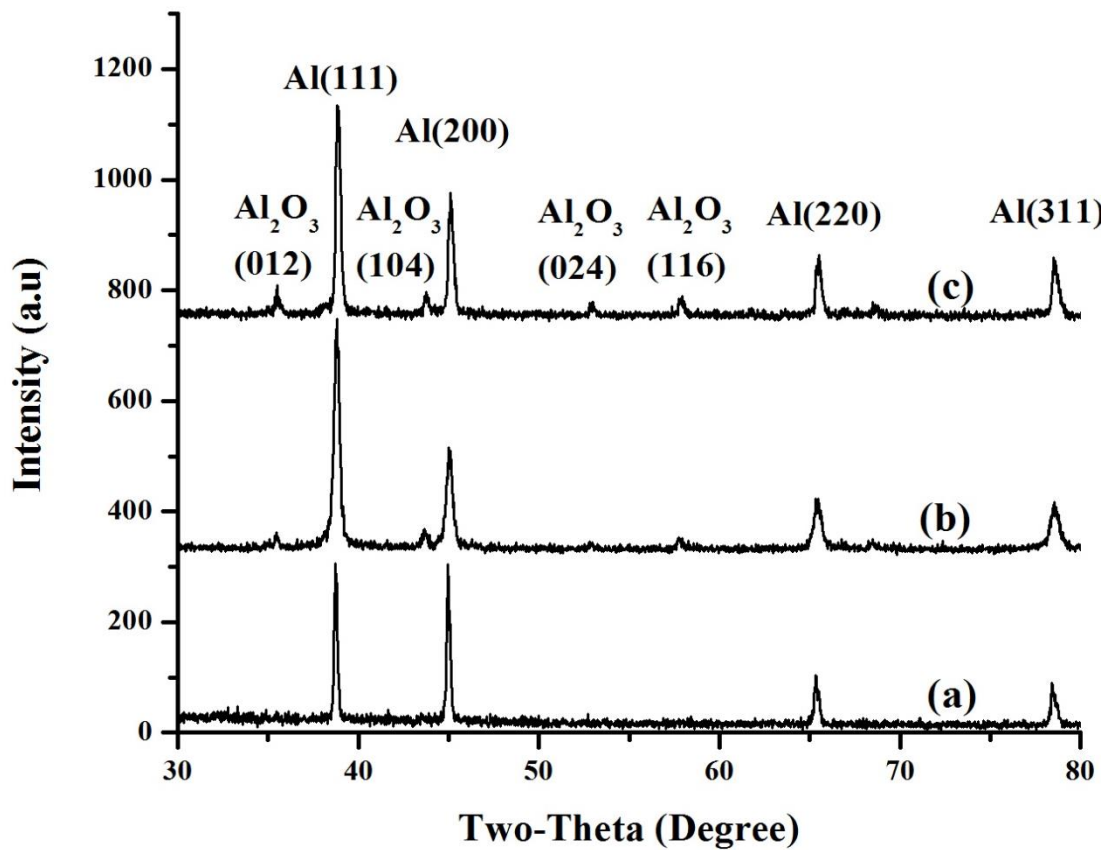


Figure 4.9 XRD spectra of Al-Al₂O₃ composites mechanically milled for 24 h (a) 2 vol. %, (b), 10 vol. %, and (c) 15vol. % Al₂O₃.

This is also an indication of the presence of little amount of alumina in the matrix of aluminum. Intensity of peaks also decreases as we proceed further to higher volume fraction with more hours of milling (24h). As milling time increase the more stresses are induced in the matrix, which results in fine particles and consequently the peaks become broadened and short. This trend is in agreement with [35, 37]. One advantage of alumina over other reinforcement like SiC etc. is its high thermal stability, which does not promote formation of new phases in the matrix. The probability of presence of new phase formation cannot be neglected in Al-Al₂O₃ system although it is not detected in XRD. There might be few reasons; it can be argued that a phase was formed but not detected due to the detectability limit of the XRD instrument and the presence of minute amount of the secondary phase in the material. In the literature, few authors reported the absence of secondary phases formation while using alumina reinforcement in aluminum matrix [40].

4.2.3 Crystallite Size

Crystallite size of α -Al and aluminum nanocomposites mechanically milled for 24h was calculated using Scherer equation. Milling and presence of Al_2O_3 rigid particles results in reduced crystallite size of the processed materials. The calculated crystallite size is represented in the form of bar chart in fig. 4.10.

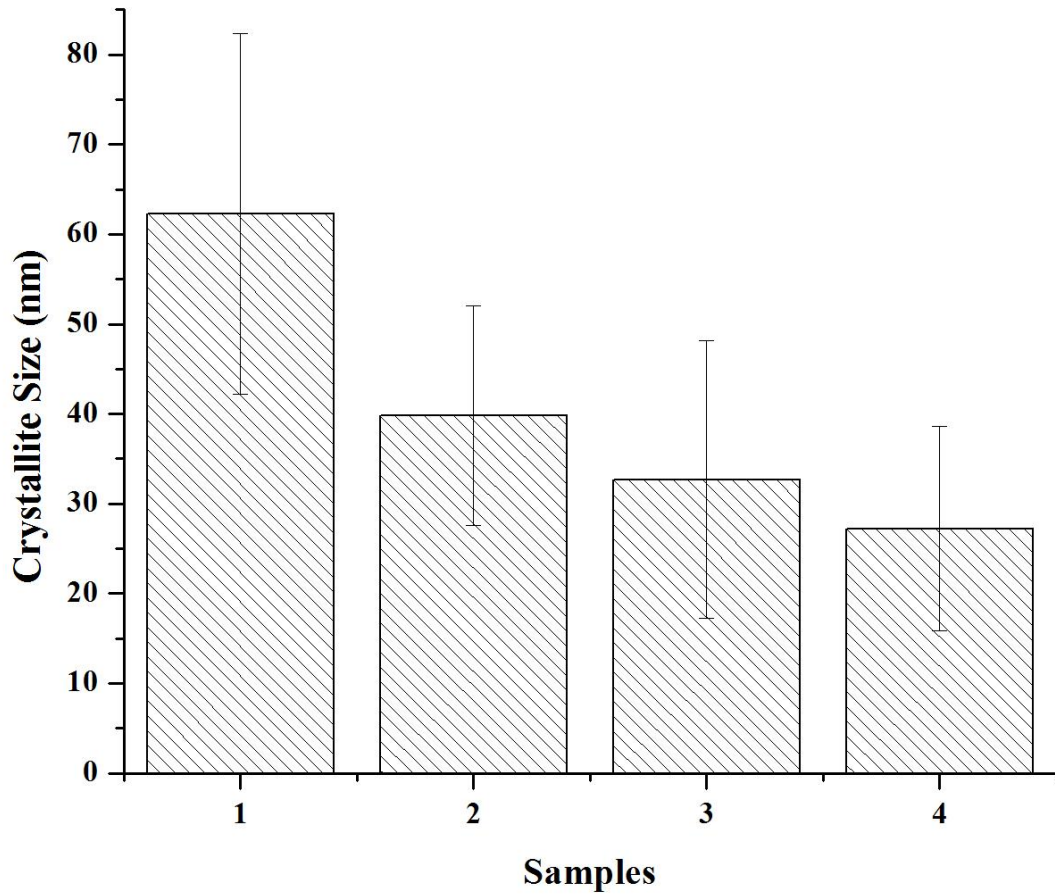


Figure 4.10 Crystallite size of (1) Al MA for 24 h, and Al- Al_2O_3 composites (2) 2 vol. %, (3), 10 vol. %, and (4) 15vol. % mechanically alloyed for 24 h

Table 4.1 Crystallite size of α -Al and mechanically milled aluminum nanocomposites

Composite	Crystallite size (nm)
Al-15 vol.% Al ₂ O ₃	27.24
Al-10 vol.% Al ₂ O ₃	32.69
Al-2 vol.% Al ₂ O ₃	39.82
Pure Al MA for 24 h	62.24
P-Al Unmilled	298

Crystallite size of monolithic aluminum is decreased to 62.24 nm although it is very ductile in nature. This was due to the application of severe plastic deformation and imparting the stresses in the matrix. In the literature, crystallite size reduction of monolithic aluminum is already discussed as 38 nm after 8h and 75 nm for 24h [56].

The crystallite size of composites reduced more than the pure aluminum due to the presence of second phase hard particles of alumina. These hard particles introduce the brittleness in the matrix (Al) and supported the process of ball milling in reduction of crystallite size. The summary of crystallite size reduction is presented in the table. 4.1. In general, the crystallite size reduction after the milling for higher times is due to induction of large stresses in the matrix which produce crystal defects. One of the line defect is said to be dislocations. When we proceed for higher milling hours, number of line defects (dislocations) per unit volume increases; This is termed as dislocation density increase. When more defects are present in the matrix it is easier to deform the material in number of smaller particles or crystals. This trend is in agreement with dislocation theory of materials [21].

4.3 Densification & Microstructure

The microstructure of un-milled aluminum sintered for 5 and 20 min is presented in figures 4.11 (a) and (b), respectively. The effect of milling on the microstructure of aluminum sintered for 5 and 20 min can be clearly seen in figures 4.11 (c) and (d), respectively. The microstructure of un-milled and sintered aluminum for 5 minutes is characterized by relatively large grains. The increase in sintering time from 5 to 20 minutes resulted in grain growth. The effect of milling for 24 h and sintering for 5 minutes can be clearly seen in figure 4.11(c) where a very fine microstructure characterized by elongated grains was obtained. The increase in sintering time from 5-20 minutes led to significant grain growth as seen in figure 4.11 (d).

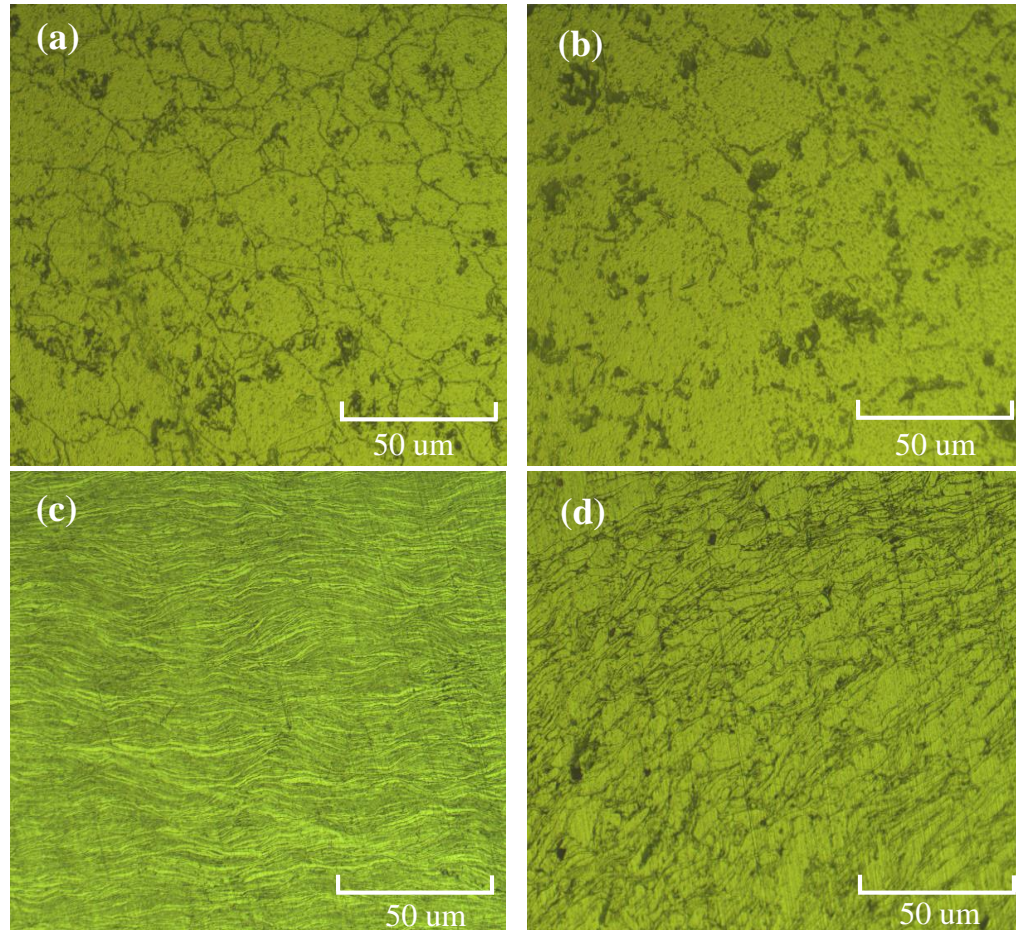


Figure 4.11 Optical micrographs (x 500) of un-milled aluminum sintered for (a) 5 min (b) 20 min, and aluminum milled for 24h and sintered for (c) 5 min, (d) 20 min.

It is well known that sintering time plays an important role in isothermal grain growth, which can be expressed with the formula $G^n - G_0^n = Kt$ where G_0 and G are the grain sizes at initial time t_0 and isothermal holding time t , respectively. K is a temperature depend parameter. It was found that the grain growth in the milled nanocrystalline aluminum was much less compared to the un-milled aluminum. This is may be due to recrystallization of the heavily milled and deformed structure. Moreover, it is claimed that nanocrystalline materials often exhibit a remarkable resistance to grain growth [29].

Typical microstructures of Al- 15 vol. % Al_2O_3 sintered for 5 and 20 min are presented in figure 4.12 (a) and (b), respectively. The increase in sintering time from 5 to 20 minutes led to marginal grain growth. Analysis of the microstructure of aluminum, figure 4.12 (c), and Al- 15 vol. % Al_2O_3 , figure 4.12 (a), milled for 24 h and sintered for 5 minutes shows that both materials have microstructures with similar features and very elongated grains. The grains in the composite material have relatively large size compared to the monolithic material. However, for the same samples sintered for 20 minutes, the monolithic material, figure 4.12 (d) had a microstructure with relatively large and equiaxed grains while the composite material, figure 4.11 (b), had a microstructure with relatively small and elongated grains. It can be concluded that Al_2O_3 significantly contributed to grain growth inhibition when samples were sintered for 20 minutes.

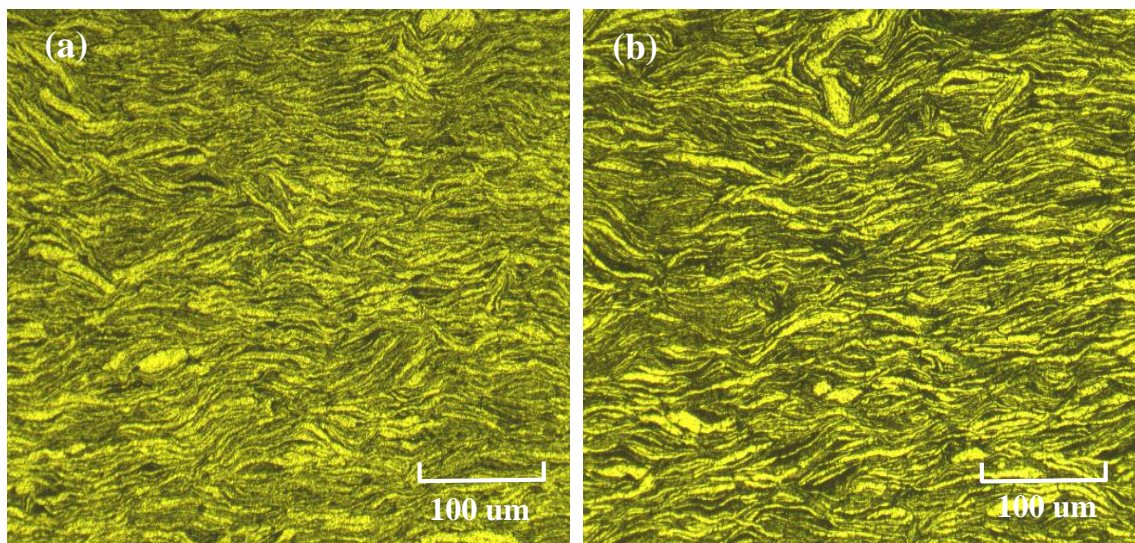


Figure 4.12 Optical micrographs ($\times 200$) of Al-15 vol.% Al_2O_3 composite milled for 24h and sintered for (a) 5 min and (b) 20 min.

Relative density of the consolidated samples is presented in fig. 4.13. The as-received pure aluminum consolidated at 550°C for 5 minutes had a relative density of 98.88 %. The increase in sintering time to 20 minutes increased its relative density to 100 %. The pure aluminum milled for 24 h and consolidated at 550°C for 5 minutes had a relative density of 95.92 %. The increase in sintering time to 20 minutes resulted in a minor change of density to 95.18 %. The pure aluminum milled for 24 h and consolidated at 550°C for 5 minutes had a relative density of 95.92 %. The increase in sintering time to 20 minutes resulted in a minor change of density to 95.18 %.

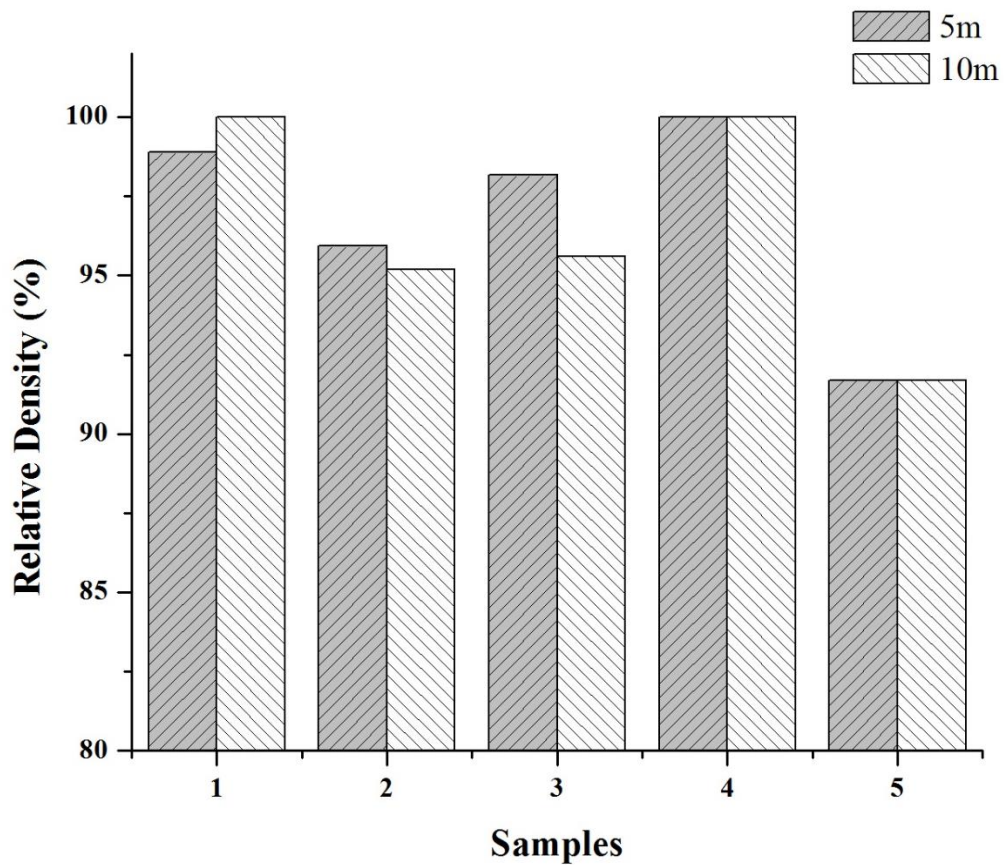


Figure 4.13 Relative density of sintered samples. (1) Al, (2) Al MA for 24 h, and Al- Al_2O_3 composites (3) 2 vol.%, (4), 10 vol.%, and (5) 15vol.%.

The Al-2 vol.% Al_2O_3 composite consolidated at 550°C for 5 minutes had a relative density of 98.16 %. The increase in sintering time to 20 minutes decreased its relative density to 95.50 %. The Al-10 vol.% Al_2O_3 composite consolidated at 550°C for 5 minutes had a relative density of 100 %. The increase in sintering time to 20 minutes did not change its density. The Al-15 vol. % Al_2O_3 composite consolidated at 550°C for 5 minutes had a relative density of 91.69 %. The increase in sintering time to 20 minutes did not affect its density.

Analysis of density results presented above shows that relative density of 100% was reached for pure un-milled aluminum sintered for 20 min i.e. it was fully densified. However, milling for 24 h reduced its densification to 95 %. Also, full densification was achieved in the Al-10 vol. % Al_2O_3 composite. However, the composites containing 2 and 15 vol. % Al_2O_3 displayed less densification compared to pure un-milled aluminum and Al-10 vol. % Al_2O_3 composite. The less densification of pure milled aluminum supports the fact that monocrystalline materials are more difficult to compact and densify. This can be attributed to the fact that consolidation of nanostructured powders is more difficult than micron-size powders of the same metal or alloy. Therefore, nanostructured materials requires larger stresses to be plastically deformed. As for mechanically milled samples, milling and the addition of Al_2O_3 improved the densification for sample containing 2 % vol. Al_2O_3 and approximately full densification was reached for sample containing 10 % vol. of Al_2O_3 . Further increase in Al_2O_3 content to 15 % decreased the densification. This shows that consolidation of nanocomposite powders become more difficult at higher fractions of ceramic nanoparticles as agglomeration of particles may take place.

4.4 Mechanical Properties

4.4.1 Hardness

The hardness of the developed materials is presented in fig. 4.14, as-received pure aluminum consolidated at 550°C for 5 minutes had a Vickers hardness of 369.3 Hv (MPa).

The increase in sintering time to 20 minutes decreased its hardness to 326.3 Hv (MPa).

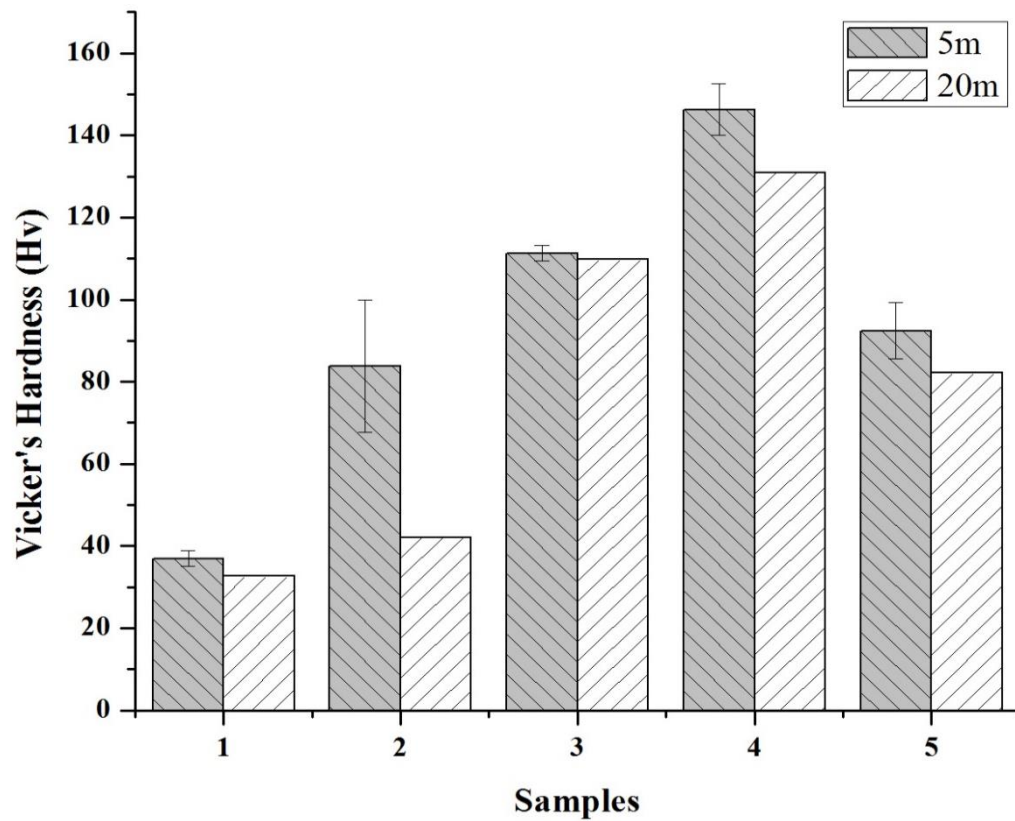


Figure 4.14 Hardness of sintered samples. (1) Al, (2) Al MA for 24 h, and Al-Al₂O₃ composites (3) 2 vol.%, (4), 10 vol.%, and (5) 15vol.%.

This can be attributed grain growth observed in figures 4.11 (a) and (b). It is understood that the yield strength of polycrystalline materials depends on the grain size according to the expression $\sigma_{ys} = \sigma_0 + kd^{1/2}$ (Hall-Petch relationship), where σ_0 is the lattice friction stress, k is a Hall–Petch slope. On the other hand, Vickers hardness and yield strength could be related through a simple formula $H_v/\sigma_{ys} \approx 3$. As a result, hardness can be related to the grain size through $H_v = H_0 + kd^{1/2}$, where H_0 and k are constants. Therefore, the hardness of a material decreases with the increase in grain size.

For example monolithic aluminum without milling shows the hardness of 369.3 Hv (MPa) for 5m holding time during sintering but when more time is provided (20 mins) then hardness decreases to 326.3 Hv (MPa). This behavior is associated with the grain growth as the coarser grains have less strength. This can also be related to Hall patch equation which concludes that smaller the grain the larger is the strength. Hardness is also related to yield strength; Hv is always three times of yield strength of the materials. Consequently, we can say that the hardness decreases with increase in grain size.

An addition of 10% alumina by volume in aluminum matrix using mechanical milling resulted in an increase in micro-Vicker's hardness up to 4-folds. Because mechanical milling for 24 h induces stresses in the grains of matrix which and second phase particles provides barriers and hurdles to the movement of dislocations. The overall contribution of mechanical milling and second phase particles results in the improvement of hardness and mechanical strength. This behavior can be clearly observed in the characterization of the developed specimen. It was also noted that the grain growth imparts slight reduction in hardness.

Table 4.2 Hardness (MPa) of spark plasma sintered materials

Composite	K (deg./min)	P (MPa)	T (°C)	Time (min)	HV (MPa)	Ref.
Al-15 vol% Al ₂ O ₃	200	50	550	5	906	This work
Al-15 vol% Al ₂ O ₃	200	50	550	20	806	This work
Al-10 vol% Al ₂ O ₃	200	50	550	5	1463.3	This work
Al-10 vol% Al ₂ O ₃	200	50	550	20	1284	This work
Al-2 vol% Al ₂ O ₃	200	50	550	5	1092	This work
Al-2 vol% Al ₂ O ₃	200	50	550	20	1077	This work
Pure Al BM 24 h	200	50	550	5	821.7	This work
Pure Al BM 24 h	200	50	550	20	413	This work
Pure Al	200	50	550°	5	362.2	This work
Pure Al	200	50	550	20	320	This work
Pure Al	200	50	600	10	313	[12]
Al-1 wt% SiC	200	50	600	10	1080	[12]
Al-5 wt% SiC	200	50	600	10	928	[12]
Al-10 wt% SiC	200	50	600	10	1715.3	[12]
Al2124+1wt.% CNTs	100	35	500	20	1181.9	[62]
Al6061	100	35	450	20	660	[62]
Al6061+1 wt.% CNTs	100	35	450	20	710	[62]
Al-7Si-0.3Mg	100	35	500	20	630	[61]
Al-7Si-0.3Mg+0.5 wt.% CNTs	100	35	500	20	680	[61]
Al-12Si-0.3Mg	100	35	500	20	680	[61]
Al-12Si-0.3Mg+0.5 wt.% CNTs	100	35	500	20	830	[61]
Al-7Si-0.3Mg	100	35	500	20	630	[9]
Al-7Si-0.3Mg+5 wt.% SiC	100	35	500	20	710	[9]
Al-7Si-0.3Mg+12 wt.% SiC	100	35	500	20	750	[9]
Al-7Si-0.3Mg+20 wt.% SiC	100	35	500	20	690	[9]

4.4.2 Compression Test

Pure aluminum (both milled for 24h, unmilled) and Al-10 vol%. Al₂O₃ composite 24h milled were investigated experimentally as given in table 4.3, and compared with theoretical values to estimate the behavior of material under compression.

Table 4.3 Experimentally calculated properties of samples sintered at 550°C, 50MPa, 200°C/min, and 20m.

Material	Relative Density (%)	Porosity (vol. %)	Compressive Strength (MPa)	Yield offset. (0.2%) MPa
Die-20 mm Diameter				
Pure Al	99.8	0.2	204.43 ± 16	74.33± 21
Pure Al-24 h	97.02	2.98	371.69 ± 69	166.9±224.0
Al-Al ₂ O ₃ 10 vol. %	96.57	3.43	432.40 ± 91	311.4± 44

Compression testing results of the developed samples such as pure Al unmilled, pure Al-24h milled, and Al-10 vol. % Al₂O₃ nanocomposite indicate the increment in the strength after processing and addition of second phase particles. In table 4.3, the variation of yield strength and compressive strength of the tested samples is listed along with the relative density and porosity of the samples. It was found that compressive strength increases with increase in milling time and addition of Al₂O₃ nanoparticles. An increase of 111.5% in compressive strength was observed for 24h milled Al-10 vol.% Al₂O₃ nanocomposite. Nanometer sized second phase particles usually restricts the motion of dislocations and therefore, a much larger force is required to deform the material permanently. Pure unmilled Al with 0.2 % porosity can bear 204.43 MPa of applied stress while pure Al milled for 24h having 2.98% can withstand 371.69 MPa applied stress. This might be

attributed with the process of milling, as milling induces defects and strains into the bulk materials and reduces the crystallite size up to nanometer scale. The defects, residual strains and smaller crystallite sizes offer more resistance to the movement of dislocations and consequently resist the deformation. The Al-10 vol. % Al_2O_3 nanocomposite exhibits 111.5 % increment in the compressive strength although it has much larger percentage of porosity in the bulk. Since residual strains, smaller crystallite size and 2nd phase particles offer resistance to the movement of dislocations, therefore, the deformation becomes more difficult. This is in agreement with literature findings [31] in which compressive strength increases with increasing the volume fraction of reinforcement.

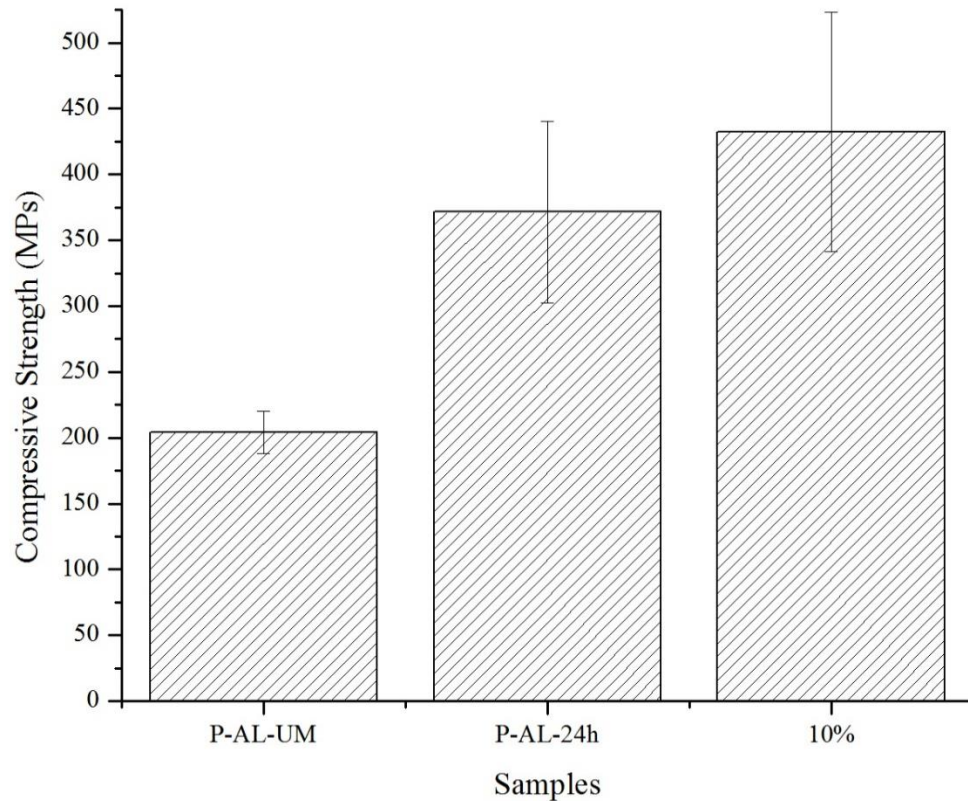


Figure 4.15 Compressive properties of samples sintered at 550°C, 50MPa, 200°C/min for 20m.

The mechanical strength of discontinuously reinforced MMNCs increases due to a variety of strengthening mechanisms benefactions. The strength of pure Al unmilled is lower than the pure Al milled for 24h. This can be explained based on the fact that mechanical milling enhances dislocation density and reduces grain and crystallite size of the material which results in more grain boundaries upon consolidation. Moreover, according to Hall-Petch strengthening mechanism; when the grain boundaries (fine grain size) are larger, yield strength will be higher $\sigma_{ys} = \sigma_0 + kd^{-1/2}$. Grain boundaries are disturbed or deformed regions in the material, and they act as barriers, which restricts the movement of dislocations upon the application of applied load. Therefore, much larger force is usually required to deform the material permanently. The microstructure of pure Al unmilled and milled for 24h can be seen in figure 4.11 (a-d) to observe the phenomenon of grain growth. The grain growth is considerable for pure Al in unmilled conditions for larger sintering time (20m) while pure Al-24h has a little grain growth after 20m of sintering, which results in finer and elongated-deformed grains after consolidation for 5 & 20m of sintering time.

Addition of second phase ceramic particles strengthened the matrix by numerous mechanisms. Since, the particulate size of the material is in submicron range, therefore, Orowan looping, CTE mismatch & Hall-Petch strengthening along with load transfer effect account for the strengthening of the matrix. Literature suggests that when the particulate size of reinforcement is lesser than 50nm, the Orowon effect and CTE mismatch are the major contributors in the strengthening of a particulate composite [3, 78-81]. The overall strengthening is considered to be the cumulative effect of all previously mentioned effects. D. Liu et al. [90] reported that the strengthening of MMNCs is mainly effected by both the grain boundaries and presence of impurities and second phase particles. The precise effect

of each mechanisms is usually approximated overall, due to difficulty in determining the individual effect of each mechanisms. The highest compressive strength for Al-10 vol. % Al_2O_3 nanocomposite milled for 24h is attributed with the addition of colossal grain boundaries, finer particle size and presence of defects and ceramic rigid nanoparticles.

Table 4.4 Mechanical properties of materials sintered using spark plasma sintering

Sample	Rel. Density (%)	Porosity (vol. %)	Comp. Strength (MPa)	Yield offset. (0.2%) MPa	Hardness (Hv)	Reference
Pure Al	99.8	0.2	204.43	74.33	32	This Work
Pure Al-24 h	97.02	2.98	371.69	166.9-224	42.1	This Work
Al- Al_2O_3 10% vol.	96.57	3.43	432.87	311.4	146.3	This Work
Pure Al	100	-	179	75	40	[95]
Al-1wt% SiC	100	-	312	251	116	[95]
Al-5wt% SiC	98	2.0	228	131	94	[95]
Al-10wt% SiC	96	4.0	534	409	172	[95]
Al	100	-	200	-	-	[92]
Al-SiO ₂ 10% vol.	87.8	13.2	83.4	-	-	[92]
Al-SiO ₂ 50% vol.	84.2	16.8	69.2	-	-	[92]

There are a few theories, which are developed by scientists to predict the strengthening of developed materials [92, 94, 95]. These theories based upon the combine or individual effect of the strengthening mechanisms as explained earlier in literature. S. Kamrani et al [94] employed a theory based upon combine effect of Orowan and Hall-Petch strengthening to predict the yield strength of mechanically alloyed Al (42 μm) and SiC (50nm) powders and consolidation was performed using double pressing/ sintering route. The strength of the fabricated composites was predicted using the equation 4.2 as given below:

$$\sigma = \sigma_{H-p} + \sigma_{orw} \quad (4.1)$$

$$\sigma = \sigma_0 + kD^{-1/2} + \left(\frac{\pi}{6V_f} - \frac{2}{3}\right)^{1/2} * \frac{Gb \ln\left(\frac{d}{b}\right)}{\pi d \sqrt{1-\nu}} \quad (4.2)$$

The detail of constants used in the relation are given in table 4.5. The grain size of the matrix after sintering was used as the grain size of the matrix in the above equation.

In compressive loading conditions, yield stress can also be considered as compressive strength if the fracture is taking place at plastic strain. Since the yield stress is also taken as compressive strength, therefore, compressive strength can also be estimated using the above described equation.

Table 4.5 Parameters used to estimate the yield strength of Al-Al₂O₃ nanocomposites [94]

Parameter	Nomenclature	Unit	Value
Inherent friction stress	σ_o	MPa	15.7
Constant of Hall-Petch equation	k	MPa.m ^{0.5}	0.0725
Reinforcement volume fraction	V_f	unitless	0-0.1
Shear modulus	G	GPa	120.3
Burger's vector	i	nm	0.286
Reinforcement particle size	d	nm	50-200
Poisson's ratio	ν	unitless	0.34

Compressive strength of particulate reinforced nanocomposites can also be determined using simple rule of mixture (ROM), relation is give in equation 4.3.

$$E_c = \eta X_p E_p + X_m E_m \quad (4.3)$$

Where X stands for composite property i.e. compressive strength etc. η is strengthening efficiency coefficient and it is a function of reinforcement aspect ratio and an approximate ratio of 0.1 is used for reinforcement in nanometer size.

Table 4.6 Theoretical and experimental values of compressive yield strength of developed nanocomposites and monolithic Al

Composite	Crystallite size (nm)	σ_y Al (MPa)	σ_y Al ₂ O ₃ (MPa)	σ_y (MPa) Eq.4.2	σ_y (MPa) Eq.4.3	σ_y (MPa) Exp.
Pure Al	366	75	49050	95.96	125.73	74.33
Pure Al-24 h	108	75	49050	174.50	221.39	166.9
Al-Al ₂ O ₃ 10% vol.	53.4	75	49050	284.91	401.71	311.40

Composite	Processing information	Y.S (MPa)	Reference
Al-Al ₂ O ₃ 10% vol.	SPS, 550°C, 50MPa, 20m	311.40	This work
Pure Al-24 h	SPS, 550°C, 50MPa, 20m	166.9	This work
Pure Al	SPS, 550°C, 50MPa, 20m	74.33	This work
Al-SiC10% wt.	SPS, 550°C, 50MPa, 15m	409	[95]
Al-SiC5% wt.	SPS, 550°C, 50MPa, 15m	131	[95]
Al-SiC1% wt.	SPS, 550°C, 50MPa, 15m	251	[95]
Al-SiC8.2% wt.	CIP, 640°C, 700MPa, 1h	269	[94]
Al-SiC6% wt.	CIP, 640°C, 700MPa, 1h	258	[94]
Al-SiC1.2% wt.	CIP, 640°C, 700MPa, 1h	207	[94]

The theoretical and experimental compressive yield strength of composites are given in the table 4.6. Theoretical values are calculated using two equations 4.2 & 4.3. Equation 4.2, 4.3 based upon the Orowan + Hall-Petch theory and modified rule of mixture (ROM) respectively. The values obtained theoretically using eqn. 4.2 are in complete agreement with the experimental values of this work. Nevertheless, values obtained theoretically using ROM are a bit higher than the experimental values.

Al-Al₂O₃10% vol. milled for 24h exhibits maximum compressive yield strength. This might be attributed to the fact that second phase rigid ceramic particles inhibit the movement of dislocations upon application of compressive load, in addition, mechanical

milling induced large amount of defects in the structure, therefore, materials withstand reasonable amount of compressive strength. The values obtained from the equation 4.2 are more reliable than 4.3 since it includes numerous strengthening mechanisms rather ROM. The variation of compressive yield strength is also compared with the literature. S. Kamrani et al. [94] presented the same variation in strength upon increasing the second phase ceramic reinforcement in the matrix and compared the results with equation 4.2. The results obtained experimentally using different weight fractions of Al-SiC were are closer to the theoretical values. From table 4.5 it can be concluded that the values obtained experimentally in Al-Al₂O₃10% vol. milled for 24h are in complete agreement with theoretical model eqn. 4.2 and with the literature [94, 95, 96].

The FESEM images of fractured surfaces of developed samples are shown in fig. 4.16 a, b &c. It can be seen that the developed pure aluminum in as received conditions fractured at the grain boundaries which is attributed with the fact that Al is usually ductile and it bears little amount of compressive loading. Since 24h of milling induces large amount of defects and lattice strains in pure Al, therefore, the fracture observed is near to brittle failure as cracking is taking place through the grains and a sharp morphology can be observed. In fig. 4.16 c. the morphology of fractured sample can be observed, since it involved 24 h of milling along with the addition of second phase particles. The failure is taking place through the grains, which is the indication of brittle mode failure. The fracture morphology of the three sintered samples is shown in the figure 4.16, which indicates that the powder was completely sintered at the mentioned conditions.

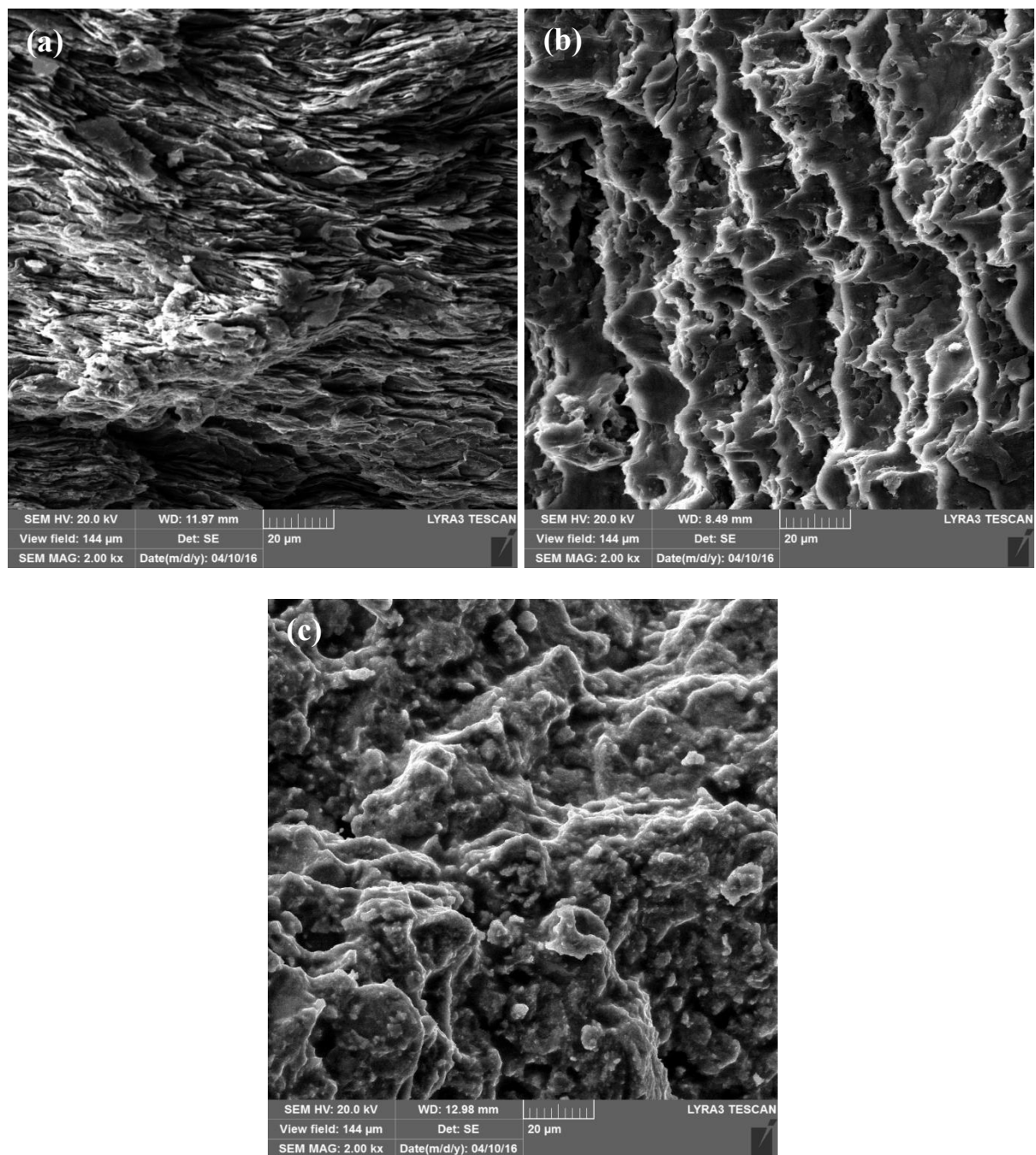


Figure 4.16 FESEM images showing fracture surfaces of (a) P-Al-unmilled (b) P-Al-24h and (c) Al-Al₂O₃ 10% vol. nanocomposite, sintered at 550°C, 50MPa, 200°C/min for 20minutes.

4.5 Thermal Properties

Thermal properties of sintered samples are listed in the table 4.6. Thermal characterization of sintered samples involve the determination of thermal conductivity, thermal diffusivity and heat capacity.

Table 4.7 Thermal properties of nanocomposite including monolithic Al, sintered at 550°C, 50MPa, 200°C, 20 m

Material	Rel. Density (%)	Porosity (vol.%)	Th. Conductivity (W/mK)	Th. Diffusivity (mm ² /s)	Heat Capacity (J/gK)
Die-20 mm Dia					
Pure Al	99.8	0.2	198.09	3.94	57.70
Pure Al-24 h	97.02	2.98	92.20	5.00	18.47
Al-Al ₂ O ₃ 10 vol.%	96.57	3.43	81.42	4.60	17.79

4.5.1 Thermal Conductivity

Thermal conductivity in metals is entirely based upon the presence of number of free moving electrons & phonons. In metals phonons (lattice vibration) also take part in the conduction but the dominant medium is free electrons [76, 89]. There are few factors which affect the conductivity of materials; grain size, presence of impurities, residual stresses and crystallographic defects [11]. In fig. 4.17, fully dense pure aluminum which bear no residual stresses, defects and impurities, exhibits 198.09 W/m.K thermal conductivity while the same materials after milling for 24h showed reduced value of thermal conductivity by around 50%. Mechanical milling induces defects and residual stresses in the lattices of materials which does not allow electrons to move freely inside the bulk. Therefore, the electronic movement and scattering are restricted. Thermally excited

electrons interact with these defects and dissipate huge amount of energy which causes reduction in thermal conductivity of materials. Regarding the comparison of pure Al and Al-Al₂O₃10% vol. milled for 24 h, the conductivity decreases by 59% for 20 mm die sintered specimens. Al-Al₂O₃10% vol. milled for 24h contains all the previously mentioned factors which affect thermal conductivity. This is because the addition of 10% by volume second phase ceramic particles of lesser thermal conductivity which not only decreases the densification but also inhibit the grain growth. While, small grains provide more hurdles to the movement of electrons which results in the reduction of thermal conductivity.

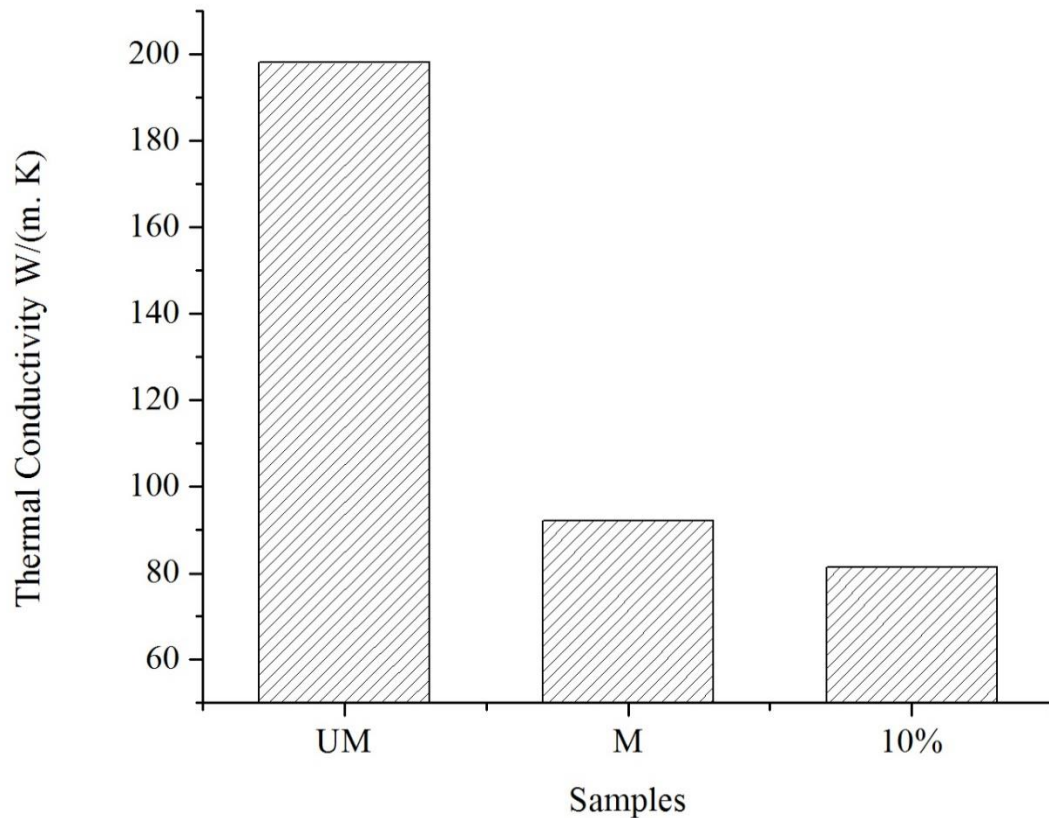


Figure 4.17 Thermal conductivities of spark plasma sintered pure Al-unmilled, pure Al and Al- Al₂O₃ 10 % vol. nanocomposite milled for 24h.

4.5.2 Thermal Diffusivity

Thermal diffusivity of sintered pure Al and composite Al-Al₂O₃10% vol. milled for 24 h at room temperature is shown in the fig. 4.18. The thermal diffusivity of pure aluminum sintered in as received conditions is lowest.

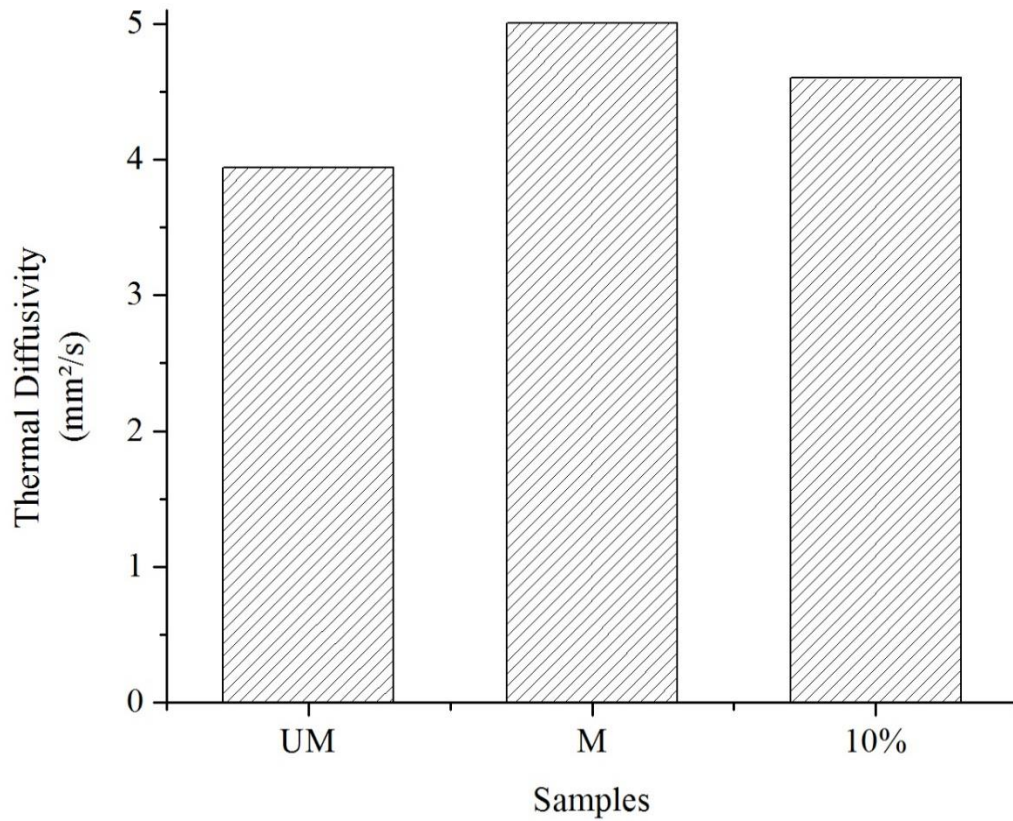


Figure 4.18 Thermal diffusivity of spark plasma sintered pure Al-unmilled, pure Al and Al- Al₂O₃ 10 % vol. nanocomposite milled for 24h.

In heat transfer analysis of materials, thermal diffusivity (thermal inertia) is the measure of the ability of a material to conduct thermal energy relative to its ability to store thermal energy. If a material has high thermal diffusivity it can conduct heat more rapidly. It is a measure of the rate at which a body with a non-uniform temperature reaches a state of thermal equilibrium. In figure 4.18, thermal diffusivity variations for the developed samples is presented.

In the relation $h = k/(C_p \cdot \rho)$, h is the thermal diffusivity, k is thermal conductivity, C_p is specific heat capacity and ρ is the temperature dependent density of the material. In case of pure Al in unmilled condition, the thermal conductivity is high but the thermal diffusivity is low this is due to the fact that the product of C_p and ρ is also high as the densification of pure Al is approximately 100% with maximum value of heat capacity as indicated in the figure 4.18. While for pure Al and Al- Al₂O₃ 10 vol. % nanocomposite milled for 24h thermal diffusivity is almost the same due to the fact that the overall relation remains unchanged due to variations in the thermal conductivity, thermal diffusivity and heat capacity.

4.5.3 Heat Capacity

Heat capacity of sintered pristine Al and composite Al-Al₂O₃10% vol. milled for 24 h at room temperature is shown in fig. 4.19. Heat capacity follows the same trend as thermal conductivity for all the three samples. Decrease in specific heat occurs as we proceed milling for 24 h and addition of second phase particles, these two factors affect the heat capacity as the densification is poorer with smaller grain size along with the second phase particles which act as barrier.

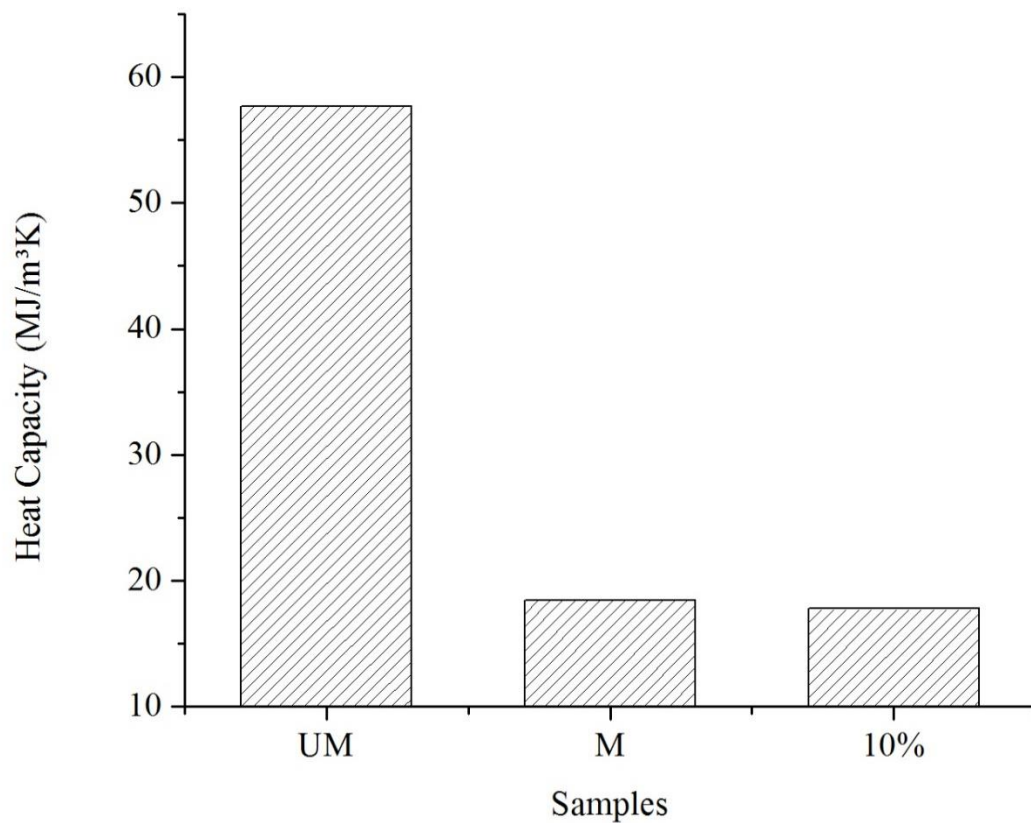


Figure 4.19 Heat capacity of spark plasma sintered pure Al-unmilled, pure Al and Al-Al₂O₃ 10 % vol. nanocomposite milled for 24h.

4.5.4 Coefficient of Thermal Expansion

Thermal expansion was measured between 25-450 °C. The change in CTE in pure Al, pure Al-24 h milled and Al-10% vol. Al_2O_3 -24h milled are shown in the fig. 4.20. It was found that the CTE of metals increased upon provision of heat. It was also observed that the processing (mechanical milling) and addition of ceramic content (Al_2O_3) in the metallic matrix (Al) resulted in a decrease in the CTE of developed materials.

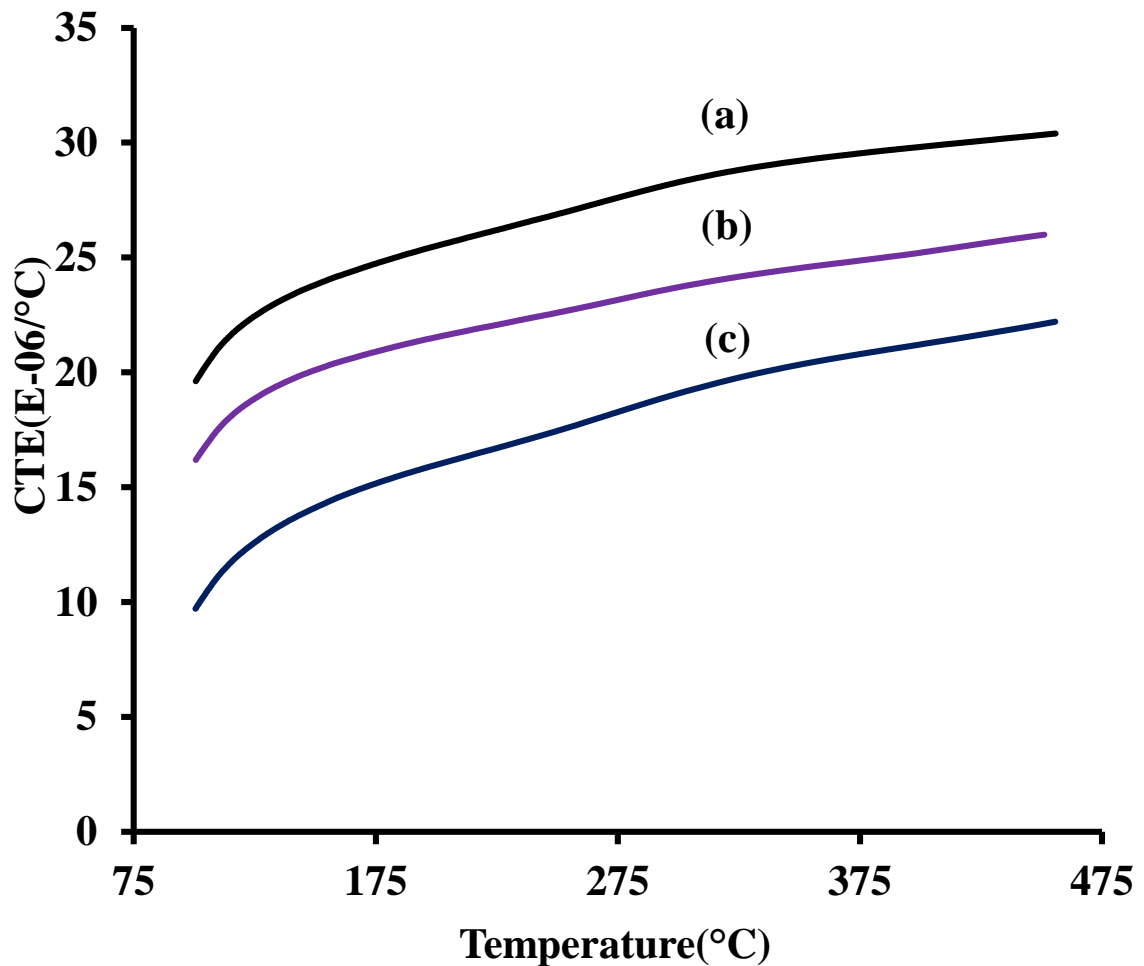


Figure 4.20 CTE variations with temperature for (a) pure Al unmilled, (b) milled 24h, and (c) Al- Al_2O_3 10% vol. nanocomposite

Coefficient of thermal expansion of particulate reinforced metal matrix composite is affected by numerous factors i.e. interfacial reactions, mismatch of CTE between reinforcement and matrix and residual stresses [82]. Chawla et al [84] stated that the thermal expansion behavior of MMCs (Al/SiC_p) depends upon the distribution, morphology, size and SiC particulate volume fraction. The addition of ceramic reinforcements in metal matrices of composites induces the residual stresses while cooling from the material processing temperature because of the difference between the CTE of reinforcement and matrix. These generated residual stresses apply compressive stresses on reinforcement and tensile stresses on the matrix. The magnitude of generated residual stresses vary by changing the characteristics and volume fraction of reinforcement and matrix along with the processing technique [69].

The overall trend in the CTE reduction can be observed in fig. 4.21 at 450 °C. It was noticed that the materials become thermally dimensional stable due to the addition of ceramic reinforcement particles and residual stresses.

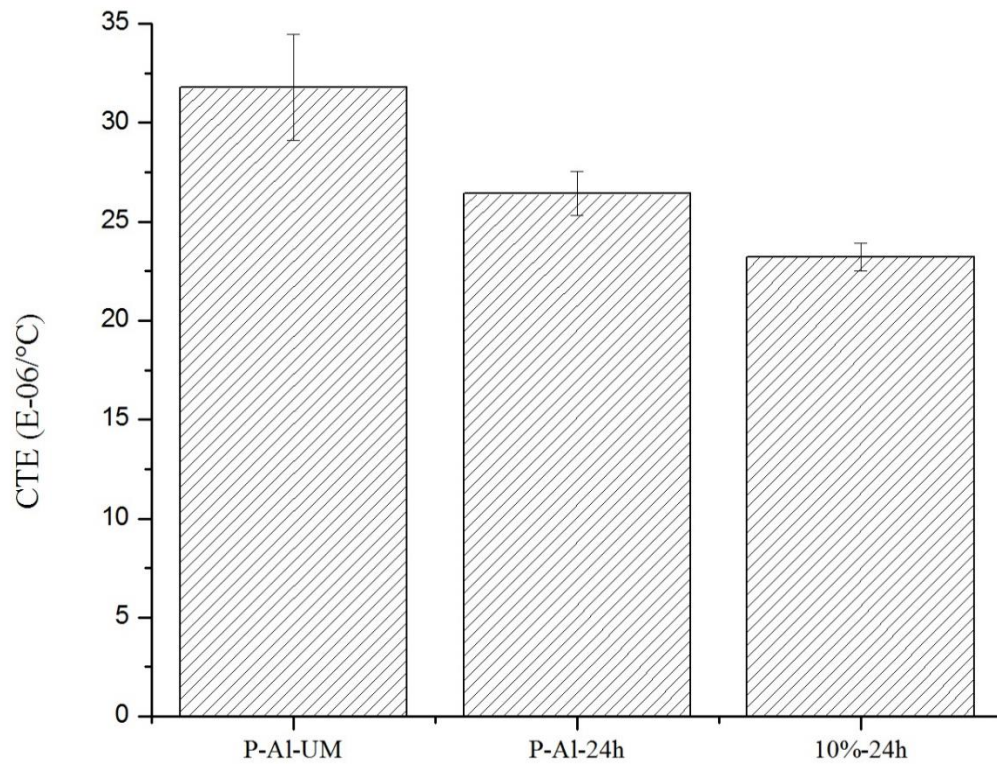


Figure 4.21 Average CTE at 450 °C for pure Al unmilled, milled 24h, and Al- Al₂O₃10% vol. nanocomposite

Ren et al. [85] claimed that while heating, the imposed tensile stresses on the matrix due to mismatch of CTE diminished as temperature increases gradually. Since, the thermal expansion of matrix is restricted by the vicinity of reinforcement, therefore, the compressive stresses on matrix started building up the pressure on reinforcement as temperature increases. This built pressure is not quite enough to push the reinforcement particles therefore the expansion of materials restricted and materials becomes thermally stable (dimensionally). S. Okumus et al. [82] investigated the thermal behavior of Al-Si/SiC/graphite prepared through casting and indicated that the aluminum metal becomes more dimensionally stable upon heating by addition of graphite and SiC particulate reinforcement due to the compressive stresses on SiC and lower CTE. S. Elomari et al. [87] concluded the decrease in CTE by the addition of SiC particles in the Al matrix and results presented were also in complete agreement with Turner's and Kerner's model.

CHAPTER 5

CONCLUSIONS

Nanocrystalline aluminum and Al-Al₂O₃ nanocomposites with uniform distribution of the reinforcement were successfully developed using mechanical and spark plasma sintering techniques. The influence of reinforcement content, milling and sintering conditions, on the microstructure, densification, mechanical and thermal properties of the developed materials was investigated. It was found that milling of pure aluminum for 24 h decreased its crystallite size beyond 100 nm. For Al-Al₂O₃ nanocomposites, milling for 24 h decreased the crystallite size of the aluminum phase and resulted in uniform dispersion of the reinforcement. Sintering of the synthesized powders led to grain growth. Al₂O₃ contributed to grain growth inhibition when samples were sintered for 20 minutes. Milling improved hardness of aluminum but reduced its densification. Addition of Al₂O₃ nanoparticles resulted in further improvement of hardness. The Al-Al₂O₃ 10 vol. % nanocomposite showed the highest Vickers hardness value of 1463 (MPa). A 111.5 % increase in compressive strength was observed for Al-Al₂O₃ 10 vol. % nanocomposite after 24 h of milling. An addition of Al₂O₃ nanoparticles to aluminum decreased its thermal conductivity and enhanced the thermal dimensional stability.

REFERENCES

- [1] M. Kevorkijan “Aluminum Composites for Automotive Applications: A Global Perspectival” JOM, Nov 1999.
- [2] A. Kelkar, R. Roth, J. Clark “Automobile Bodies: Can Aluminum Be an Economical Alternative to Steel” *Journal of Materials*, Vol 53, pp.28-32, 2001.
- [3] C. Riccardo, V. Maurizio “Metal Matrix Composites Reinforced by Nano-Particles-A Review” *Metals*, 4, 65-83; doi: 10.3390/met4010065, 2014.
- [4] I.A. Brahim, F.A. Mohamed, and E.J. Lavernia “Particulate reinforced metal matrix composites-a review”, *Journal of Materials Science*, Vol. 26, pp.1137-1156, 1991.
- [5] G.A. Sweet, M. Brochu, R.L. Hexemer, I.W. Donaldson, D.P. Bishop, “Microstructure and mechanical properties of air atomized aluminum powder consolidated via spark plasma sintering” *Materials Science and Engineering A*, 608, pp. 273-282, 2014.
- [6] M. Rahimiana,, N.Parvinb, N. Ehsania “Investigation of particle size and amount of alumina on microstructure and mechanical properties of Al matrix composite made by powder metallurgy” *Materials Science and Engineering A* 527, 1031–1038, 2010.
- [7] M. Rahimian, N. Ehsani, N. Parvin, H.R. Baharvandi “The effect of sintering temperature and the amount of reinforcement on the properties of Al–Al₂O₃ composite” *Materials and Design* 30, 3333–3337, 2009.
- [8] A. R. Othman, Ali Sardarinejad & Abdul Kadir Masrom “Effect of milling parameters on mechanical alloying of aluminum powders” *Int J Adv Manuf Technol*, 2014.
- [9] N. Aqeeli, K. Abdullahi, C. Suryanarayana, T. Laoui, and S. Nouari “Structure of Mechanically Milled CNT-Reinforced Al-Alloy Nanocomposites” *Materials and Manufacturing Processes*, 28: 984–990, 2013.

- [10] B.W. Chua, L. Lu, M.O. Lai “Processing Routes for Aluminum based Nano-Composites” Dissertations and thesis 2010.
- [11] C. Tatar, N.O zdemir “Investigation of thermal conductivity and microstructure of the -Al₂O₃ particulate reinforced aluminum composites (Al/Al₂O₃-MMC) by powder metallurgy method” *Physica B* 405, 896–899, 2010.
- [12] N. Saheb, I. K. Aliyu, S. F. Hassan and N. Al-Aqeeli “Matrix Structure Evolution and Nano-reinforcement Distribution in Mechanically Milled and Spark Plasma Sintered Al-SiC Nan-ocomposites” *Materials* 7, 6748-6767; doi: 10.3390/ma7096748, 2014.
- [13] M.Y. Zheng, K. Wu, C.K. Yao, Mater “Microstructure and mechanical properties of aluminum borate whisker-reinforced magnesium matrix composites” *Materials Letters* 57, 558– 564, 2002.
- [14] R.Z. Valiev, R.K. Islamgaliev, I.V. Alexandrov, Bulk nanostructured materials from severe plastic deformation, *Progress in Materials Science* 45, 103-189, 2000.
- [15] F. He, Q. Han, M. J. Jackson ‘Nano-particulate reinforced metal matrix nanocomposites-a review’, *Int. J. Nanoparticles*, Vol.1, No.4, pp.301- 309, 2008.
- [16] L. Fischer, R. Raj, A. Saha “Literature Survey Report: Nano- dispersion Strengthening of Aluminum” 2004.
- [17] N. Crainic, and A. T. Marques ”Nanocomposites: A State-of-Art Review” *Key Eng. Mater.*, 230–232, pp. 656–659, 2002.
- [18] S. Rawal, “Metal-Matrix Composites for Space Applications, *ASME J. Offshore Mech. Arct. Eng.*, 53, pp. 14–17, 2001.
- [19] M. Varuzan, Kevorkijan “Aluminum Composites for Automotive Applications: A Global Perspective” *JOM*, Nov 1999.

- [20] S.W. Hadley, S. Das, J.W. Miller “Aluminum R&D for Automotive Uses. And the Department of Energy’s Role” *U.S. Department of Energy Washington, D.C.* 2000.
- [21] G.E. Dieter, Mechanical Metallurgy, *McGraw Hill Inc*, U.S.A, 1986.
- [22] E.T. Thostenson, C. Li, T.W. Chou “Review: Nanocomposites in context” *Composites Science and Technology* 65, 491–516, 2005.
- [23] J. He, M. Ice, S. Dallek, and E. J. Lanernia “Synthesis of Nanostructured WC-12 Pct Co Coating Using Mechanical Milling and High Velocity Oxygen Fuel Thermal Spraying” *Metallurgical and Materials Transactions A*, Volume 31A-541, Feb, 2000.
- [24] C. Borgonovo, D. Apelian, and M. Makhlof, "Aluminum nanocomposites for elevated temperature applications," *JOM Journal of the Minerals, Metals and Materials Society*, vol. 63, pp. 57-64, 2011.
- [25]] H. Khorsand a, M. Ghaffari b, E. Ganjeh “Microstructural association between mechanical behavior with bending fracture surfaces in Astaloy CrA sintered parts alloyed by Cu and C” *Materials and Design*, 55 979–986, 2014.
- [26] J. Lan, Y. Yang, and X. Li, "Microstructure and microhardness of SiC nanoparticles reinforced magnesium composites fabricated by ultrasonic method," *Materials Science and Engineering: A*, vol. 386, pp. 284-290, 2004.
- [27] Y. Yang, J. Lan, and X. Li, "Study on bulk aluminum matrix nano-composite fabricated by ultrasonic dispersion of nano-sized SiC particles in molten aluminum alloy," *Materials Science and Engineering: A*, vol. 380, pp. 378-383, 2004.
- [28] T. Rostamzadeh and H. Shahverd, "Microstructure Study On Al-5% Sic Nanocomposite Powders," *Iranian Journal of Materials Science and Engineering*, vol. 8, pp. 32-39, 2011.

- [29] Y. Saberi, S. Zebarjad, and G. Akbari, "On the role of nano-size SiC on lattice strain and grain size of Al/SiC nanocomposite," *Journal of Alloys and Compounds*, vol. 484, pp. 637-640, 2009.
- [30] M. Singla, D. D. Dwivedi, L. Singh, and V. Chawla, "Development of aluminum based silicon carbide particulate metal matrix composite," *Journal of Minerals & Materials Characterization & Engineering*, vol. 8, pp. 455-467, 2009.
- [31] C. Suryanarayana and N. Al-Aqeeli, "Mechanically alloyed nanocomposites," *Progress in Materials Science*, 2012.
- [32] M. Sadeghi and J. Mahmoudi, "Experimental and Theoretical Studies on the Effect of Die Temperature on the Quality of the Products in High-Pressure Die- Casting Process," *Advances in Materials Science and Engineering*, vol. 2012.
- [33] K. A. Gujba, "Development and characterization of carbon nanotubes (CNTs) and silicon carbide (SiC) reinforced Al-based nanocomposites," *ProQuest Dissertations and Thesis*, pp. 156. 2012.
- [34] U. Anselmi-Tamburini, J. Garay, Z. Munir, A. Tacca, F. Maglia, and G. Spinolo, "Spark plasma sintering and characterization of bulk nanostructured fully stabilized zirconia: Part I. Densification studies," *Journal of materials research*, vol. 19, pp. 3255-3262, 2004.
- [35] A. Khalil, "Synthesis and wear behavior of aluminum 6061 alloy reinforced with carbon nanotubes," *ProQuest Dissertations and Thesis*, pp. 129. 2012.
- [36] A. Csanády, I. Sajó, J. Lábár, A. Szalay, K. Papp, G. Balaton, and E. Kálmán, "Al-Pb nanocomposites made by mechanical alloying and consolidation," *Current Applied Physics*, vol. 6, pp. 131-134, 2006.

- [37] N. Al-Aqeeli, K. Abdullahi, A. Hakeem, C. Suryanarayana, T. Laoui, and S. Nouari, "Synthesis, characterization and mechanical properties of SiC reinforced Al based nanocomposites processed by MA and SPS," *Powder Metallurgy Journal*, Volume 56, Issue 2 (April 2013), pp. 149-157, 2013.
- [38] R. Orrù, R. Licheri, A. M. Locci, A. Cincotti, and G. Cao, "Consolidation/synthesis of materials by electric current activated/assisted sintering," *Materials Science and Engineering: R: Reports*, vol. 63, pp. 127-287, 2009.
- [39] H. Mahboob, S. A. Sajjadi, S. M. Zebarjad "Synthesis of Al-Al₂O₃ Nano-Composite by Mechanical Alloying and Evaluation of the Effect of Ball Milling Time on the Microstructure and Mechanical Properties" *The International Conference on MEMS and Nanotechnology*, ICMN'08 13-15, Kuala Lumpur Malaysia, 2008.
- [40] C. Suryanarayana, "Synthesis of nanocomposites by mechanical alloying," *Journal of Alloys and Compounds*, vol. 509, pp. S229-S234, 2011.
- [41] Z. R. Hesabi, A. Simchi, S. M. S Reihani "Structural evolution during mechanical milling of nanometric and micrometric Al₂O₃ reinforced Al matrix composites" *Mater Sci Eng A* 428:159–68, 2006.
- [42] Z. R. Hesabi, HR. Hafizpour, A. Simchi "An investigation on the compressibility of aluminum/nano-alumina composite powder prepared by blending and mechanical milling" *Mater Sci Eng A*, 454–455:89–98, 2007.
- [43] B. Prabhu, C. Suryanarayana, R. Vaidyanathan "Synthesis and characterization of high volume fraction Al–Al₂O₃" *Materials Science and Engineering A* 425 192–200, 2006.

- [44] N. Saheb., Z. Iqbal., A. Khalil., A. S. Hakeem., N. Al Aqeeli, T. Laoui, A. Al-Qutub, and R. Kirchner “Spark Plasma Sintering of Metals and Metal Matrix Nanocomposites A Review” *Journal of Nanomaterials*, Volume-2012.
- [45] V. Yadav, "Spark plasma sintering of aluminum matrix composites," PhD Thesis, 2011.
- [46] L. Lü and M. O. Lai “Mechanical alloying” *Kluwer Academic Publishers*, 1998.
- [47] H. Zoz, D. Ernst, and R. Reichardt "High Energy Milling/Mechanical Alloying/Reactive Milling," *Zoz GmbH*, 1998.
- [48] D. L. Zhang "Processing of advanced materials using high-energy mechanical milling," *Progress in Materials Science*, vol. 49, pp. 537-560, and 2004.
- [49] C. Suryanarayana "Mechanical alloying and milling," *Progress in Materials Science*, vol. 46, pp. 1-184, 2001.
- [50] S. Nouari "Spark Plasma Sintering of Al6061 and Al2124 Alloys" *Advanced Materials Research*, vol. 284, pp. 1656-1660, 2011.
- [51] X.C. Tong “Advanced Materials for Thermal Management of Electronic Packaging” ISBN 978-1-4419-7759-5, 2011.
- [52] D. D. L.Chung “Materials for thermal conduction” *composite materials research laboratory*, state university of New York, 2001.
- [53] C.R. Smith “Graphite aluminum metal matrix composite microelectronic packaging” *US Patent*, 5998733, 1999.
- [54] P. Wang, Z. Xiu, L. Jiang, G. Chen, X. Linc, G. Wu “Enhanced thermal conductivity and flexural properties in squeeze casted” *Materials and Design*, 88 (2015) 1347–1352.

- [55] E9-89A “Standard Test Methods of Compression Testing of Metallic Materials at Room Temperature” *ASTM international*, 2000.
- [56] N. Saheb, M. S. Khan, A. S. Hakeem “Effect of *Processing* on Mechanically Alloyed and Spark Plasma Sintered Al-Al₂O₃ Nano-composites” *Journal of nanomaterials*, Volume 2015, Article ID 609824, 13 pages.
- [57] W. Zhou, Q. Wangb, W. Ling, L. He, Y. Tang b, F. Wub, J. Liao, K.S. Hui, K.N. Hui “Characterization of three- and four-point bending properties of porous metal fiber sintered sheet” *Materials and Design*, 56- 522–527, 2014.
- [58] B 528–99 “Standard Test Method for Transverse Rupture Strength of Metal Powder Specimens” *ASTM International*, 2000.
- [59] T. Huber, H. P. Degischer, G. Lefranc, and T. Schmitt “Thermal expansion studies on aluminum-matrix composites with different reinforcement architecture of SiC particles” *Compos. Sci. Technol*, vol. 66, no. 13, pp. 2206–2217, 2006.
- [60] J. S. Benjamin "Mechanical alloying-A perspective" *Metal powder report*, vol. 45, pp. 122-127, 1990.
- [61] N. Al-Aqeeli “Processing of CNTs Reinforced Al-Based Nanocomposites Using Different Consolidation Techniques” *Journal of Nanomaterials*, 2011.
- [62] N. Saheb “Characterization of mechanically milled and spark plasma sintered Al₂O₃-CNTs Nanocomposite” *Science of Sintering*, 47 (2015) 119-129.
- [63] G.Saravanan, K. Shanmugasundaram, M. Prakash, M. Natesan “Influence of aging temperature on mechanical properties and thermal expansion of aluminum hybrid composite” *Rev. Téc. Ing. Univ. Zulia*, Vol. 39, N° 1, 10 - 17, 2016.

- [64] M. Balog, J. Nagi “Heat resistant ultra-fine grained Al profiles” *Rev.Adv.Mater.Sci*, 18(2008) 415-421.
- [65] A.S. Edelstein, R.C. Cammarata “Nanomaterials: synthesis, properties and application” *Institute of Physics*, Bristol and Philadelphia, PA, 2002.
- [66] A. A. El-Daly, M. Abdelhameed, M. Hashish, and A. M. Eid "Synthesis of Al/SiC nanocomposite and evaluation of its mechanical properties using pulse echo overlap method," *Journal of Alloys and Compounds*, vol. 542, pp. 51-58, 2012.
- [67] W. D. Callister “Materials Science and Engineering-An introduction” sixth edition, *John Wiley & Sons*, Inc. 2004.
- [68] ASM Handbook, Metallography and Microstructures, *ASM International*, Materials Park, OH, 1985.
- [69] T. Ettera, M. Papakyriacoub, P. Schulzb, P.J. Uggowitzera “Physical properties of graphite/aluminum composites produced by gas pressure infiltration method” *Carbon*, Volume 41, Issue 5, 2003, Pages 1017–1024.
- [70] H.J. Yeom, Y. W. Kima, K. J. Kim “Electrical, thermal and mechanical properties of silicon carbide–silicon nitride composites sintered with Yittria and Scandia” *Journal of the European Ceramic Society*, 35 (2015) 77–86.
- [71] S. Li, H. Izui, M. Okano, W. Zhang, T. Watanabe “Microstructure and mechanical properties of ZrO₂ (Y₂O₃)–Al₂O₃ nanocomposites prepared by spark plasma sintering” *Particuology*, 10 (2012) 345– 351.
- [72] ASTM-E-290 “Standard Test Methods for Bend Testing of Material for Ductility” *ASM Internationals*.

- [73] ASM Handbook “Mechanical testing and evaluation” *ASM International*, Materials Park, OH, 2000.
- [74] M. Tokita, Proceeding NEDO Int. Symp. Funct. Graded Mater. (1999).
- [75] Z. Balak, Mohammad Zakeri “Application of Taguchi L_{32} orthogonal design to optimize flexural strength of ZrB_2 -based composites prepared by spark plasma sintering” *Int. Journal of Refractory Metals and Hard Materials*, 55 (2016) 58–67.
- [76] U Harms, T.D Shen, R.B Schwarz “Thermal conductivity of $Pd_{40}Ni_{40-x}Cu_xP_{20}$ metallic glasses” *Scripta Materialia*, Volume 47, Issue 6, 16 September 2002, Pages 411–414.
- [77] L. Jianga, P. Wanga, Z. Xiub, G. Chena, X. Linc, C. Daia, G. Wua “Interfacial characteristics of diamond/aluminum composites with high thermal conductivity fabricated by squeeze-casting method” *Materials Characterization*, Volume 106, August 2015, Pages 346–351.
- [78] Z. Zhang, D.L. Chen “Consideration of Orowan strengthening effect in particulate-reinforced metal matrix nanocomposites: A model for predicting their yield strength” *Scripta Materialia*, Volume 54, Issue 7, April 2006, Pages 1321–1326.
- [79] Z. Zhang, D.L. Chen “Contribution of Orowan strengthening effect in particulate-reinforced metal matrix nanocomposites” *Materials Science and Engineering: A*, Volumes 483–484, 15 June 2008, Pages 148–152.
- [80] K.M. Shorowordi, T. Laoui, A.S.M.A. Haseeb, J.P. Celis, L. Froyen “Microstructure and interface characteristics of B_4C , SiC and Al_2O_3 reinforced Al matrix composites: a comparative study” *Journal of Materials Processing Technology*, 142 (2003) 738–743.

- [81] T.P.D. Rajan, R.M. Pillai, B.C. Pai, “Review: reinforcement coatings and interfaces in aluminum metal matrix composites” *J. Mater. Sci.* 33 (1998) 3491–3503.
- [82] S.C. Okumus, S. Aslan, R. Karslioglu, D. Gultekin, H. Akbulut “Thermal Expansion and Thermal Conductivity Behaviors of Al-Si/SiC/graphite Hybrid Metal Matrix Composites (MMCs)” ISSN 1392–1320 *MATERIALS SCIENCE*, (MEDŽIAGOTYRA). Vol. 18, No. 4. 2012.
- [83] H. E. Nassini, M. Moreno “Thermal expansion behavior of aluminum alloys reinforced with alumina planar random short fibers” *JOURNAL OF MATERIALS SCIENCE*, 36 (2001) 2759 – 2772.
- [84] N. Chawla, X. Deng, D.R.M. Schnell “Thermal expansion anisotropy in extruded SiC particle reinforced 2080 aluminum alloy matrix composites” *Materials Science and Engineering A*, 426 (2006) 314–322.
- [85] S. Ren, X. He, X. Qu, I. Humail, Y. Li, “Effect of Mg and Si in the Aluminum on the Thermo-mechanical Properties of Pressureless Infiltrated SiC_p/Al Composites” *Composites Science and Technology*, 67 (2007): pp. 2103 – 2113.
- [86] S. Elomari, R. Boukhili, D. J. Lloyd “Thermal expansion studies of prestrained Al/Al₂O₃ metal matrix composite” *Acta mater.* (1996) Vol. 44, No. 5, pp. 1873-1882.
- [87] S. Elomari, M. D. Skibo, A. Sundarrajan, H. Richards “Thermal expansion behavior of particulate metal matrix composites” *Composites Science and Technology*, 58 (1998) 369-376.
- [88] J.K. Chen, I.S. Huang “Thermal properties of aluminum-graphite composites by powder metallurgy” *Composites Part B: Engineering*, Volume 44, Issue 1, January 2013, Pages 698–703.

- [89] J. Wu, H. Zhang, Y. Zhang, J. Li, X. Wang “Effect of copper content on the thermal conductivity and thermal expansion of Al–Cu/diamond composites” *Materials and Design* 39 (2012) 87–92.
- [90] D. Liu , Y. Xiong, P. Li, Y. Lin, F. Chen, L. Zhang, J. M. Schoenung, E. J. Lavernia “Microstructure and mechanical behavior of NS/UFG aluminum prepared by cryomilling and spark plasma sintering” *Journal of Alloys and Compounds*, 679 (2016) 426-435.
- [91] J.E Daw, J.L Rempe, D.L Knudson, K.G. Condie, J.C. Crepeau “Viability of pushrod dilatoetry techniques for high temperature In-pile measurements” *Idaho National Laboratory (INL)*, USA, (2008) INL/EXT-07-13120.
- [92] M.G.A. Kumar, S.Seetharamu, Jagannath Nayak, L.N.Satapathy “A Study on Thermal Behavior of Aluminum Cenosphere Powder Metallurgy Composites Sintered in Microwave” *International Conference on Advances in Manufacturing and Materials Engineering, AMME Procedia Materials Science*, 5 (2014) 1066 – 1074.
- [93] J.J. GRACIO, R.P.CATALIN, V.GABRIELA, M.NITHIN, S.THOMAS, L. AUGUSTO, and C.BUCHHEIM “Mechanical Behavior of Al-SiC Nanocomposites Produced by Ball Milling and Spark Plasma Sintering” *METALLURGICAL AND MATERIALS TRANSACTIONS A VOLUME 44A*, NOVEMBER 2013—5259.
- [94] S. KAMRANI, R. RIEDEL, S. M. SEYED REIHANI, H. J. KLEEBE “Effect of Reinforcement Volume Fraction on the Mechanical Properties of Al-SiC Nanocomposite Produced by Mechanical Alloying and Consolidation” *Journal of Composite Materials*, 2009, Vol. 0, No. 00/2009.
- [95] A. Ismaila," Effect of Process Parameters on Microstructure and Properties of Spark

Plasma Sintered Al-SiC Nanocomposites," ProQuest Dissertations and Thesis, pp. 156.
2013.

[96] N. Saheb, "Compressive Behavior of Spark Plasma Sintered CNT Reinforced Al2124 and Al6061 Nanocomposites," Advanced Materials Research, vol. 652-654, pp. 33-37, 2013.

VITAE

Name: *Muhammad Shah Zeb Khan*
Date of Birth: 20/08/1990
Email: engr.shahzeb07@gmail.com
Academic Background: *M.Sc. (Materials Science & Engineering)* May 2016
King Fahd University of Petroleum & Minerals (KFUPM),
Dhahran, Saudi Arabia.
B.Sc. (Metallurgical & Materials Engineering), April 2012.
University of the Punjab, Lahore, Pakistan.

Research Achievements:

- N. Saheb, M.S.Khan, A.S.Hakeem “Effect of Processing on Mechanically Alloyed and Spark Plasma Sintered Al-Al₂O₃ Nanocomposites” Journal of Nanomaterials Volume 2015 (2015), Article ID 609824, 13 pages.
- B.S. Yilbas, C.Karatas, H. Karakoc, B.J.Abdul Aleem, M.S.Khan, N.Al-Aqeeli “Laser Surface Treatment of Aluminum Based Composite Mixed with B₄C Particles” Optics & Laser Technology, Volume 66, March 2015.

Professional Experience:

- May 2014-June 2016: Research Assistant, Center of Excellence in Nanotechnology, King Fahd University of Petroleum & Minerals (KFUPM), Dhahran, Saudi Arabia.
- June 2012-Oct 2013: Research Associate, Materials Science & Engineering Department, Institute of Space Technology, Islamabad, Pakistan.